関西学院大学博士学位論文

Optical properties of a newly developed fiber-optic miniaturized Raman probe and its application to nondestructive biomedical tissue measurement

A Thesis for the Degree

of

Doctor of Engineering

Submitted to School of Science and Technology

Kwansei-Gakuin University

By

Yuko S. Yamamoto

In July 2011

1

Contents

Chapter 2: High axial resolution Raman probe made of single hollow optical fiber

Chapter 3: Subsurface Sensing of Biomedical Tissues Using a Miniaturized Raman Probe: Study of Thin-layered Model Samples

Chapter 4: Noninvasive Subsurface Analysis Using Multiple Miniaturized Raman Probes: Basic Study of Thin-Layered Transparent Models of Biomedical Tissues

Chapter 5: Raman Study of Brain Functions in Live Mice and Rats: a Pilot Study

General Introduction

1. Thesis perspective – Development of Raman depth profiling method for in vivo measurements of layered tissues

The aim of this research is to investigate optical properties of a newly developed fiber-optic miniaturized Raman probe and develop of methodologies for obtaining depth-resolved Raman signals from biomedical tissues.

In recent years, fiber-optic Raman spectroscopy has become a more prospective method for real-time "optical biopsy" in place of conventional biopsy along with the progression of miniaturized fiber-optic probes.[1-3] For a noninvasive in vivo diagnosis and detection of epithelial precancer and cancer in organs, it is highly desirable to develop a depth-resolved Raman spectroscopic technique in order to characterize depth-dependent pathological changes associated with disease transformation in tissue.[4] I developed depth profiling methods using a newly fiber-optic Raman probe, called ball-lens mounted hollow-fiber Raman probe (BHRP) as a term of endearment, on the basic knowledge of optical properties of the Raman probes. Optical biopsy using Raman spectroscopy would improve by introducing the methodology by allowing layered tissues to be monitored in noninvasive manner.

The novelty and originality of this thesis can be described as follows: First, detailed information of scattering effects in layered sample are shown experimentally and generally by Raman spectroscopy. I eliminate an absorption effect of scattering media from the experimental system to highlight a scattering effect for a size of Raman sampling volume in depth direction. Second, BHRP are introduced as a miniaturized Raman probe for a

miniaturized endoscope. Basic properties and functions of BHRPs are investigated in detail. In this study, it is shown that BHRP has a high-sensitivity, limited depth-of-field optical property and considerably little background noise enough to use with the miniaturized endoscope. Third, I present a shape of Raman sampling volume of BHRPs along depth direction in a layered transparent sample. A calculation using chemometrics is introduced to depict a real form of Raman sampling volumes inside a layered transparent sample. Fourth, I propose a simple methodology to extract a pure Raman spectrum from embedded layer by using multiple BHRPs. In contact with surface layer of layered transparent materials, multiple BHRPs with different working distances measure different Raman spectra. These spectra includes Raman signal from surface and subsurface layer at the same time if the Raman sampling volume of BHRPs are thicker than each layers. I clarify a relationship between a size of Raman sampling volume of BHRPs, thicknesses of surface layers, and measured Raman spectra. Finally, I show a potent example to apply this system to *in vivo* measurements of a living rat.

The goal of this research is to demonstrate a performance of BHRP for in vivo measurement of animals in a living state, and show future prospects of optical biopsy using BHRP.

2. Why Raman? - Optical biopsy using near-infrared Raman spectroscopy

To diagnose disease, the physician's ability is enhanced by the timely availability of objective, quantitative diagnostic information.[5] Novel biomedical applications of optical spectroscopy, such as fluorescence, reflectance and Raman scattering have made advances by their needs to provide such information in clinical practice.[5]

6

Raman spectroscopy is a vibrational spectroscopic technique and can provide the most detailed information about the chemical composition of tissue at the molecular level. Since light can be delivered and collected rapidly via optical fibers, which can be incorporated into catheters, endoscopes, cannulas and needles, Raman spectroscopy can be performed *in vivo* in real time.A promising study of clinical Raman system using a fiber-optic Raman probe has firstly reported by Shim et al. in 1997.[6] They introduced a fiber-bundle Raman probe which consists of a central illumination fiber surrounded by several detection fibers with integrated filters.[6, 7] After this report, many kinds of Raman probes were developed in similar or different manner by a number of research groups. Most Raman fiber probes are bundled-silica-fiber probes mainly 6 to 15-around-1 multi fiber probes made of silica optical fibers.[8-14]Another type of Raman probesarefabricated usinga hollow-optical fiber, a new type of optical fiber.[15] Note that a new type of Raman probe made of a hollow fiber will be introduced in this thesis.

For *in vivo* diagnosis and detection of epithelial cancer and precancer nondestructively, Near-infrared (NIR) Raman spectroscopy has certain advantages. Interference of water is relatively small in comparison to Fourier transform IR spectroscopy in NIR region.And a penetration depth of NIR excitation light is deeper than that in shorter wavelength.[16]Moreover, strong and broadband fluorescence from tissue decreases very rapidly at NIR excitation comparing to visible excitation.[5] For CCD-based dispersive spectrometers, excitation wavelengths shorter than 850 nm is useful with silicon-based CCD detectors because detector efficiency drops of sharply from 1000 to 1100 nm which is corresponding to the Raman fingerprint region for 850 nm excitation.[5] Fluorescence interference in tissue Raman spectra can be reduced even further with 830 nm excitation

than 810 nm.[5] These descriptions may indicate that the laser source at 830 nm or longer wavelength has advantages for Raman measurement of biomedical tissues with CCD detector. However, for practical Raman systems, laser sources at 830 nm wereinitially used for the fiber-optic Raman systems[8, 9, 17, 18] but those at shorter wavelength e.g. 785 nm were introduced especially in the past few years.[1, 2, 7, 13, 14]

Despite the great advantage that Raman spectroscopy with NIR excitation light could offer, there are technical challenges to overcome using fiber-optic Raman probe.[3] First, achieving a high signal-to-noise (S/N) ratio is difficult because Raman scattering from tissue is inherently very weak. Second, conventional fiber-optic Raman probe made of bundled silica fibers exhibit strong Raman scattering in the fingerprint region. High background Raman signal must be interfere the real Raman spectra. To collect Raman spectra from tissue with high S/N ratio, optical design problems including spectral interference from the optical fibers themselves must be resolved.

3. Development a newly miniaturized fiber-optic Raman probe with high signal-to-noise ratio

In 2009, this optical design problems of miniaturized Raman probes dramatically solved using a new type of optical fiber, called a hollow optical fiber (HOF) developed by Prof. Matsuura.[19]The HOF consists of thin glass capillary tubing with a smooth silver film coating its inner surface, and can delivery light in wide range including NIR region with low loss.[19] It generates very little Raman scattering noise during the laser transmission from core material because the core material of HOF is air. A newly miniaturized Raman probe, ball-lens mounted hollow-fiber Raman probe (BHRP, Fig. 2) was developed with attaching

a single ball lens at the distal end of HOF as describes in Chapter 2. So that practically nought of Raman scattering noise, BHRP performs to collect Raman signal from any sample with high S/N ratio. Thus, BHRP have great advantage for optical biopsy using Raman spectroscopy.

The simple design of BHRP brings two merits for Raman optical biopsy system. First, it's not necessary to use an intricate filter system at the distal end of the probe. Second, BHRP can be fabricated not only specialists for optics but also researchers in other field, even though students like the author. These merits give us the way to make a research of Raman optical biopsy with low-cost. It means that a high-quality *in vivo* Raman measurement is available inexpensively and simply by introducing BHRP.

Furthermore, the design strategy of BHRP made a huge improvement in an axial resolution and sensitivity. By introducing a single ball lens to a single HOF, the Raman sampling volume of BHRP is relatively smaller than that of other types of fiber-optic Raman probes. A measured working distance and axial resolution of BHRP with a sapphire ball lens are only 28 and 23 um (FWHM) in air (Fig. 3). These are small enough to measure in particular layer in thick-layered biomedical tissues which are already well-known.

BHRP was introduced immediately to a newly-developed optical biopsy system by H. Sato and his collaborators.[1] The system produced by H. Sato consists of a miniaturized endoscope, a NIR laser at 785 nm, and a dispersive spectrometer with cooled CCD detector (Fig .1). Hattori et al[1] succeeded to measure esophagus of living rat *in vivo*using the proposed system.

However, for diagnostic use, it is highly desirable to develop a depth-resolved Raman spectroscopic technique because dysplasia-related changes may be associated with

the thickening of epithelial tissue.[4] Axial resolutions of fiber-optic Raman probes in air are almost ten to several hundred times bigger than a conventional Raman confocal microscope.[20] For facilitating the wide applications of Raman spectroscopy in biomedical diagnosis, it is efficient to introduce depth-selected measurement in layered tissue using fiber-optic Raman probes.

4. How to achieve Raman depth profiling using BHRP - Optical properties of BHRPs and its application

As written in previous section, axial resolutions of miniaturized Raman probes including BHRPs are relatively much bigger than those of conventional microscopes. To measure a particular layer by using a BHRP, a depth resolution of the BHRP must be smaller than the thickness of the layer. However, in case of BHRPs, the depth resolution cannot be improved by modifying any optical configuration. This is because a spatial resolution of BHRP is limited by an aberration of a ball lens and a numerical aperture of the HOF. To solve this problem, I started trying to imagine an excitation volume, called Raman sampling volume of a BHRP with thought experimental measurement of a layered transparent material.

Let me consider a place of origin of Raman signals measured by a BHRP (Fig. 4). If a particular layer of a layered sample is thick enough to cover whole Raman sampling volume of a BHRP, a Raman spectrum obtained by BHRP includes only pure Raman signal from single layer. But if a thickness of a particular layer is thinner than a Raman sampling volume of a BHRP, the Raman spectrum has contributions from not only the layer but also other layers. In other words, when I measure a Raman spectrum by using a probe with a large Raman sampling volume, the Raman spectrum shouldinclude all signals coming from

inside a whole Raman sampling volume. It means that BHRP can capture all information within a Raman sampling volume at once including each layer's pure Raman spectrum, chemical compositions and so on. Therefore, I thought that it is possible to extract particular signal or spectrum of a particular layer from a Raman spectrumwhich is obtained by BHRP.

According to my first inspiration above, I completed to show a potency to extract quantitative information about a thickness of a subsurface layer by using a BHRP combined with chemometrics as described in Chapter 3. The result proposed a methodology to provide simultaneous determination of the location and chemical composition of subsurface layer. The result is also able to improve a depth resolution of a BHRP at the same time. Moreover, I completed to develop a noninvasive subsurface analytical method using multiple BHRPs as described in Chapter 4. I represented a basic theory for explaining a relationship between spectra from embedded layer and a surface layer thickness of a layered transparent sample. A pure Raman spectrum of subsurface layer successfully reconstructed using multiple BHRPs with different working distances non-invasively.

These results strongly suggest that my prediction model of Raman sampling volume of BHRP is essentially correct. Combined with light-scattering effect as described in Chapter 1, BHRP can assuredly be used to depth-resolved Raman measurement for layered tissue *in vivo*.

5. Further prospects for measuring layered biomedical tissues using BHRP

BHRP has two major advantages for measuring biomedical tissues and bring new eyes to us for real-time optical biopsy using fiber-optic miniaturized Raman probes. One of the advantages is low signal-noise ratio.This is because very little Raman scattering noise is

generated from HOF. Another is that we can easily change a working distance of BHRP by selecting a ball lens at distal end.

I show an example of *in vivo* optical biopsy of live animal using BHRP in Chapter 5. Particular striking of this study is that Raman spectra of a brain tissue were successfully measured from rats and mice which are kept in a living state. Under anesthesia, the spectra show differences of water condition including water concentration and cluster conformation in the brain. BHRP is sufficiently narrow, flexible enough to measure a brain *in vivo* and can bring high-quality Raman spectra. This study opens up a new possibility for brain researchesof live experimental animals.

Furthermore, in combination with proposal methodologies of Raman depth profiling, I suppose that the system can also be used for *in vivo* human blood diagnosis in noninvasive manner (Fig. 5). A working distance of a BHRP made of a fused silica lens is several hundred micrometers, enough to achieve capillary blood vessels embedded under human skin. Thus, we may reconstruct pure Raman spectrum of human blood by using multiple BHRPs noninvasively. Moreover, applying chemometrics, it may be possible to extract quantitative and qualitative information about human blood glucose, human blood cells and so on. I have completed an application form for a budget about this study. A challenge for noninvasive diagnosis of human blood will be performed by the author and the collaborators in near future.

6. Thesis outline

This thesis consists of five chapters. First, a basic study of scattering effect in depth-resolved Raman measurement is described in Chapter 1. Second, a new type of

miniaturized Raman probe is introduced in Chapter 2. Third, a methodology of Raman depth profiling using the Raman probes is reported in Chapter 3 and 4. And last, an *in vivo* study using BHRP is shown in Chapter 5 as an important example.

6-1.　Chapter 1: Basic Study of Raman Sampling Volume in Diffusely Scattering Media

In Chapter 1, I experimentally disclose a scattering effect for a depth-resolved Raman measurement of layered scattering media. An objective lens of conventional Raman microscope is used as an analogue of a BHRP. The layered sample consists of Si wafer, Intralipid™dilution as light-scattering medium, and silica window.

I investigate a Raman signal from the silicon substrate beneath Intralipid suspension layer with varying a thickness of the scattering layer. Raman collection efficiency depending on the thickness of scattering medium is clearly reported in this section. I also show Raman sampling volume, response curves in depth directionby using Raman signal from embedded layer (Si wafer) through scattering media (Intralipid). I finally succeeded in this chapter to develop a quantitative model for evaluation of describe an extinction of Raman signal coming through scattering media detected by lens system quantitatively. These results present a potential of depth-resolved Raman measurements for layered tissues using BHRPs.

6-2.　Chapter 2: High axial resolution Raman probe made of single hollow optical fiber

In Chapter 2, I introduce a miniaturized Raman probe, ball-lens mounted hollow fiber Raman probe (BHRP). BHRP is specially-fabricated to a newly miniaturized endoscope system,[1] simply made of single hollow optical fiber and single lens. This miniaturized endoscope is designed for diagnosing diseases of the esophagus, stomach, colon, and rectum in order to continuously study the physiological changes in small living experimental animals.[1]WithBHRP, the endoscope system is able to measure *in vivo*Raman spectra from gastrointestinal tract in rats or mice.

I report a summary of BHRP especially to a structure and optical properties in depth in this section. Detailed optical properties of the miniaturized Raman probes changinglens materials anddiameters are described here. Merits and weak points of BHRP are also discussed in the same section.

6-3.   Chapter 3: Subsurface Sensing of Biomedical Tissues Using a Miniaturized Raman Probe: Study of Thin-layered Model Samples

In Chapter 3, I discuss a basic knowledge of a Raman sampling volume of a BHRP in layered model samples. The model sample consists of two kinds of transparent polymers. I also propose a technique to measure a thickness of surface and subsurface layer of two-layered sample using single BHRP in a nondestructive manner. To extract a thickness of the first layer, a partial least square (PLS) regression analysis was employed. Curiously, a shape of Raman sampling volume of BHRP in transparent sample is showed up using PLS regression analysis at the same time. A principle of the proposed technique is demonstrated by a simulation study and an empirical study.

6-3.   Chapter 4: Noninvasive Subsurface Analysis Using Multiple Miniaturized Raman Probes: Basic Study of Thin-Layered Transparent Models of Biomedical Tissues

In Chapter 4, I describe a noninvasive approach for subsurface probing using multiple BHRPs with different working distances. The model sample is also made of two kinds of transparent polymers, a polymethylmethacrylate (PMMA) substrate covered with polyethylene (PE) films. I present a theory to reconstruct a pure Raman spectrum of an embedded layer noninvasively. The theory shows a relationship between a thickness of surface layer and sizes of Raman sampling volumes of BHRPs, and indicates a simple way to extract a pure Raman spectrum from embedded layer.I succeeded to extract a pure Raman spectrum from embedded layer, PMMA, without any invasive measurement experimentally. The method is essentially applicable to other Raman systems, including bundle-fiber Raman probes, Raman microscopes and so on.

6-4.   Chapter 5: Raman Study of Brain Functions in Live Mice and Rats: a Pilot Study

In Chapter 5, I introduce an application of a BHRP for *in vivo* measurement in small living animals. Brain tissues of live rats and mice under anesthesia are measured using the BHRP in minimally-invasive manner. This study was successfully demonstrated*in vivo* layered tissue measurements by BHRP. The results would strongly provide us an effective way to study chemical compositions of biomedical tissues *in vivo*at the molecular level.

References

[1]   Y. Hattori, Y. Komachi, T. Asakura, T. Shimosegawa, G. Kanai, H. Tashiro, and H. Sato, Applied Spectroscopy 61, 6, 579 (2007).

[2]   Z. Huang, S. Teh, W. Zhen, J. Mo, K. Lin, X. Shao, K. Ho, M. Teh, and K. Yeoh, Optics Letters, 758 (2009).

[3]   A. Beljebbar, S. Dukic, N. Amharref, and M. Manfait, Analytical and Bioanalytical Chemistry, 477 (2010).

[4]   J. Mo, W. Zheng, and Z. Huang, Biomedical Optics Express 1, 1, 17 (2010).

[5]   E. B. Hanlon, R. Manoharan, T. W. Koo, K. E. Shafer, J. T. Motz, M. Fitzmaurice, J. R. Kramer, I. Itzkan, R. R. Dasari, and M. S. Feld, Physics in Medicine and Biology 45, 2, R1 (2000).

[6]   M. G. Shim and B. C. Wilson, Journal of Raman Spectroscopy 28, 2-3, 131 (1997).

[7]   M. Shim, B. Wilson, E. Marple, and M. Wach, Applied Spectroscopy, 619 (1999).

[8]   H. P. Buschman, E. T. Marple, M. L. Wach, B. Bennett, T. C. B. Schut, H. A. Bruining, A. V. Bruschke, A. van der Laarse, and G. J. Puppels, Analytical Chemistry 72, 16, 3771 (2000).

[9]   J. Motz, M. Hunter, L. Galindo, J. Gardecki, J. Kramer, R. Dasari, and M. Feld, Applied Optics, 542 (2004).

[10]   Y. Komachi, H. Sato, K. Aizawa, and H. Tashiro, Applied Optics 44, 22, 4722 (2005).

[11]   Y. Komachi, H. Sato, and H. Tashiro, Applied Optics 45, 30, 7938 (2006).

[12]   Y. Komachi, T. Katagiri, H. Sato, and H. Tashiro, Applied Optics 48, 9, 1683 (2009).

[13]   M. A. Short, S. Lam, A. McWilliams, J. H. Zhao, H. Lui, and H. S. Zeng, Optics Letters 33, 7, 711 (2008).

[14] N. D. Magee, J. S. Villaumie, E. T. Marple, M. Ennis, J. S. Elborn, and J. J.

McGarvey, Journal of Physical Chemistry B 113, 23, 8137 (2009).

[15] Y. Komachi, H. Sato, Y. Matsuura, M. Miyagi, and H. Tashiro, Optics Letters 30, 21,

2942 (2005).

[16] S. K. Teh, W. Zheng, K. Y. Ho, M. Teh, K. G. Yeoh, and Z. Huang, British Journal of

Cancer 98, 2, 457 (2008).

[17] T. C. B. Schut, M. J. H. Witjes, H. Sterenborg, O. C. Speelman, J. L. N. Roodenburg,

E. T. Marple, H. A. Bruining, and G. J. Puppels, Analytical Chemistry 72, 24, 6010

(2000).

[18] J. Day, R. Bennett, B. Smith, C. Kendall, J. Hutchings, G. Meaden, C. Born, S. Yu,

and N. Stone, Physics in Medicine and Biology, 7077 (2009).

[19] Y. Matsuura, G. Takada, T. Yamamoto, Y. W. Shi, and M. Miyagi, Applied Optics 41,

3, 442 (2002).

[20] N. Everall, I. Priestnall, P. Dallin, J. Andrews, I. Lewis, K. Davis, H. Owen, and M.

George, Applied Spectroscopy, 476 (2010).

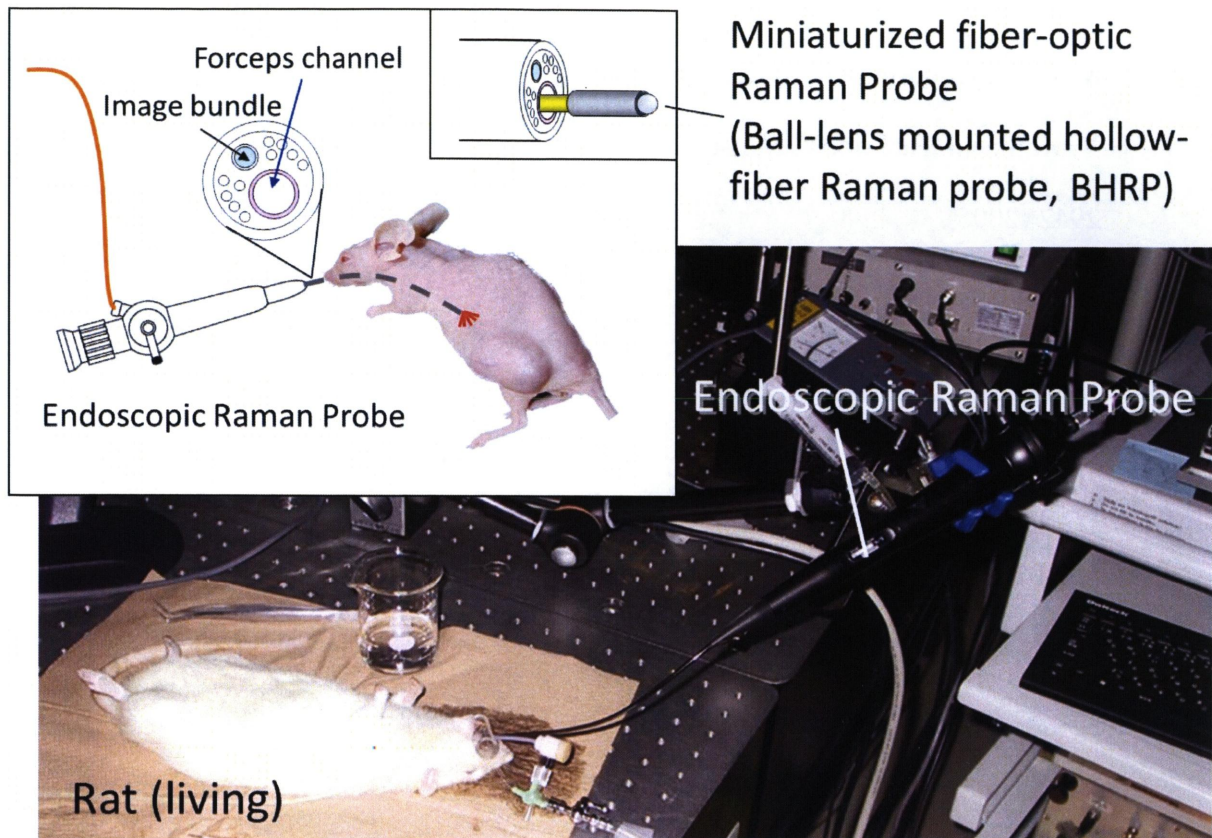Figure 1. Schematic representation of *in vivo* Raman measurements using a miniaturized endoscopic Raman system.
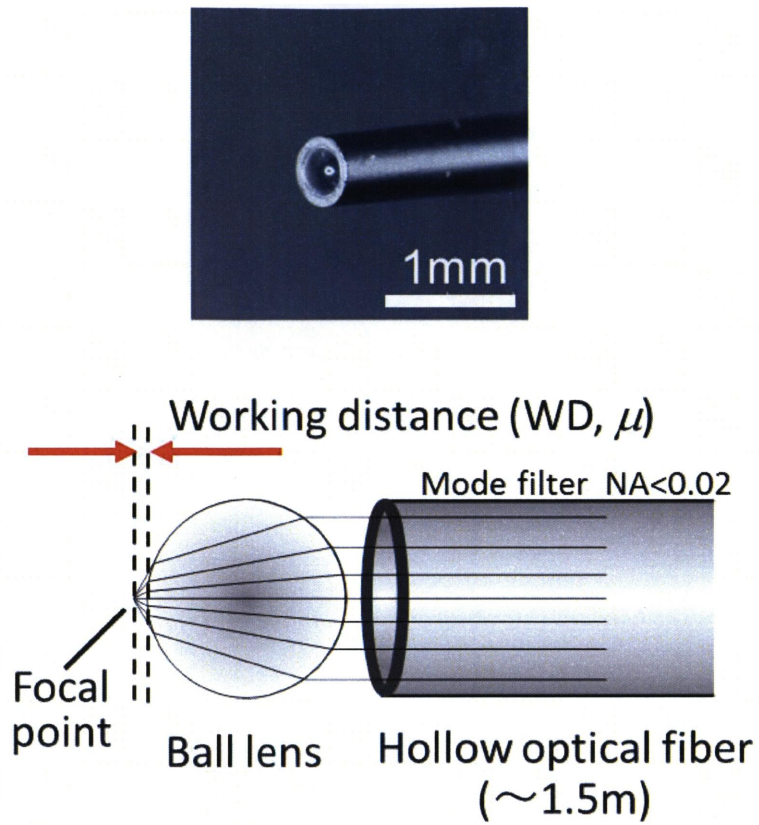
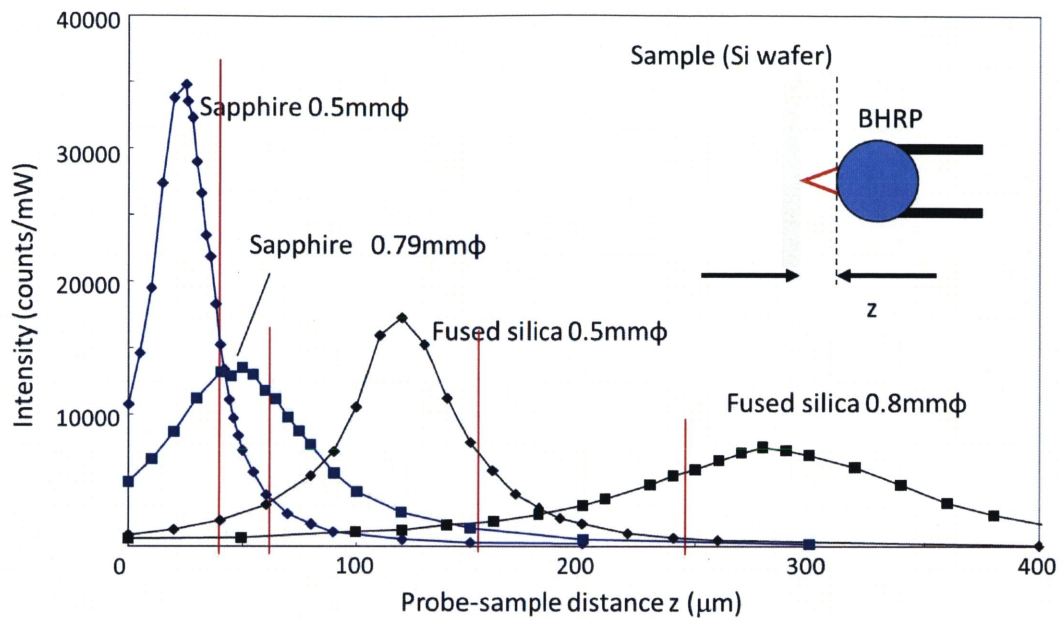Figure 2.   Architectureof Ball-lens mounted hollow-fiber Raman probe (BHRP).

Figure 3. Response curves of Raman spectral intensity to probe-sample distances for four probes with different ball lens. Red lines indicate working distances calculated by a formula (1) in Chapter 2.
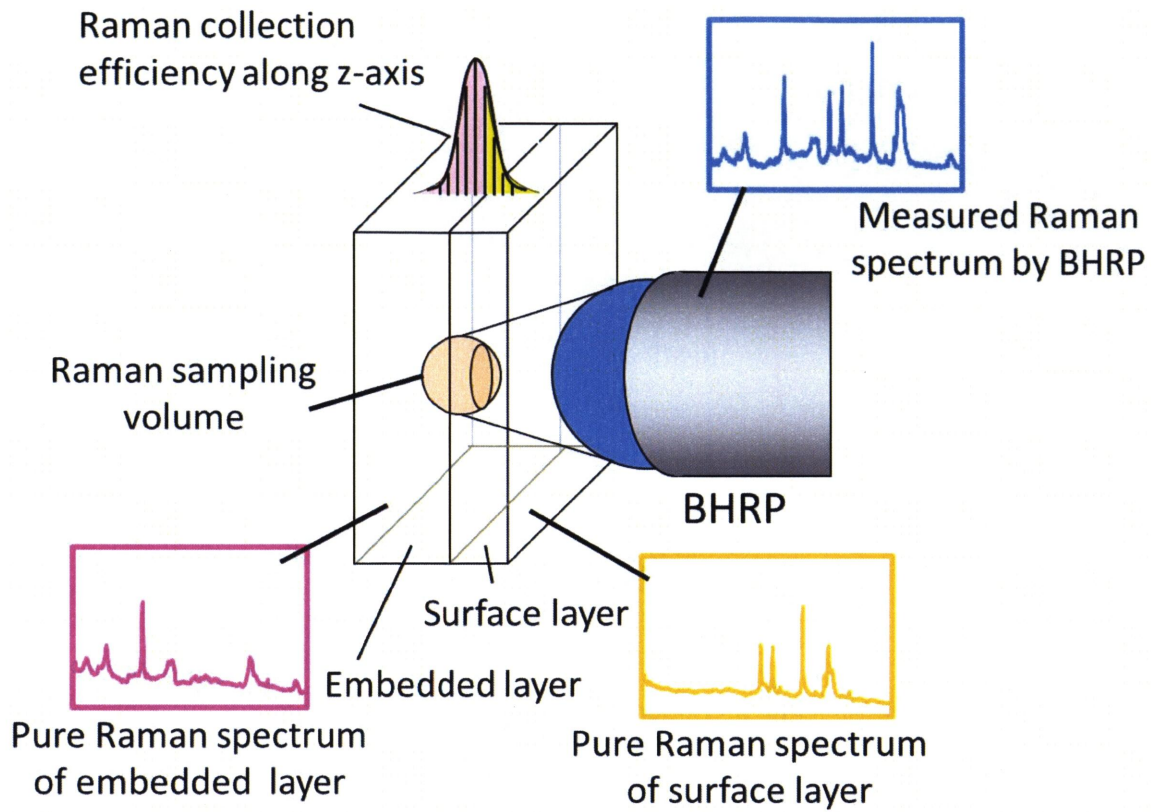
Figure 4.   Raman sampling volume of BHRP in layered sample.

Rat or mouse (living)

PC

NIR laser

Chemometrics
(PLS, PCA)

Raman
spectrometer

BHRP

Human (living)

Hair

Epidermis

Capillary
blood
vessel

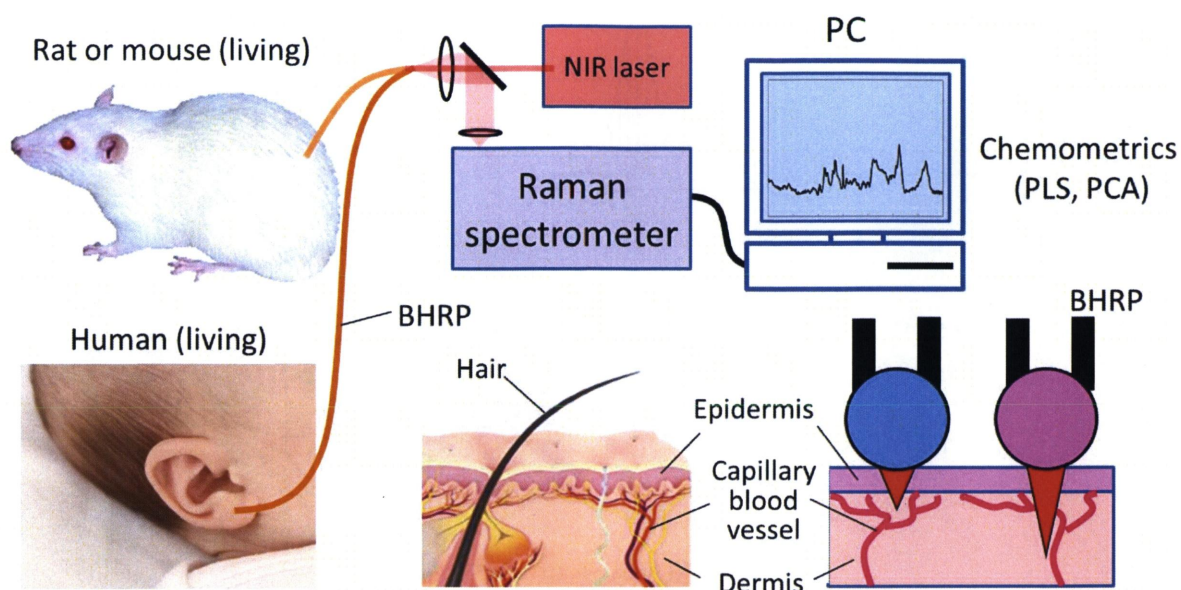Dermis

BHRP

Figure 5.   Proposed scheme of optical biopsy system for *in vivo* blood analysis using BHRP.

Chapter 1

Basic Study of Raman Sampling Volume in Diffusely Scattering Media

Abstract

To quantitatively evaluate a scattering effect on Raman sampling volume in layer structured samples, which is common for biomaterials including skin, we experimentally and theoretical developed a simple model using conventional Raman microscope. We showed shapes of Raman sampling volumes along depth direction both in air and in scattering condition. The layer structured samples are Si wafer covered with aqueous dilution of Intralipid™ as a scattering media, and silica window. We succeeded to develop a quantitative model for evaluation of an extinction of Raman signal coming through scattering media detected by lens system quantitatively. A simple function introduced from Lambert-Beer's law was well fitted to the experimental results. In combination with a previous report, the model is useful for application of fiber-optic Raman probes to real biomaterials.

Introduction

Raman spectroscopy is a promising tool for in situ diagnosis of epithelial precancerous region. It provides information of molecular compositions from live tissue without labeling or staining processes.[1,2] In the past decade, fiber-probe Raman spectroscopy has become a more prospective method for real-time "optical biopsy" in place of conventional biopsy.[3] For most medical application, fiber-optic Raman probes must be thin, generally smaller than 1-2 mm in diameter, to apply to *in vivo* observation of human organs and tissue for incorporation into needles, endoscopes, angioscopes and other clinical devices.[4] Several types of Raman probes which meet these criteria are reported previously[6-13] and have been applied for *in vivo* measurements with an endoscope.[3, 10, 12] Meanwhile, analyzing Raman spectroscopic information emitted from tissue still remains complicated for tissue diagnosis and characterization.[1, 6] The main reason is that the overall Raman signals acquired from the tissue surface usually contain a mixture of Raman information originating from different tissue depths. To clarify the origins of Raman signals collected from tissue by using Raman fiber-optic probes experimentally, it is highly important to depict a sampling volume of the Raman probe which is introduced for *in vivo* measurements.

However, to investigate a shape of a sampling volume inside scattering media is very difficult because several optical parameters (e.g. absorption coefficient, scattering coefficient, anisotropic factor, refractive index) are may significantly affect it. Moreover, sampling volumes of fiber-optic Raman probes must be different from one probe to another depending on the optical designs. For these reason, we should measure or calculate a shape of Raman sampling volumes one by one. Early experimental trials have been reported by

Shim et al.[6] and Komachi et al.[9] In both studies, a phantom target was placed in a container

filled with scattering liquid and then the probe was retracted from a contact position to the

phantom step by step on the order of hundreds of micrometers. Their results successfully

showed a shape of the sampling volume of their own probes in turbid liquid, however, these

results are essentially not applicable to the other probes directly. Another way to speculate a

sampling volume's shape of one's own probe in turbid media is to measure that in air

condition. The results have been shown by J. Motz, Komachi and Katagiri.[5, 9, 11, 14] The other

way to speculate that in transparent polymer substances is shown in our previous study.[15]

For one of our fiber-optic Raman probe namely Ball-lens mounted hollow-fiber Raman

probe (BHRP),[11] the function representing the Raman sampling volume along the depth

direction is Gaussian curve in those substances. Nevertheless, the Raman sampling volume

in turbid media such as biomedical tissue must be different from these results because of the

several optical parameters including scattering effect. In other studies, the Monte Carlo

(MC) simulations have been introduced to calculate the spatial distributions of Raman

sensitivity of fiber-optic Raman probes using several optical properties of samples.[1, 2, 16] MC

is a powerful method because it is applicable to a wide range of fiber-optic Raman systems,

however, there are substantial needs for experimental study to understand the principles of

Raman sampling volumes in turbid media comprehensively. Although Reble et al[16]

succeeded to combine MC simulation and experimental results quantitatively using several

optical properties such as absorption coefficient μ_a, scattering coefficient μ_s, and Raman

scattering cross-section σ, the alternative inspection is necessary to clarify the meaning of

optical parameters for the shape of Raman sampling volume using another experimental

approach.

In the present study, we focused on scattering effect of turbid media for the size of Raman sampling volumes experimentally and quantitatively by using a scattering coefficient μ_s. A lens of Raman microscope is used as an analogue of fiber-optic Raman probe to clarify the scattering effect in several tens to hundreds micrometers. The confocal cross-slit of the Raman microscope was broaden compared with standard setting to broaden the focal volume of the lens similar to conventional high-volume fiber-optic Raman probes. We drew out a Raman collection efficiency along the depth direction from whole Raman sampling volume because the analysis in depth direction is very important for diagnostic application.[1, 2, 15, 17] To eliminate the absorption effect, we used Intralipid suspension as an scattering sample and applied 514 nm laser source. Conventional Lambert-beer's law leads a simple formula of Raman signal coming from inside layered sample quantitatively and the formula was connected to scattering coefficient μ_s directly in this study. We note that the present results are well agreed with the report by Reble et al.[16]

Experiments

a. Instrumentation.

Raman spectra were acquired using an ultra-high-performance Raman microscope (Photon Design Corporation, Japan). The Raman microscope system consists of Ar+ laser (Spectra Physics, U. S. A.); deep-depletion CCD camera (2048 × 512 pixels at 13.5 um×13.5 um per pixel; image area 27.6 mm ×6.9 mm, -120°C, Princeton Instruments); spectrograph (PDP320, f = 320mm, F/4.9, range of wavelength 0-13000 Å (at 1200 gr / mm), Photon Design Corporation, Japan); ultra-long working distance objective lens (Photon

Design Corporation, Japan); and a variable cross-slit in front of a vertical slit of a spectrograph.

The cross-slit was set to 1000 um to broaden a spatial resolution of a 9× objective lens (NA 0.28) than conventional Raman confocal microscope. The measured spatial resolution of the objective lens along z-axis was 170 um as a full width at half-maximum (FWHM) (Fig. 1). The 514 nm line of the Ar+ laser was employed as a light source. The laser power was typically 80 mW at the sample and the exposure time was typically 60 s. Raman scattering was collected in a 180° back scattering geometry. The spectral resolution was 5 cm^{-1}.

b. Samples and Data processing

10 % Intralipid™ stock solution purchased from Fresenius Kabi (France) was introduced as a light scattering medium. The stock solution was diluted with distilled water to 0.1 − 1.0 % and mix slowly by upside-down and used within several hours. The scattering coefficient μ_s of 10 % stock solution was obtained by Staveren et al.[18]

The layered model samples consist of 0.1 - 1.0 % intralipid suspension and silicon substrate as shown in Fig. 1. Thicknesses of the intralipid suspensions are varied with 50 um to 800 um by changing a spacer made of polytetrafluoroethylene (PTFE).

A background spectrum originating from a silica window covering the intralipid suspension was subtracted from raw Raman spectra. Zero depth ($\Delta=0$) in Fig. 3 was defined as the maximum point of Raman signal which is measured by Raman microscope by changing the distance between the sample and the lens. The error limit was within 10 um along depth

direction. The fitting calculations in Fig. 3 were performed by Origin 8.5 software (Lightstone corp., Japan)

Results and discussion

a. Raman Sampling Volume along Depth Direction under Scattering Condition

Figure 2 shows a typical Raman spectrum dataset measured from a layered sample with changing the distance from sample's surface and lens as shown in Fig. 1. The layered sample consists of Si wafer, 0.5 % intralipid suspension and silica window. To emphasize a feature of the scattering layer and the embedded Si layer, a spectrum originating from a silica window covering the intralipid suspension was subtracted from raw Raman spectra dataset individually. A sharp band at 519 cm^{-1} is assigned to Si-Si bonding in the Si wafer and bands at 1439 and 1654 cm^{-1} are assigned to C-H deformation and C=C stretching modes of the lipid vesicle in Intralipid suspension. A broad band due to water at 1640 cm^{-1} overlaps the band due to the C=C stretching mode.

As shown in Fig.2, we succeeded to measure both layer of Si wafer and Intralipid layer at the same time. And the spectral features changed depending on the distance between the sample and the lens. The result indicates that the sampling volume of this setting is large enough to cover both layers by not only a focal point of the lens but also surrounding area. It suggests that the optical setting of present work is similar to that of fiber-optic Raman probe as we described in previous work.[15]

Figure 3 depicts Raman response curves along depth direction determined in air, water, and 0.5 % Intralipid suspension. Band areas at 519 cm^{-1} were plotted against the sample-lens distance as described in Shim et al.[6] These curves were well fitted by Voigt

function. Figure 4 indicates a difference of the full width at half maxima (FWHM) of the Raman response curves shown in Fig. 3. It is clear from Figure 3 and 4 that the FWHM of the response curves are slightly changed due to the refractive indexes of materials, and strongly affected by the scattering effect of them. FWHM of 0.5 % Intralipid becomes 1.5 times larger than that of air and water.

b. Attenuation of Raman Signal Passed Through Scattering Media

b-1. Theoretical Approach describing Quantitative Raman Signal through Scattering Media using Lambert-Beer's Law

Let us consider total amount of Raman signal generated from inside the scattering media macroscopically. The basic property of light attenuation written by Lambert-Beer law is given by:

$$(z) = Uo\exp(-\mu_t z) \qquad \text{-----(1)}$$

Where Uo is the intensity of radiation energy, μ_t is an extinction coefficient. This basic formula simply shows that a collimated beam is attenuated in a media of thickness z. Note that the extinction coefficient is connected with the extinction cross section σ_t as $\mu_t = \rho\sigma_t$, where ρ is the density of particles. [19]

Raman signal which is generated inside media by incident light is also attenuated as shown in Lambert-Beer's law. Thus,

$$U_{Raman}(z) = Uo_{Raman}\exp(-\mu_t z) \qquad \text{-----(2)}$$

Then the intensity of Raman scattering light must be proportional to the intensity of radiation energy. [20]

$$Uo_{Raman}(z) \propto U(z) = Uo\exp(-\mu_t z) \qquad \text{-----(3)}$$

$$Uo_{Raman}(z) = A \cdot Uo\exp(-\mu_t z) \qquad \text{-----(4)}$$

$$U_{Raman}(z) = A \cdot Uo \cdot \exp(-\mu z) \cdot \exp(-\mu_t z) \qquad \text{-----(5)}$$

$$U_{Raman}(z) = A \cdot Uo \cdot \exp(-2\mu_t z) \qquad \text{-----(6)}$$

Where A is constant. The extinction coefficient μ_t can be separated to the absorption coefficient μ_a and the scattering coefficient μ_s as $\mu_t = \mu_a + \mu_s$. When the scattering media doesn't absorb the excitation light which is used in Raman measurement, the absorption coefficient μ_a is zero and the extinction coefficient μ_t must be equal to the scattering coefficient μ_s. Therefore,

$$\mu_t = \mu_s = \rho \sigma_s \qquad \text{-----(7)}$$

b-2. Comparison Theoretical Approach to Experimental Results

Figure 5 shows an experimental result of Raman signal's attenuation in different concentration of the scattering media which is measured as shown in Fig. 1. The band intensities at 519 cm^{-1} generated from the Si wafer were plotted as a function of the thicknesses of scattering layer for 0.1 %, 0.5 % and 1.0 % Intralipid suspension. The absorption coefficient μ_a of 10 % Intralipid suspension at 514 nm is 0.99 $\times$ 10$^{-5}\mu$m^{-1}[18] and negligible in this studybecause it is minus four orders of magnitude of μ_s. The solid lines were fitted by $z = z0 + A \cdot U \cdot \exp(-2\mu_t z)$ referring from Eq. 6 and the fitted parameters are shown in Table 1.

Of note is that the parameters μ_t in Table 1 obtained by the fitting calculation are very reasonable to that of 10 % Intralipid obtained by Staveren et al.[18] As shown in Eq. 7, if the sizes and the number of particles in Intralipid suspension does not changed by dilution with water, an extinction coefficient μ_t must be proportional to a density of particle ρ. Therefore, the μ_t of 0.1, 0.5 and 1.0 % Intralipid suspension should be a hundredth,

twentieth and tenth part of the μ_t of 10 %. From Table 1, the μ_t of 0.5 and 1.0 % are well agreed with that of 10 % and the errors in the results are within ten to twenty percent. However, the μ_t of 0.1 is twice larger than that of 10 %. These results might show that the size distribution of Intralipid doesn't change significantly at the concentrations from 10 % to 0.5 %, while that might be change at that of 0.1 %.

The present results demonstrate that the present theoretical model is potentially useful to estimate of Raman signal coming through a scattering medium quantitatively. It should be noted that the present results which is simply based on the Lambert-Beer's law are totally agreed with that of Reble et al. which were calculated based on the MC simulation[16]. As we described in this paper, our approach focused on the extinction of Raman signal from embedded substrate due to the scattering effect without any absorption. Although Reble et al.[16] used both reduced scattering coefficient μ_s' and absorption coefficient μ_a to fit a MC simulation to their experimental results, the models in Reble et al.[16] are well fitted to our present results. Then we concluded that the present model is much simpler and easier to make a prediction of Raman sampling volume of fiber-optic Raman probes in light scattering samples. Moreover, according to the result of Reble et al[16] and the present one, a coefficient of absolute Raman signal μ_{Raman}[16] seems to be connected generally to $U_{Raman}(z)$ in Eq. 6. in the present study as a function of depth in scattering sample.,

Conclusion

We show a prediction for Raman sampling volumes of fiber-optic Raman probes along depth direction under scattering condition. We introduced a conventional Raman microscope as an analogue of fiber-optic Raman probes. The Raman response curves along depth direction were well fit by Voigt function. Scattering phantom was made of 0.1 to 1.0 % Intralipid suspension. Compared with no scattering condition, the response curve in scattering condition extended to 1.5 times in depth direction. Very little effect is appeared by refractive indexes of layered samples including scattering media.

We also propose a quantitative analysis of Raman signal from embedded Si wafer coming through scattering layer. Our results simply show that the Raman signal is extinct while through a scattering layer exponentially. And in case of no absorption, the total amount of Raman signal measured by a lens system can be described by a simple equation introduced from Lambert-Beer's law. This result is well agreed with Reble et al.

References

[1] M. Jianhua, Z. Wei, and H. Zhiwei, Biomedical Optics Express 1, 1, 17 (2010).

[2] C. Reble, I. Gersonde, C. A. Lieber, and J. Helfmann, Biomedical Optics Express 2, 3, 520 (2011).

[3] Y. Hattori, Y. Komachi, T. Asakura, T. Shimosegawa, G. Kanai, H. Tashiro, and H. Sato, Applied Spectroscopy 61, 6, 579 (2007).

[4] E. B. Hanlon, R. Manoharan, T. W. Koo, K. E. Shafer, J. T. Motz, M. Fitzmaurice, J. R. Kramer, I. Itzkan, R. R. Dasari, and M. S. Feld, Physics in Medicine and Biology 45, 2, R1 (2000).

[5] Y. Komachi, T. Katagiri, H. Sato, and H. Tashiro, Applied Optics 48, 9, 1683 (2009).

[6] M. Shim, B. Wilson, E. Marple, and M. Wach, Applied Spectroscopy, 619 (1999).

[7] Y. Komachi, H. Sato, K. Aizawa, and H. Tashiro, Applied Optics 44, 22, 4722 (2005).

[8] Y. Komachi, H. Sato, Y. Matsuura, M. Miyagi, and H. Tashiro, Optics Letters 30, 21, 2942 (2005).

[9] Y. Komachi, H. Sato, and H. Tashiro, Applied Optics 45, 30, 7938 (2006).

[10] M. A. Short, S. Lam, A. McWilliams, J. H. Zhao, H. Lui, and H. S. Zeng, Optics Letters 33, 7, 711 (2008).

[11] T. Katagiri, Y. Yamamoto, Y. Ozaki, Y. Matsuura, and H. Sato, Applied Spectroscopy, 103 (2009).

[12] Z. Huang, S. Teh, W. Zhen, J. Mo, K. Lin, X. Shao, K. Ho, M. Teh, and K. Yeoh, Optics Letters, 758 (2009).

[13] N. D. Magee, J. S. Villaumie, E. T. Marple, M. Ennis, J. S. Elborn, and J. J. McGarvey, Journal of Physical Chemistry B 113, 23, 8137 (2009).

[14] J. Motz, M. Hunter, L. Galindo, J. Gardecki, J. Kramer, R. Dasari, and M. Feld, Applied Optics, 542 (2004).

[15] Y. Yamamoto, Y. Oshima, H. Shinzawa, T. Katagiri, Y. Matsuura, Y. Ozaki, and H. Sato, AnalyticaChimicaActa, 8 (2008).

[16] C. Reble, I. Gersonde, S. Andree, H. J. Eichler, and J. Helfmann, Journal of Biomedical Optics 15, 3 (2010).

[17] Y. S. Yamamoto, H. Sinzawa, Y. Matsuura, Y. Ozaki, and H. Sato, Applied Spectroscopy 65, 8, 34 (2011).

[18] H. J. Vanstaveren, C. J. M. Moes, J. Vanmarle, S. A. Prahl, and M. J. C. Vangemert, Applied Optics 30, 31, 4507 (1991).

[19] V. Tuchin, *Tissue Optics: Light Scattering Methods and instruments for Medical Diagnosis* (SPIE press, USA, 2007), 2nd ed.

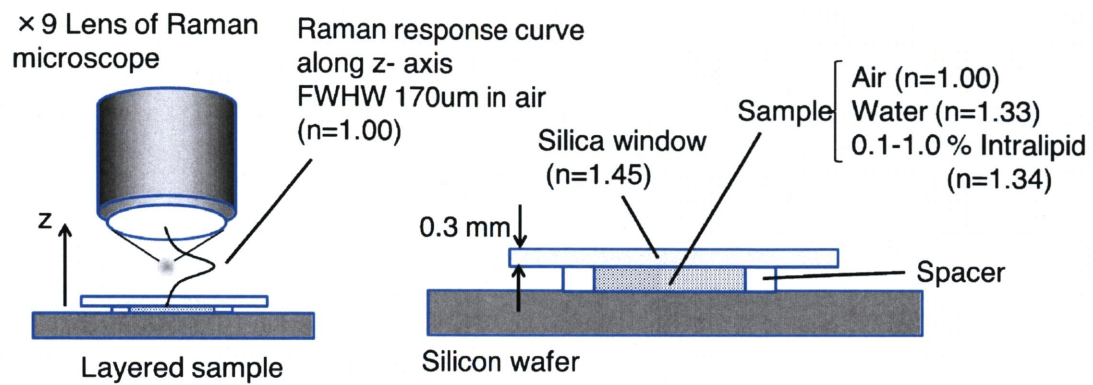[20] *Raman bunko-hou* (Raman spectroscopy) (GakkaiShuppan Center, Japan, 1988).

Figure. 1. Schematic representation of Raman measurements for layered scattering medium. 9× microscope objective lens was introduced with relatively larger confocal cross-slit to broaden a spatial resolution of the lens.
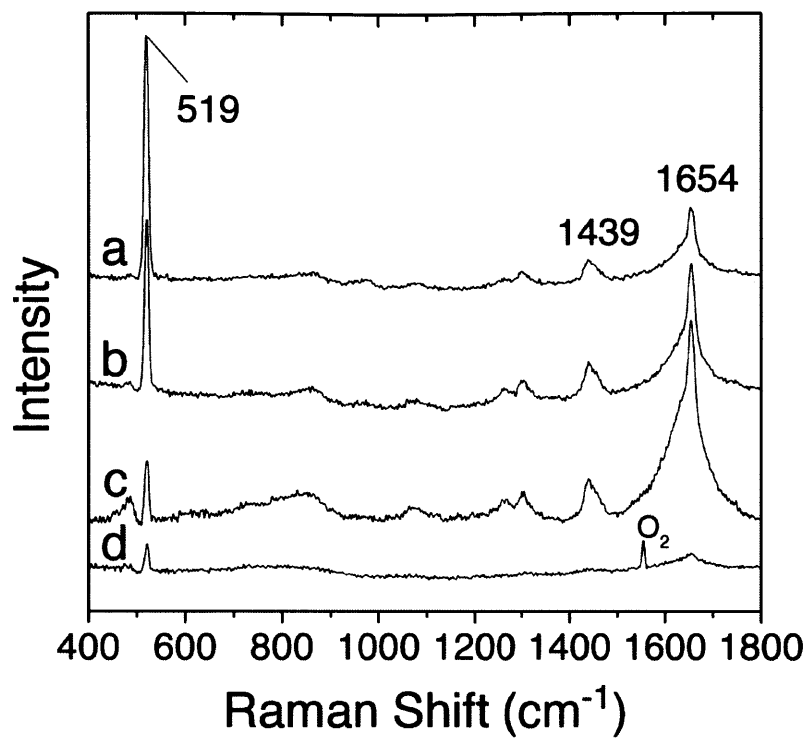
Figure 2. Raman spectra dataset acquired from layered scattering sample with changing the distance from sample's surface and lens. The concentration and the thickness of scattering media is 0.5 % and 800 um, respectively. The position of the objective lens are (a) 0.6mm, (b) 0.4mm, (c) 0.2mm, and (d) -0.9mm from the focal point, respectively.
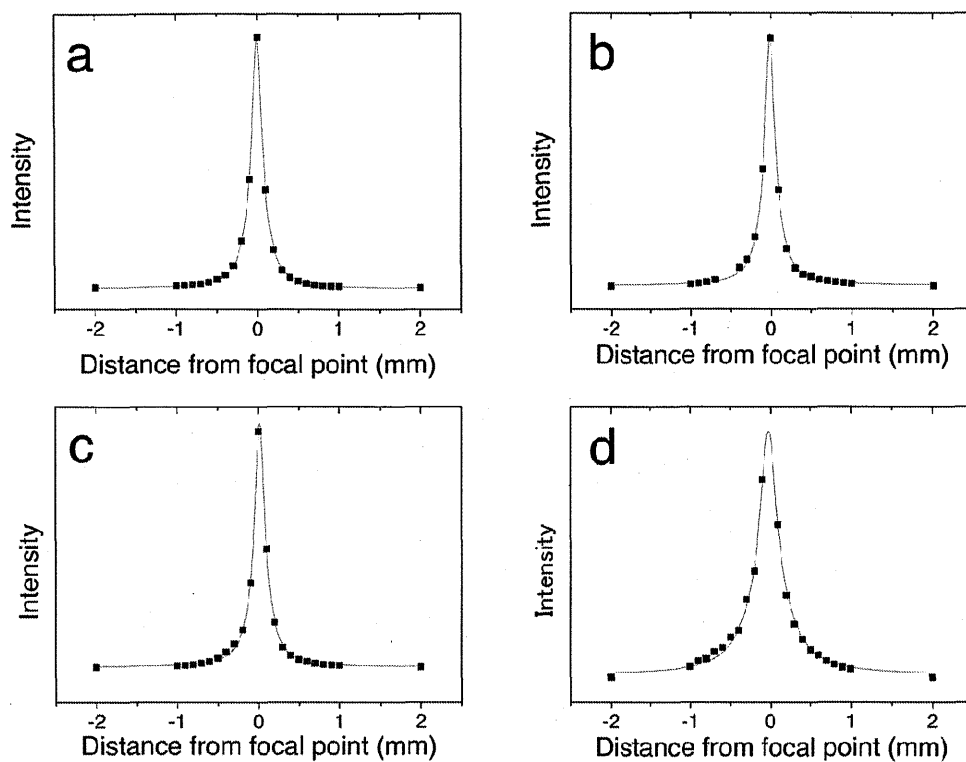
Figure 3. Raman response curves of spectral intensity at 519 cm^{-1} along z-axis which are measured with layered samples made of (a) Si-air, (b) Si-air-silica, (c) Si-water-silica and (d) Si-0.5 % Intralipid-silica as shown in Fig. 1. The z=0 was set at the maximum point of Raman signal. These curves were fitted by Voigt function (solid lines).
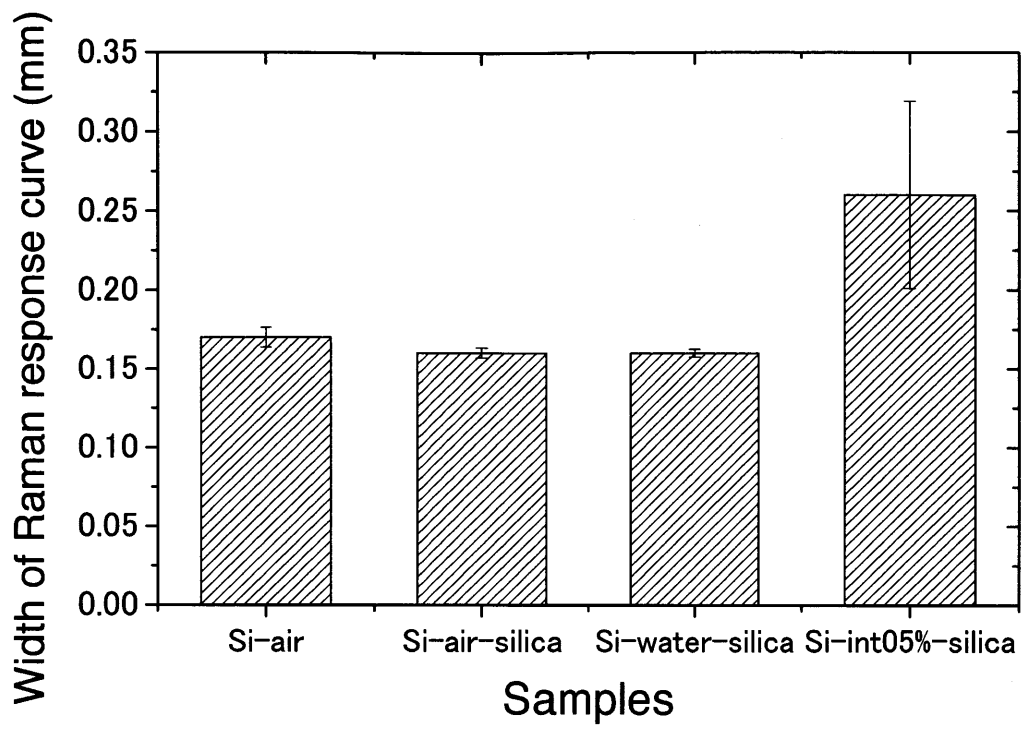
Figure 4. FWHMs of Raman response curves along z-axis which are shown in Fig. 3. The significant figure was two.
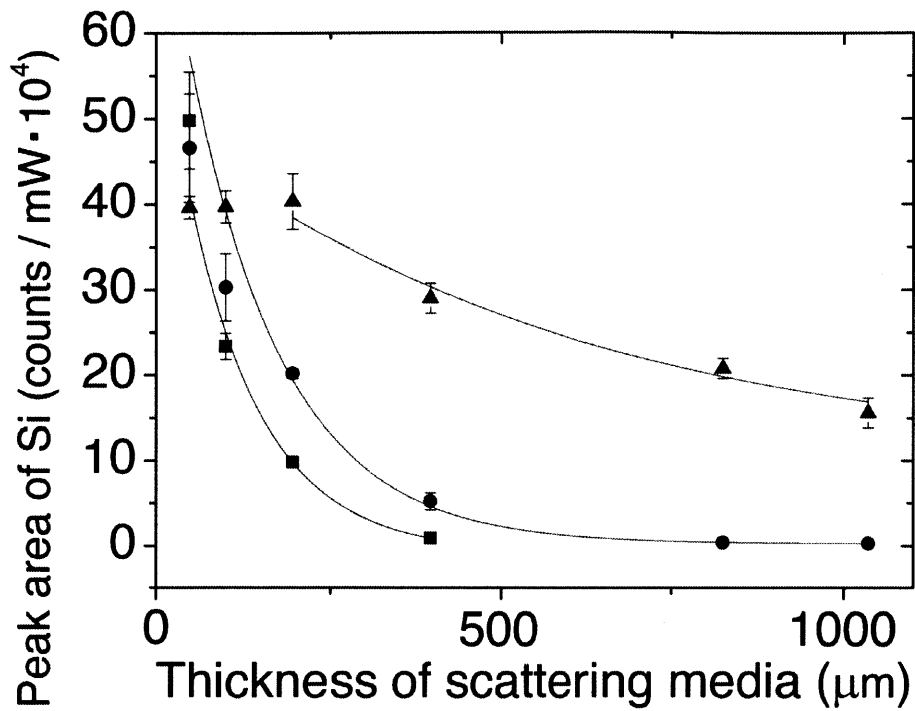
Figure 5. Response curve of the Si 519 cm-1 band obtained from a Si wafer beneath a scattering layer which is made of (▲) 0.1 % , (●) 0.5 % and (■) 1.0 % Intralipid suspension.The solid lines were fitted by $z = z0 + A \cdot U \cdot \exp(-2\mu_t z)$ referring from Eq. 6 and the fitted parameters are shown in Table 1. The measuring points were defined as the maximum point of Raman signal searched by changing the distance between the sample and the lens.

Table 1. Fitted parameters calculated in Fig. 5.

Intralipid™	z0	A	U	$\mu_t \doteq \mu_s$ (μm-1)	ρ (density of particle, rate)	σ (extinction cross section, rate)
0.1%	129253	428813	-0.00234	0.0012	1	120
0.5%	2066	608056	-0.00619	0.0031	5	62
1.0%	15958	929775	-0.01387	0.0069	10	69
10%(ref. 2)	-	-		0.077	100	77

Chapter 2

High Axial Resolution Raman Probe Made of Single Hollow Optical Fiber

Abstract

A ball lens mounted hollow optical fiber Raman probe (BHRP) consisting of a single hollow optical fiber (HOF) and a micro-ball lens was developed for performing a high-axial resolution and high-sensitivity remote Raman analysis of biomedical tissues. The totaldiameter of the probe head is 640 μm. The BHRP is useful in the measurement of thin-layered tissues that are in contact with the probe's surface because the probe has a limited depth-of-field optical property. An optical calculation studysuggested that it is possible to vary the probe's working distance by selecting different materials and diametersfor the ball lens. Empirical studies revealed that this probe has a higher axial resolution and a higher sensitivity than an HOF Raman probe without the ball lens. Thespectrum of a mouse stomach measured with the BHRPhad better quality and considerably lowernoisethan that measured with a conventional Raman microscope. These results strongly suggest that the BHRP can be used effectively in biomedical applications.

Introduction

A miniaturized Raman probe is an attractive tool for the *in vivo* measurement of living tissues. It can beused with an endoscope to directly observe diseased tissues in a noninvasive or a minimally invasive manner. These narrow fiber-optic probes have been developed by several groups and have been applied to the study of biological tissues. [1-3]A Raman probe with a diameter of 1.5 mm was developed by Shim *et al.* for performing *in vivo* medical Raman spectroscopy.[1]Motz*et al.* developed a Raman probe (diameter: 2 mm) equipped with filters and a ball lens following Shim *et al.*'s optical design strategy in order to optimize the collection efficiency and minimize the noise of the Raman probe.[2] The performance of Motz*et al.*'s probe was tested by conducting simulations and experiments using tissue models and several *in vitro* tissue types. Further,Komachi*et al.* developed a micro-Raman probe with a diameter of 0.6 mm for intravascular application. The abovementioned three miniaturized Raman probes are made of bundled optical fibers and equipped with an optical noise filtering system made of band-pass and long-pass filters for suppressing the fluorescent and Raman background noisedue to the core materialof the optical fibers.[3]The technological hurdle of constructing a narrow fiber-optic Raman probe can be eliminated by using the high-wavenumber region (2000–4000cm^{-1}) of a Raman spectrum. Because no Raman signal is generated in the fiber itself in this spectral region, a single optical fiber can be used for guiding the laser light to the tissue and collectingthe scattered light.[4-6]Kolhenović et al. used the single fiber-optic Raman probe for examining a sliced porcine brain and succeeded in distinguishing between adjacent brain structures on the basis of their biochemical composition.[5]Nijssen et al. used the single fiber-optic probe for obtaining high-wavenumber (2800 to 3125 cm^{-1}) Raman spectra of basal cell carcinoma

and perilesional biopsy specimens.[6]In contrast, Komachi*et al.* developed a different type of

miniaturized Raman probeby using a hollow optical fiber (HOF).[7] This HOF consists of thin

glass capillary tubing with a smooth silver film coating its inner surface, giving it unique

characteristics.[8,9] It generates no Raman scattering or fluorescence noise during the laser

transmission. This property brings two major advantages to the Raman probe made by using

an HOF. One is that the complex filter system at the distal end of the probe is unnecessary,

and the other is that the single HOF can be used bidirectionally, i.e., for sending the

excitation light and for collecting the Raman scattered light.

We developed a miniaturized endoscope system for diagnosing diseases of the

esophagus, stomach, colon, and rectum in order to continuously study the physiological

changes in small living experimental animals.[10] The endoscope has a small channel

(diameter: 800 μm)that guides the miniaturized Raman probes to the measuring point. In our

recent experiments, it was found that the Raman probe should be used in contact with the

sample surface for the best measurement because the tissues in a living body beat

continuously because of blood pulsation and breathing. It is difficult to hold the focus on the

beating tissue surface. It is also preferable for the probe to have a limited depth-of-field

optical property for the analysis of the layered structure of many tissues such as the stomach

wall and skin. Boere*et al.* adjusted the focal length of a Raman probe by placing a quartz or

CaF_2 window at the end of the probe tip in order to limit the actual measurement volume

near the surface in the measurement of Barrett's epithelium.[11]

We have reported a brief summary of a miniaturized Raman probe made of a single

HOF with a ball lens in the previous work.[12] In the present paper, the detailed optical

properties of the probe are described along with a method to control the probe's working

distance and weak point. The HOF has a considerably smaller numerical aperture (NA) than conventional glass fibers.[7] A small NA is generally considered to be a disadvantage in optical devices; however, in the case of the BHRP, this property plays a key role in realizinga high axial resolution.

Experimental

a. Fabrication of BHRP

Figure 1 presentsthe structure and a photograph of the head of the BHRP. The probe is made of a single HOFthattransmits both excitation and collected light. The HOF (core diameter: 320 μm, outer diameter: 435 μm, and length: 1.5 m) was fabricated by coating a thin silver film on the inner surface of a flexible glass capillary tube.[8,9]A ball lens was mounted on an Al sheath and sealed with an epoxy resin in order to prevent water leakage. Then, the sheath was glued to the distal end of the HOF. A fiber chuckwas attached to the other end of the HOFto attach to the fiber coupling stage.The mounting position of the ball lens was modified in order to improve the efficiency of the contact of the top of the ball lens to the sample as compared to the BHRP reported previously.[12] In the present study, two kinds of ball lenses were utilized:a ball lens (diameter: 400 μm) made of sapphire glass and purchased from Edmund Optics (USA) and a ball lens (diameter: 500 μm) made of fused silica from Swiss Jewel Co. (USA). The total diameter of the probe head was 640 μm.

b. Raman system setup

Figure 2 represents an optical setup of a coupling stage for the BHRP. The 785-nm excitation light from a background-free electronically tuned Ti:sapphire laser[13,14] (BF-ETL,

homemade, pulse repetition rate: 1.8 kHz) is reflected by a long-pass filter (LF, cut-off at 795.2 nm), and then focused into the HOF-Raman probe via a lens (L_a, focal length: 150 mm). The returned light, which includes Raman scattered light,is then collimated by lens L_a. This light passes through the long-pass filter LF and the 785-nm notch filter (NF, Kaiser Optical Systems Inc., USA) and is focused by lens L_b (focal length:80 mm) onto slit S (width:100μm). The Raman spectra were recorded with a single polychromatic Raman spectrometer (F/4.9,focal length: 320 mm, grating: 600 gr/mm, blaze: 750 nm, Photon Design Co. Ltd., Japan) and a CCD detector (DU420-OE, Andor Technology Co. Ltd., Northern Ireland). For making the Raman microscope measurements, a conventional microscope head with an objective lens (0.4 NA, M Plan NIR 20×, Mitutoyo Co. Ltd., Japan) was attached to the Raman spectrometer.

Results and Discussion

a. Optical properties of the BHRP

A silicon wafer sample with a smooth surface was measured with three types of Raman probes in order to evaluate theoptical properties of these probes in the depth direction, such as the axial resolution and the location of the focal point. A comparison was then made among the three probes that utilized the same HOF. Probe A had a sapphire ball lens (diameter: 400 μm) having a refractive index of 1.76. Probe B had a fused silica ball lens (diameter: 500 μm)having a refractive index of 1.45. Probe C did not have a ball lens. The curves in Fig. 3 represent the intensities of a strong silicon Raman band at 519 cm^{-1}plotted as a function of the sample probe distance measured with the probes. The response curve of probeC was almost flat in the measurement range because of the small

NA of the HOF, as reported by Komachi*et al.*[7] In contrast, the response curvesofprobes A

andB had maximums at 28 and 220 μm for the sample-probe distances, suggesting that the

BHRP has a limited depth-of-field optical property. In the following discussion, the distance

from the topsurface of the ball lens to the sample point at the maximum intensity is referred

to as the working distance (WD) of the BHRP. The maximum signal intensities of probes A

and B were, respectively, approximately twelveand three times larger than the intensity of

probeC, i.e., the probe without the ball lens.These results indicate that the sensitivity of a

Raman probe made of HOF is dramatically improved by attaching a ball lens at the probe

head. The small NA of HOF is considered to play the role of a modal filter, which passes

only well-collimated light to the HOF. The hollow fiber very preferentially transports light

that has a minimum interaction with the hollow fiber walls. The light entering the hollow

fiber at considerably large incident angles (light path A in Fig. 1) has many relatively

high-loss reflections against the hollow fiber wall and is hence lost. The light that reached

the ball lens at the end of the hollow fiber is almost collimated and can therefore be focused.

For the same reason, light scattered from the laser focus and collected by the ball lens is

recollimated when it travels through the hollow fiber (light path B in Fig. 1). Light scattered

from other locations does not enter the hollow fiber in a collimated beam and will therefore

experience more interactions with the hollow fiber wall and be lost.As a result, the

well-known weak point of the HOF,which transports only collimated light or light having as

little interaction with the hollow fiber wall as possible very well, is turned into an advantage

by placing the ball lens at the tip of the fiber.This results in the limited depth-of-field optical

property of the probe. The response curves suggest that the shorter the probe focal length,

the higher is the probe sensitivity.The depth resolutions, which are defined by the FWHMs

of the response curves in Fig. 3, are estimated to be 23 μm for probe A and 110μm for probe

B. A conventional miniaturized fiber-optic Raman probe consisting of multiple glass fibers

is supposed to have a focal depthof more than several hundred micrometers. It is suggested

that the BHRP has an advantage in subsurface Raman measurementsbecause of its high

axial resolution, as compared toa miniaturized fiber-optic Raman probe.[1-3]

Figure 4 depicts the Raman spectra of a two-layer model sample, consisting of a

100-μm-thick polyethylene (PE) layer and a poly(methylmethacrylate) (PMMA) substrate,

measured with probesA and B. The measurementswere carried out with the probes held

perpendicular to the substrate, in contact with the surface of the PE layer (as shown in Fig.

1). The Raman bands at 1118, 1289, and 1434 cm^{-1} observed in spectrum (a), measured

with probe A, were assigned to the C-C stretching mode, CH_2 twisting mode, and CH_2

bending mode of the PE, respectively. Those at 799, 976, 1448, and 1731 cm^{-1} observed in

spectrum (b), measured with probe B, were assigned to the CH_3 rocking mode, C-O

stretching mode, CH_2 bending mode, and C=O stretching mode of the PMMA, respectively.

Spectra (a) and (b) resemble those of pure PE and PMMA very well, although trace bands

due to the PE were observed in spectrum (b). According to their WDs, the focal points of

probeA and probeB were in the PE and PMMA layers, respectively, suggesting that isolated

information at the focal pointswas obtained by using the BHRP. The resultssuccessfully

demonstrated that the BHRP has a limited depth-of-field optical property and that its WD

can be varied by selecting different focal lengths for the ball lenses.

The BHRP will be used in a miniaturized endoscope system reported in ref. 10. The

probe will be used under a bending condition as shown in Fig. 2. The head of the endoscope

has an angle section with a curvature radius of approximately 10 mm. Consequently, the

performance of the bent BHRP is examined when the probe is used in the endoscope. The curves in Fig. 5 show the attenuation of the excitation energy and Raman signals when the BHRP is curved. The probe is bent at an angle of θ_1 near the coupling stage, with a curvature radius of 200 mm. When θ_1 reaches 180°, the probe is bent at an angle of θ_2 near the distal end, with a curvature radius of 10 mm. The HOF has high flexibility, but its transmission efficiency decreases when it is bent. Curve (a) depicts the attenuation of the excitation power. It shows that the excitation power was reduced almost proportionallyto the total bent angle, but was independentof the curvature radius. In contrast, it seems that curve (b), showing the Raman intensity, has a sharp reduction when the probe is bent with a small curvature radius, showing a strong dependency on the curvature radius. This fact suggests that the optical pathways for the excitation light and the collected light are different, even in the single HOF in the BHRP. This result suggests that the BHRP is suitable for use without strong bending.

b. Theoretical study of the working distance and depth resolution forthe BHRP

The theoretical working distance(WD_t) for the ball lens to the collimated paraxial incident light is estimated by using the following equation:

$$WD_t = \frac{Dn_{med}(n_{ball} - 2)}{2(2n_{med} - n_{ball} - n_{ball}n_{med})} \qquad (1)$$

where D is the diameter of the ball lens and n_{med} and n_{ball} are the refractive indexes of the surrounding medium andball lens.In the present BHRPs, the surrounding mediumwas air, where$n_{med} = 1$ and the calculated WD_t values were 32 μm for probe A and 153 μm for probe B. The given function suggests that it is possible to control the working distance by

50

selecting materials with differentrefractive indices and/or varying the diameter of the ball

lens. The theoretically calculated WDs of the BHRP with various lenses are presented in

Table 1. The measured WD agrees well with the theoretical value, but these values are not

identical.The optical property of the HOF is considerably different from that of the

conventional glass optical fiber. In principle, a transmission mode thathas the highest

transmitting efficiency has a Gaussian-like distribution in the HOF cross section when the

fiber is held linearly. However, in the empirical study, the unavoidable slight bent of the

HOF and/or subtle deviation of the incident angle might result in a mode transition from the

Gaussian-like mode to another mode such as a ring shape mode. The ring shape mode

consists of a ray having a large spread angle that elongates the effective focal length. In

contrast, the spherical aberration of a ball lens might shorten the effective focal length. The

difference between the measured and theoretical WDs seems to be attributed to the

abovementioned phenomena.

An attempt was made to use ball lenses made of other glass materials, as well as

gradient-index (GRIN) lenses instead of the ball lens, but it turned out that the strong

fluorescent and/or Raman emission from the lens material often caused interference,

resulting in weak Raman signals for the biological tissues. Accordingly, out of the lenses

investigated, only ball lenses made of sapphire glass and quartz were found to be adequate

for the entire range (0–4000 cm^{-1}) of Raman measurementsin the case of the tissue samples.

c. Measurements for biological tissues

Figure 6 shows the Raman spectra of the resected stomach of a rat measured

withprobe A and with a conventional Raman microscope. Both spectra were measured

under the same excitation power, exposure time, slit width, and Raman system, with the only difference being the objective heads of the BHRP and the microscope. The laser power was 29 mW at the sample and the exposure time, 60 s. The spectra shown in the figure are raw and are not treated for baseline correction. Bands marked * appearing below 600 cm^{-1} are due to the interference from the LP and notch filters. A sharp band at 1560 cm^{-1} observed only in spectrum (b) was assigned to the oxygen in the air contained in the HOF of the BHRP. The Raman bands at 367, 407, 630, and 738 cm^{-1} observed in spectrum (b) were assigned to the vibration modes of sapphire, the material of the ball lens. It should be noted that the intensities of these unnecessary bands generated by the BHRP itself are considerably low,and are comparable to the weak Raman bands of the biological tissue. Therefore, it is possible to remove them by the usual subtraction with a background spectrum. The spectrum below 300 cm^{-1} is cut off by the edge of the LP filter in order to remove the Rayleigh line. It is suggested that the Raman bands can be observed with a high signal-to-noise ratio even in the low-frequency region by using the BHRP. It is generally difficult to measure the low-frequency spectrum with a miniaturized Raman probe made of glass optical fibers. In a glass-fiber Raman probe, the interference filters, such as the BP and LP filters, are attached to the distal end of the optical fibers in order to cut off light with unnecessary frequencies. Althoughthe optical fiber has a rather large NA, the angular acceptance of the interference filter is very small. Consequently, it is impossible to remove a part of the unnecessary light, and the broad Raman bands due to the glass core appear in the low-frequency region. The Raman bands at 1257, 1439, and 1654 cm^{-1} are assigned to the amide III mode, CH_2 bending mode, and amide I mode of the protein, respectively. The signal-to-noise ratio of the spectrum measured by the BHRP is similar to that measured by

the conventional Raman microscope, although the spectral intensity of the former is approximately one-half of the latter.

Conclusion

The high performance of the BHRP was successfully demonstrated in the present study. It suggested that the axial resolution and sensitivity were dramatically improved by attaching a ball lens to a single HOF Raman probe.The maximum diameter of the probe is only 640 μm, which is as narrow as the micro-Raman probe developed by Komach*et al.*, which, as far as we know, is the narrowest Raman probe for measuring the fingerprint region.[4]The measured WD and axial resolution in airof the BHRP with a sapphire ball lens (diameter: 400μm) were 28 and 23 μm, and those of the BHRP with a quartz ball lens (diameter: 500 μm) were220 and 110 μm. The measurement of a layered model sample demonstrated that the BHRP has a limited depth-of-field optical property and is suitable for depth-resolved Raman measurement.The calculation study showed that it is possible to control the WD of the probe by selecting different materials and diametersfor the ball lens. The Raman spectrum of a rat stomach tissue was successfully measured with the BHRP. The obtained spectra had high quality,as compared to that measured with a conventional Raman microscope, strongly suggesting that the BHRP emits considerably little background noise. We also discovered a drawback of the BHRP. The collection efficiency of the Raman scattered light was reduced when the BHRP was used with a small curvature radius. This suggests that the BHRP is only suitable for use without strong bending. For example, it is useful for the measurement of surface tissues such as the walls of the digestive organs and skin, and/or the measurement of inner tissues by inserting it into the tissues. However, when it is necessary to pass a probe through a winding pathway such as a blood vessel, it is better to use a micro-Raman probe made with glass fibers.

References

[1] M. G. Shim, B. C. Wilson, E. Marple and M. Wach, *Appl. Spectrosc.* **53**, 619 (1999).

[2] J. T. Motz, M. Hunter, L. H. Galindo, J. A. Gardecki, J. R. Kramer, R. R. Dasari and M. S. Feld, *Appl. Opt.* **43**, 542 (2004).

[3] Y. Komachi, H.Sato, K.Aizawa,H.Tashiro, *Appl. Opt.*, **44**, 4722 (2005).

[4] L. F. Santos, R.Wolthuis, S. Koljenovic´, R. M. Almeida and G. J. Puppels, *Anal. Chem.***77**, 6747 (2005).

[5] S. Koljenovic´, T. C. Bakker Schut, R. Wolthuis,A. J. P. E. Vincent, G. Hendriks-Hagevi,L. Santos, J. M. Kros, and G. J. Puppels,*Anal. Chem.* **79**, 557 (2007).

[6] A. Nijssen, K. Maquelin, L. F. Santos, P. J. Caspers, T. C. Bakker Schut, J. C. den Hollander, M. H. A. Neumann, and G. J. Puppels,*J. Biomedical Opt.***12**, 034004 (2007).

[7] Y. Komachi, H. Sato, Y. Matsuura, M. Miyagi, and H. Tashiro, *Opt. Lett.*, **30**, 2942 (2005).

[8] Y. Matsuura, G. Takada, T. Yamamoto, Y. Shi, and M. Miyagi, *Appl. Opt.* **41**, 442 (2002).

[9] M. Mohebbi, R. Fedosejevs, V. Gopal, and J. A. Harrington, *Appl. Opt.* **41**, 7031 (2002).

[10] Y. Hattori, Y. Komachi, T. Asakura, T. Shimosegawa, G. Kanai, H. Tashiro, H. Sato, *Appl. Spectrosc.*, **61**,579 (2007).

[11] I. A. Boere, T. C. Bakker Schut, J. van den Boogert, R. W. F. de Bruin andG. J. Puppels,*Vibrational Spectrosc.*, **32**, 47 (2003).

[12] Y. Matsuura, S. Kino, E. Yokoyama, T. Katagiri, H. Sato, and H. Tashiro, *IEEE J. Selected Topics in Quantum Electronics*, **13**, 1704 (2007).

[13] H. Sato, S. Wada, M. Ling and H. Tashiro, *Appl. Spectrosc.* **54**, 1163 (2000).

[14] H. Sato, S. Wada and H. Tashiro, *Appl. Spectrosc.* **56**, 1303 (2002).

Table 1. Calculated working distances of the BHRPs made with different types of ball

lenses.

Table 2

Lens Material	Sapphire				Quartz			
Lens Diameter (mm)	0.4	0.5	0.6	0.7	0.4	0.5	0.6	0.7
Working Distance (μm)	32	39	47	55	122	153	183	214
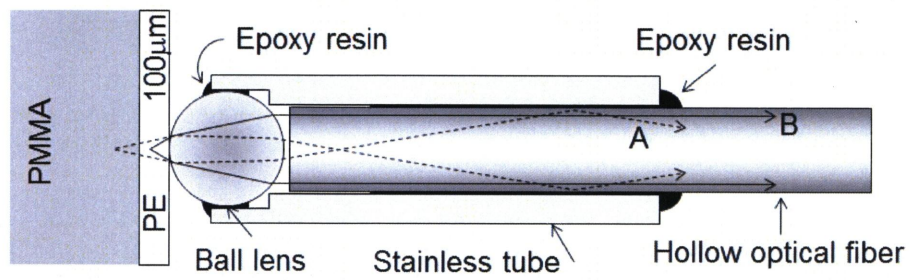
Figure 1.   Structure of the BHRP head and its photograph.
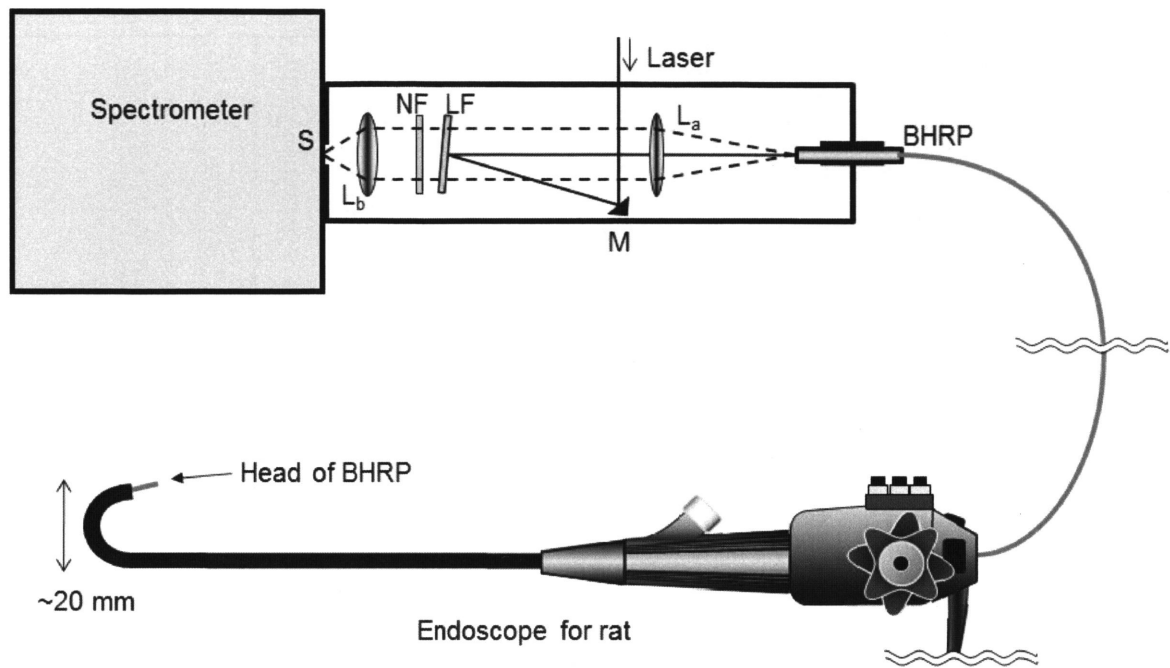
Figure 2. Schematic representation of the system setup for Raman measurement using the BHRP.
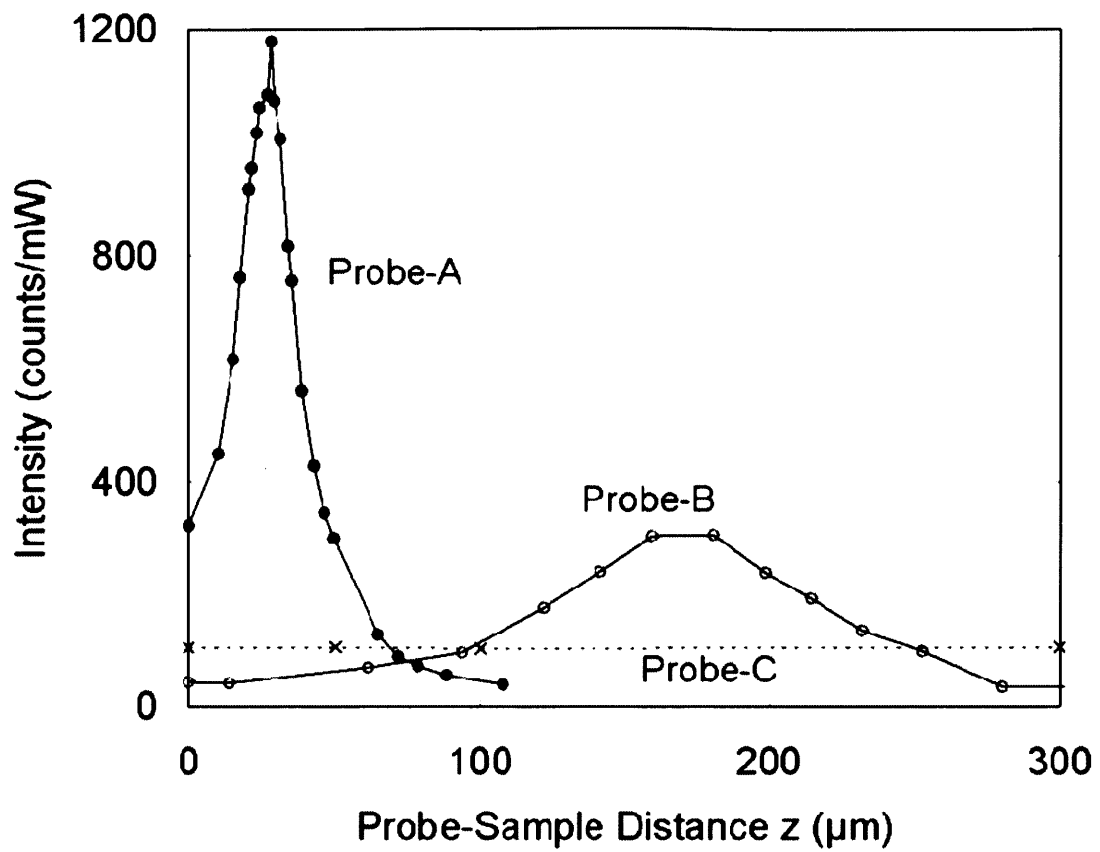
Figure 3. Response curves of Raman spectral intensity to probe-sample distances for three

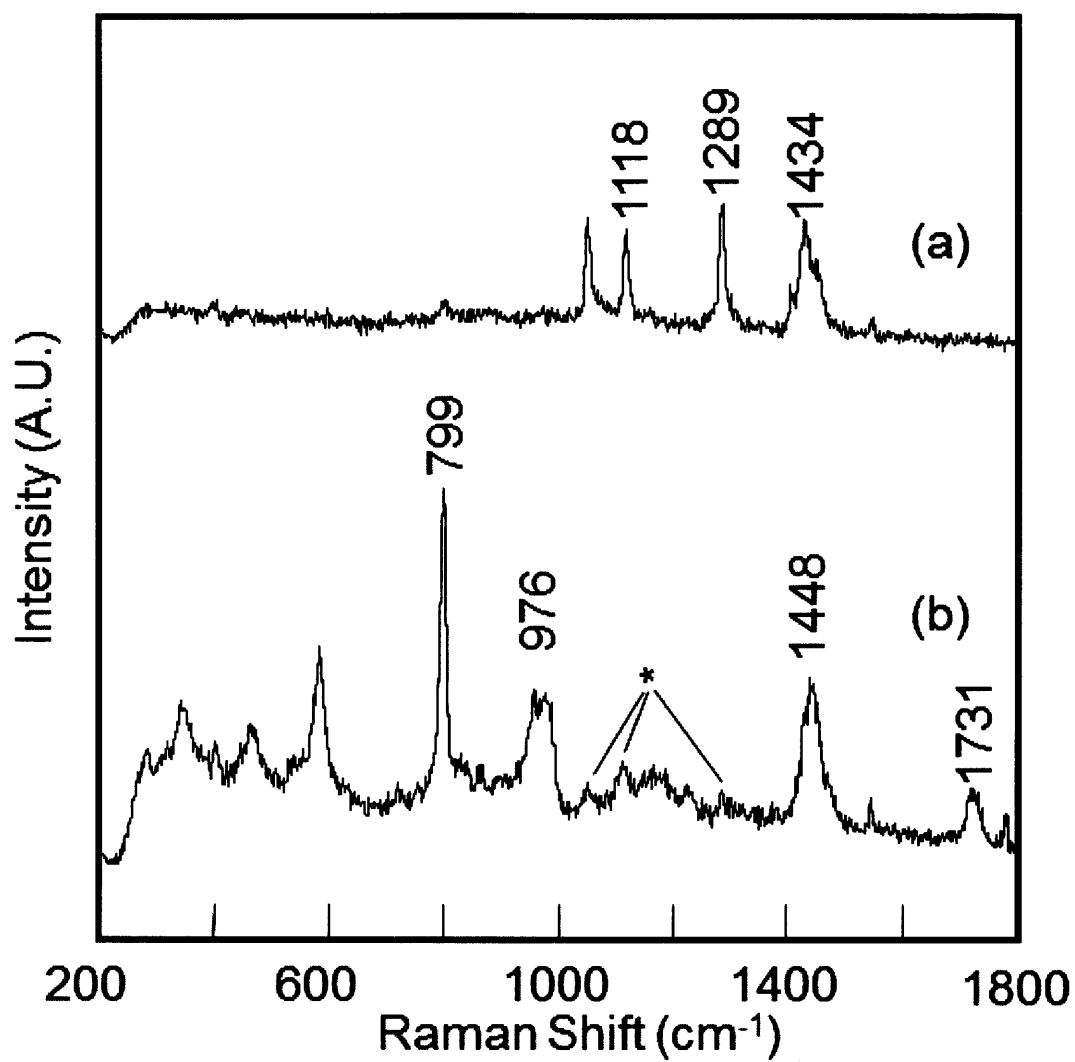probes A(sapphire, 400 μm), B(quartz, 500 μm), and C(no lens).

Figure 4. Raman spectra of a two-layer model sample in which a 100-μm-thick PE film covers a flat PMMA substrate, measured with probeA (a) and probeB (b).
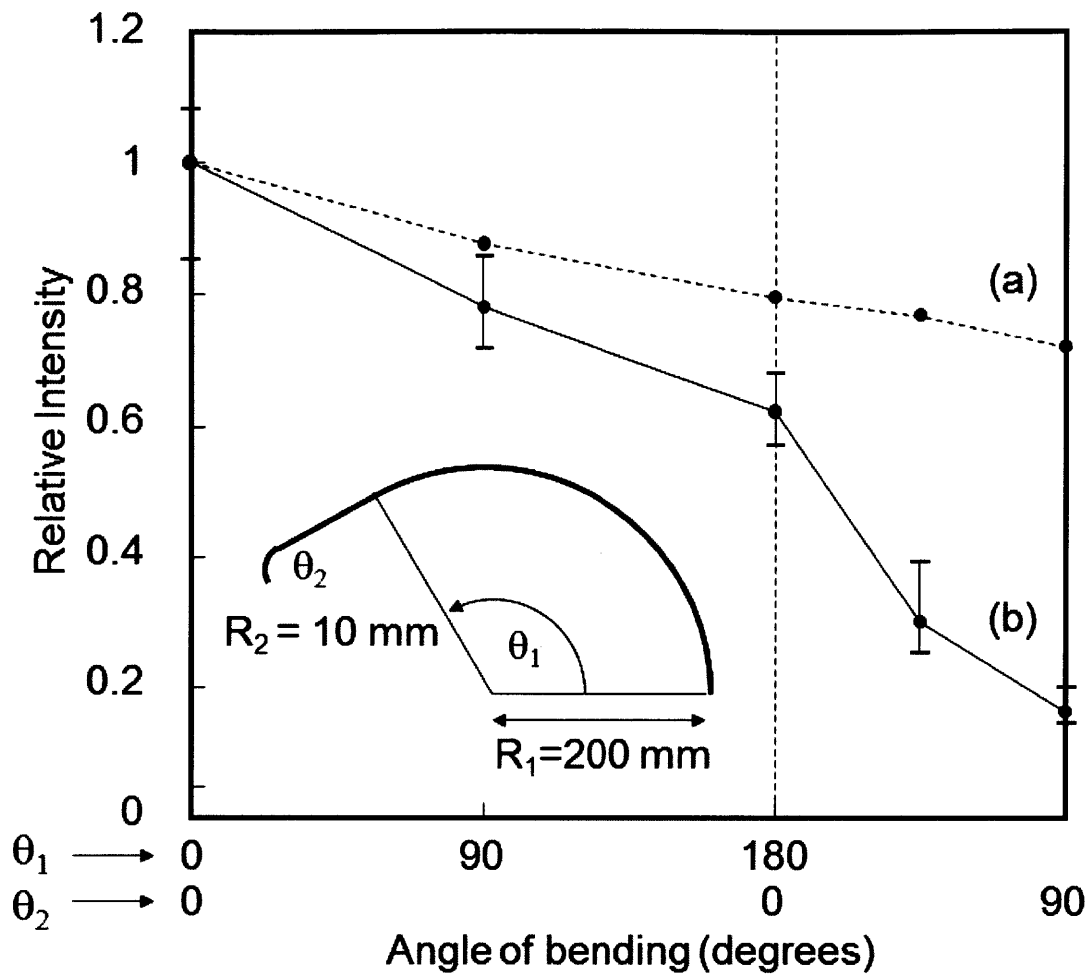
Figure 5. Response curves of intensities of transmitted excitation light (a) and collected Raman scattered light (b) to changes in the curvature and curvature radius. The BHRP is bent up to 180° at acurvature radius of 200 mm; then, the distal end of the probe is bent at a curvature radius of 10 mm.
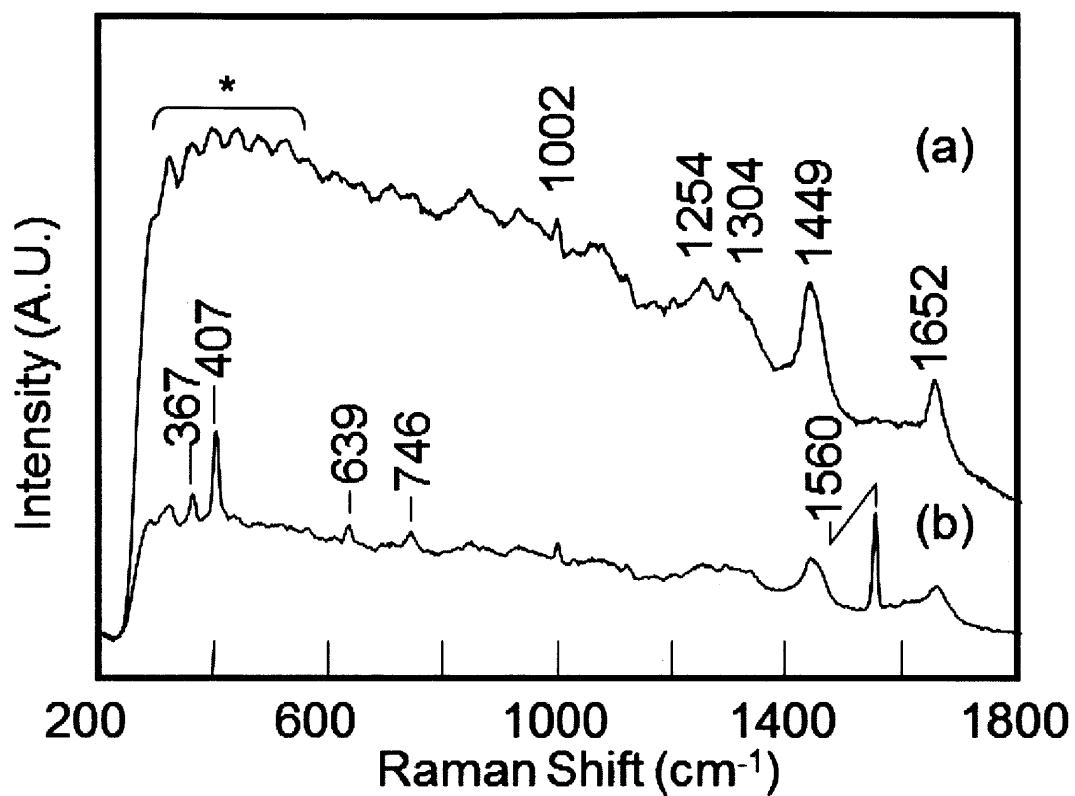
Figure 6.   Raman spectra of a resected rat stomach measured with a conventional Raman microscope (a) and BHRP (b). Bands marked with "*" are generated by filters.

Chapter 3

Subsurface Sensing of Biomedical Tissues Using a Miniaturized Raman Probe: Study of Thin-layered Model Samples

Abstract

A ball lens hollow-fiber Raman probe (BHRP) is a powerful tool for *in vivo* nondestructive subsurface analysis of biomedical tissues in a living body. It has confocal-like optical properties, but its collection volume is rather large in comparison with that of a conventional confocal Raman system. Therefore, the obtained Raman spectra have contributions from the upper and lower layers at different rates dependingon the thickness of the upper layer when the measurement point is close to the boundary surface of the two layers. In the present study, we describe a methodology to extract quantitative information about the thickness of the subsurface layer structure by using a BHRP combined with the partial least-square regression (PLSR) analysis. The simulation study indicates that distribution of the collection efficiency in the collection volume of the BHRP is similar to a Gaussian distribution. The empirical study suggests that the PLSR model built with only a principal component (PC) 1 based on the linearized depth data gives good prediction.

Introduction

Raman spectroscopy finds applications in various fields, particularlyin biomedical fields[1-3]. It has recently been identifiedas a potential alternative diagnostic method for variousforms of cancer. One of the major objectivesof biomedical Raman spectroscopy is to provide a method forthe simultaneous determinationof the location and chemical composition of subsurface tissues in a less-invasive or non-invasive manner. The required depth resolution is varied depending on the size of the tissue under study. Komachi*et al.* developed a micro-Raman probe comprising optical fibers;the probe, which is 600 μm in total diameter, is as narrow as an intravascular endoscope and can be inserted into arteries[4]. Hattori *et al.* succeeded in obtaining the Raman spectra of the esophagus and stomach walls of live rats by using a miniaturized endoscope with a diameter of 2.5 mm equipped with the micro-Raman probe[5]. The use of the miniaturized Raman probe under endoscopic guidance enables us to obtain the Raman spectrum of tissues that are present deep in the entire body. The depth resolution is assumed to be a few millimeters, depending on the resolution of the endoscopic image and the skill of the manipulator. The accessible region will extend to most of the digestive organs and other organs through which thick arteries pass. Matousek*et al.* described several methodologies for the effective retrieval of the Raman spectra of the subsurface layers in diffusely scattering media[6,7]. Ultrafast temporal gating and spatially offset technologies are extremely beneficialfor obtaining information regarding subsurface biological tissues. In the former technique, the detection of the subsurface Raman signals was optimized by varying the time delay using a Kerr gate[6]. In the latter technique, the Raman spectrum was collected from the regions spatially offset from the point of incidence of the probe laser beam on the surface of a diffusely scattering sample[7]. In such a small

region, the location accuracy would be defined by the depth and lateral resolutions. According to these papers, it is estimated that the depth resolution and detectable depth are a few hundred micrometers and several millimeters, respectively. The lateral resolution of the spatially offset method depends on the offset distance, and that of the ultrafast temporal gating method would depend on the optical setup used in the measurement. On the other hand, a conventional confocal Raman microscope has very high spatial resolution. Froud investigated the use of a confocal Raman microscope with immersion lenses in Raman depth profiling, and eleven layers of polymer laminate over a depth of 100μm were successfully resolved[8]. According to their results, it is estimated that the depth resolution is less than 1 μm.

In situ biomedical applications often require that the following two conditionsbe satisfied simultaneously: remote sampling and depth resolved measurement. The miniaturized fiber Raman probe is suitable for the remote sampling[4,5,9–13]. Since the anatomic considerations strictly limit the size of the probes, the use of the conventional confocal microscope and spatial offset method is not suitable for the purpose. Bakker Schut*et al.* employed a miniaturized optical-fiber Raman probe to study a dysplastic tissue in the epithelium of the palate of a rat model[9]. Their probe efficiently recorded a Raman signal at a distance of 100–600μm from the probe tip end. To achieve the maximum signal collection efficiency at the palatal tissue surface, which was in contact with the probe tip during the measurement, a 200-μm thick CaF_2 window was used as a spacer between the probe tip and the tissue.

We have developed miniaturized Raman probes based on hollow optical fibers $(HOFs)$[10,11]. The ball lens hollow-fiber Raman probe (BHRP) is well-suitedfor investigating

67

layered biomedical samples. It comprisesa single HOF and a ball lens at the distal end. Since the HOF has a very low numerical aperture that plays the role of a mode filter, the BHRP shows a confocal-like performance. The working distance can be controlled by selecting a suitable ball lens. The depth resolution of the BHRP is several tens to one hundred micrometers, depending on its working distance. Motz*et al.* developed a Raman probe made of bundled conventional glass fibers and a ball lens[12]. They implemented an optical design calculation to optimize the collection efficiency of the Raman scattering. The spatial resolution of their Raman probe is not high because of the use of glass fibers with a large numerical aperture (NA).

Here, we examine an approach for improvingthe depth profiling performance of the BHRP based on the multivariate analysis. Since the spatial resolution of the BHRP is limited by the aberration of the ball lens and NA of the HOF, as described in Fig. 1, it cannot be improved by modifying the optical configuration. We attempt to employ a PLSR analysis, which is one of the most prevailing multivariate analysis techniques, to ascertain the thickness of the embedded tissue layer[1,13]. The tissues chosen for our study are obtained from very early esophageal and stomach cancer specimens and skin samples, suggesting that the desirable desirable depth resolution is approximately 10μm. Oshima*et al.* demonstrated that the PLSR analysis is useful for extracting quantitative information from Raman spectra,particularlythoserecordedby the miniaturized Raman probe[14]. Everall suggested that the most effective and reliable general method for obtaining the pure spectra of embedded layers is to mechanically section the sample[15]. However, recent progresses in multivariate analysis, such as PLSR and self-modeling curve resolution (SMCR) methods, will be usefulin resolvingthe spectra of embedded layers and ascertaining their thicknesses[16]. These

methods generally construct models on the basis of the combination of linear functions. If the real phenomenon cannot be explained by the combination of the linear functions, as in the case described in the present study, it is necessary to transform the inherently nonlinear response to fit the linear functions, and then, the prediction model is calculated based on the transformed data. The principle of this proposed technique is demonstrated by a simulation study and an empirical study by measuring a two-layered sample using the BHRP. This is a preliminary study,wherein transparent samples are used instead of diffusely scattering samples. This technique must be extended to light-scattering samples with more layers in future in order to apply itto practical biomedical samples.

Experimental

1. Raman system

A schematic diagram of the experimental setup for the Raman measurements is shown in Fig. 2. A 785-nm line of a diode laser (XTRA, Toptica, Germany) was employed as an excitation light source. The BHRP is fabricated with a hollow optical fiber (homemade) and a sapphire ball lens (diameter: 0.5 mm, Edmund Optics Inc., USA). The total diameter of the probe head is 640μm. The Raman spectra measurements are carried out with a single polychromatic Raman spectrometer (grating: 600 lines/mm; blazed wavelength: 800 nm; f/4.9, focal length: 320 mm, Photon Design Co. Ltd., Japan). The BHRP is connected to the spectrometer via a coupling stage that equips a notch filter (785nm, Kaiser optical Systems Inc., MI) and a long-pass (LP) filter (785nm, Semrock Inc., USA). The excitation light is reflected by the LP filter and focused into the BHRP by a lens. The excitation light and Raman scattered light are transmitted with the same HOF. The

Raman scattered light is collimated with the lens, filtered with two filters to cut-off the Rayleigh scattering light, and focused into the slit of the spectrometer whose width is 120μm, which corresponds to 10 cm^{-1} in the spectral resolution. The Raman signals are integrated on a Peltier-cooled CCD detector (DU420-OE, Andor Technology Co. Ltd., Northern Ireland) operated at 188 K. The power of the excitation light is approximately 10 mW at the sampling point. The exposure time is typically 20 s.

The model sample comprises polyethylene (PE) films and a polymethyl methacrylate (PMMA) substrate. The PE films are transparent and approximately 10 μm thick;they are attached to the flat PMMA substrate one by one in order to vary the thickness of the PE layer, as shown in Fig. 2. After the measurements, the model sample is cut vertically with a sharp cutter, and the thickness of the PE layer is measured with a digital microscope (Keyence, Japan).

2. Data processing and simulation study

The obtained raw spectra were converted into evenly spaced data by using GRAMS/AI version 7 software (Thermo Electron Corporation, Waltham, MA). To eliminate the optical noises generated by the lenses and filters, the spectrum without any sample, which does not emit Raman signals, was recorded and subtracted from the sample spectra. Since the transmission efficiency of the HOF changes with the manner in which it is bent, the laser power was monitored after every measurement, and the intensities of the spectra were calibrated. The Unscrambler software package (ver. 7.8, CAMO Software Inc., US) was employed for the PLSR analyses of the empirical and simulation spectra. The PLSR analyses were carried out for the spectral region ranging from 400 to 1868 cm^{-1} for

the dependent variables. The PLSR models were validated with the leave-one-out cross-validation method.

Results and discussion

1. Simulation study

The proposed technique that appliesthe PLSR analysis to the data set measured with the BHRP, which has a nonlinear response to the sample depth, involves the following three steps.

1. A feature of the correction volume of the BHRP in the sample is considered and then, a function that describes the collection coefficient along the z-axis, which is in the depth direction, is estimated. At this point, it is not necessary to select a linear function.

2. The measured data set,which should have a response following the estimated function, is linearized.

3. The PLSR analysis is applied to the transformed data set to construct a prediction model. It should be noted that the transformed value does not denote the real thickness of the sample. If necessary, the predicted values must be re-transformed into the true values.

In this simulation study, let us analyze what type of data set is obtained when the Raman spectra of the model samples comprising two transparent materials, (A) and (B), are measured by the BHRP, as shown in Fig. 1, and verify the proposed technique using the simulated data set. Eleven imagined samples,where the material (A) is attached onto the substrate (B), are demonstrated; the thickness of (A) varies with the z-value, as shown in Table 1.It is estimated that the dispersion of the Raman collection efficiency along the z-axis in the depth direction is capableofapproximatingthe Gaussian distribution. It is easily

71

assumed that the measured spectra are linear combinations of the pure spectra of (A) and (B). Their mixing ratios follow the integrated values of the left and right sides of the Gaussian curve split by the boundary at z between (A) and (B), as schematically presented in Fig. 1. The integrated values (in percentage) for the various z values are shown in the second and third columns of Table 1. The integrated values also represent a cross-sectional volume in the collection volume appropriated by each sample. The basic model spectra representing samples (A) and (B) are presented as follows.

$$y_A = f_1(x) + f_3(x) + f_5(x) + f_7(x)$$
$$y_B = f_2(x) + f_4(x) + f_6(x) + f_8(x)$$

$$f_i(x) = a_i \exp\left(-\frac{(x - \mu_i)^2}{2\sigma^2}\right)$$

Here, σ is a constant, 4000, and the values of a_i and μ_i are depicted in Table 2. Each spectrum exhibits four bands of different frequencies, intensities, and bandwidths. Fig. 3 exhibits the model spectra $g_j(x)$ fabricatedfrom these two basic model spectra,y_A and y_B, mixed in the ratio shown in Table 1.

$$g_j(x) = t_1 y_A + t_2 y_B$$

Here, t_1 and t_2 are the ratios of areas A and B in percentage. Now, the z value is transformed into the linearized data set, t_1 and t_2; therefore,g_j are expressed by their linear functions. The first and second steps of the proposed technique are completed at this point.

The PLSR analysis is applied to the transformed data set in the third stepsince it is a powerful tool for the quantitative analyses of Raman spectra. Initially, for the comparison, the raw z-values are used as explanatory variables, and the PLSR model is constructed. All the data in Fig. 3 are used for this calculation, and no test data is isolatedto investigate the

robustness of the model. The calibration curve of the PLSR model (-O-) built with only the

principal component (PC) 1 is depicted in Fig. 4. The PC1 explains 90.2% of the data. The

residual value drops to the minimum at the PC1, and almost no improvement is observed

when other components are added to the PC1. This fact indicates that the PLSR analysis

cannot extract further information from the spectra; in other words, the Gaussian curve can

not be resolved into a combination of the linear functions. The result reveals that it is not

possible to evaluate the thickness of the sample from the raw data set by the PLSR analysis.

The calibration curve calculated using the spectra as dependent variablesand the converted

z-value in the second column of Table 1 (-▲-) is presented in Fig. 4. The correlation

coefficient of the calibration curve is apparently 1.0, and 100% of the information is

effectively extracted with only the PC1. This result indicates that the PLSR technique is

applicable to ascertain the sample thickness if to the correct method of linearizing the

z-value is known.

2. Empirical study

Figure 5 exhibits the Raman spectra of pure PMMA, pure PE, and four model

samples selected from the series of eleven spectra. The model samples are made of PE films

attached on the PMMA substrate, as represented in Fig. 2. The bands at 596, 813, and 1453

cm^{-1} are assigned to the C–C stretching, CH_3 rocking, and CH_3 bending modes of PMMA,

respectively[17]. The bands at 1062, 1131, 1299, and 1443 cm^{-1} are assigned to the CH_2

rocking, C–C stretching, CH_2 twisting, and CH_2 bending modes of PE, respectively[18]. The

spectral intensities of PMMA and PE are comparable. The measured thicknesses of the PE

layer are 0.0, 11.9, 21.7, 29.5, 46.7, 51.2, 61.0, 72.1, 83.5, 93.4,and 101.2 mm, respectively,

for the 11 model samples. For comparison, the PLSR prediction model is calculated for all the spectra and the measured thickness of PE. The calibration curve (-○-) built with only the PC1 is represented in Fig. 6. The feature of the calibration curve is analogous to a sigmoid, and resembles that of the simulation result shown in Fig. 4. The PC1 explains 94.4% of the data. The residual value drops to a minimum at the PC1 and is not improved by adding other components to it. The empirical result shows atendency similar to that of the simulation result. These facts strongly suggest that the actual distribution of the Raman collection efficiency along the z-axis resembles a Gaussian distribution, as we had previously assumed in the simulation study. According to the procedure of the proposed technique, the raw z-values are linearized by transformation following the integrated Gaussian curve. The problem in this case is that we do not yet know the central value and range of the Gaussian curve forachieving the best fit to the shape of the collection volume of the real BHRP. Here, the best-fit Gaussian curve is randomly searched. A matching degree is judged by the correlation coefficient of each cross-validated prediction model constructed with only the PC1. We started with theoretically obtained working distance, 63μm, and the value of full width at half maxima (FWHM), 46 μm;these are shifted by 1-μm intervals until the best correlation coefficient is obtained[11]. Consequently, the best result is obtained for the working distance of 58μm and FWHM of 46μm. The PLSR prediction curve calculated with only the PC1 (-▲-) is depicted in Fig. 6. Its correlation coefficient is 0.995. The PC1 explains 99.2% of the information and contributions from the subsequent components are remarkably small. These facts suggest that the present method has highlyviablefor analyzingthe thickness of the layered structure by using the BHRP. All the data are used for this calculation, and no test data areseparated to investigate the robustness of the model

because the purpose of this process is to determine the parameters of the Gaussian curve that gives the best prediction result.

The result shows a silhouette of the shape of the focal volume of the BHRP. Figure 7 depicts the Gaussian curve plotted for z-value and thicknesses of the real samples indicated by dotted lines. It should be noted that the actual distribution of the Raman collection efficiency is never identical to the Gaussian function. For example, there is no PE sample or Raman signal at the point of $z = 0$ in the empirical study;however, in the simulation study, the Gaussian curve always has a finite value. In the Raman spectrum, at $z = 11.9\mu m$ (Fig. 5(b)), bands of PE appear much smaller than that expected, according to the Gaussian curve shown in Fig. 7. On the other hand, the Raman spectrum (d; $z = 114.7\mu m$; not shown) shows a larger contribution of the Raman signal of PMMA than expected. These results suggest that the real collection volume assumesa smaller value in the area adjacent to the lens surface and a larger value in the area beyond 100 μm.

Conclusion

The present study has demonstrated that the BHRP has high viability in subsurface analyses,particularlyinthe estimationof the thickness of thin-layered samples. The comparison between the simulation and empirical studies has suggested that the collection volume of the probe has a Gaussian-distribution-like shape. The working distance, z, and FWHM are 58 μm and 46 μm, respectively, in the transparent PE sample. According to the result, the spatial resolution appears to be approximately10 μm. The PLSR prediction model built only with the PC1 based on the measured spectra and linearized z-values gives the best prediction, and its correlation coefficient is 0.995. The present preliminary study has successfully demonstrated that the PLSR analysis can be a powerful tool to ascertain the thickness of the sample when the data is processed following the proposed technique. In our future work, we will modify the present technique to make it applicable to light-scattering samples such as biomedical tissues.

References

[1] C.A. Owen, I.Notingher, R. Hill, M. Stevens, L.L. Hench, *J. Mater. Sci: Mater. Med.*,**17**,1019 (2006).

[2] P.J. Caspers, G.W. Lucassen, G.J. Puppels, *Biophysical J.*,**85**, 572 (2003).

[3] M.V.P. Chowdary, K.K. Kumer, J. Kurien, S. Mathew, C.M. Krishna, *Biopolymers,***83**,556 (2006).

[4] Y. Komachi, H.Sato, K.Aizawa,H.Tashiro, *Appl. Opt.*, **44**, 4722 (2005).

[5] Y. Hattori, Y. Komachi, T. Asakura, T. Shimosegawa, G. Kanai, H. Tashiro, H. Sato, *Appl. Spectrosc.*,**61**,579 (2007).

[6] P. Matousek, N. Everall, M. Towrie and A.W. Parker, *Appl. Spectrosc.*,**59**, 200 (2005).

[7] P. Matousek, L.P. Clark, E.R.C. Draper, M.D. Morris, A.E. Goodship, N. Everall, M. Towrie, M. Towrie, A.W. Parker, *Appl. Spectrosc.* **59**, 393 (2005).

[8] C.A.Froud, I.P. Hayward and J. Laven, *Appl. Spectrosc.*,**57**, 1468 (2003).

[9] T.C. Bakker Schut, M.J.H. Witjes, H.J.C.M. Sterenborg, O.C. Speelman, J.L.N. Roodenburg, E.T. Marple, H.A.Bruining, G.J. Puppels, *Anal. Chem.*,**72**, 6010 (2000).

[10] Y.Komachi, H. Sato, Y. Matsuura, M. Miyagi, H.Tashiro,*Opt. Lett.*,**30**,2942 (2005).

[11] T. Katagiri, Y. Komachi, Y. Hattori, Y. Matsuura, M. Miyagi, H. Tashiro, H. Sato, *SPIE*,**6083**,60830E-1(2006).

[12] J. T. Motz, M. Hunter, L.H. Galindo, J.A. Gardecki, J.R. Kramer, R.R. Dasari, M.S. Feld, *Appl. Opt.*,**43**, 542 (2004).

[13] F. Estienne, D.L. Massart, *Anal. Chim. Acta*, **450**,123 (2001).

[14] Y. Oshima, Y. Komachi, C. Furihata, H. Tashiro, H. Sato, *Appl. Spectrosc.*,**60**,964 (2006).

[15]N. J. Everall, *Appl. Spectrosc.*,**54**, 1515 (2000).

[16]H. Shinzawa, J. Jiang, M. Iwahashi, I. Noda, Y. Ozaki, *Anal. Chim. Acta*, **595**,275(2007).

[17]J. Dybal, S. Krimm, *Macromolecules*, **23**, 1301 (1990).

[18]K. Sano, M. Shimoyama, M. Ohgane, H. Higashiyama, M. Watari, M. Tomo, T. Ninomiya, Y. Ozaki, *Appl. Spectrosc.*,**53**,551 (1999).

Table 1. Thickness,z, of the layer A and the integrated areas beneath the Gaussian curve overlapped with layer A (area A) and layer B (area B) in the simulation study.

z	area A (%)	area B (%)
0.0	0.13	99.87
16.7	2.28	97.72
25.0	6.03	93.97
33.3	15.87	84.13
41.7	31.30	68.70
50.0	50.00	50.00
58.3	68.70	31.30
66.7	84.13	15.87
75.0	93.97	6.03
83.3	97.72	2.28
100.0	99.87	0.13

Table 2. Parameters of bands in the simulation spectra (Fig. 3).

	a_i	μ_i
A	0.15	700
B	0.60	700
C	1.00	800
D	1.00	900
E	1.20	1100
F	0.15	1200
G	0.70	1300
H	0.80	1400
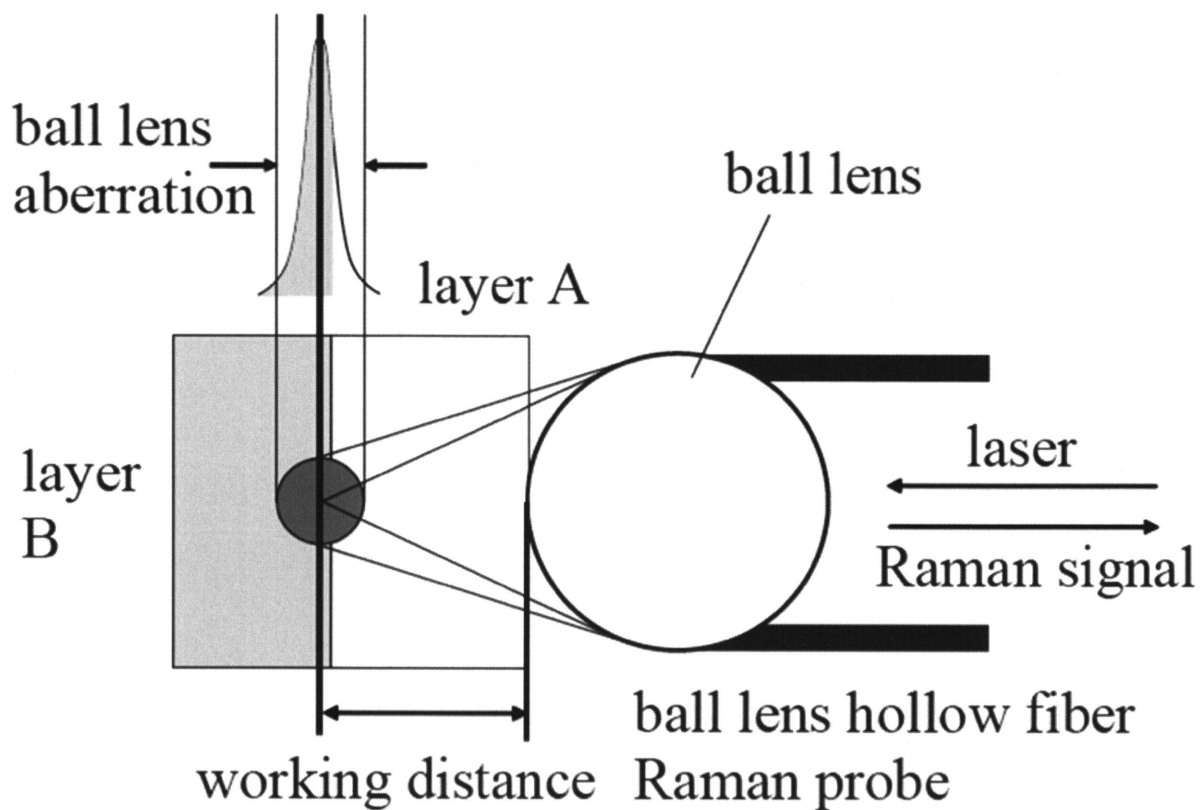
Figure 1. Schematic representation of the excitation volume of the BHRP placed near the boundary of two-layered sample.
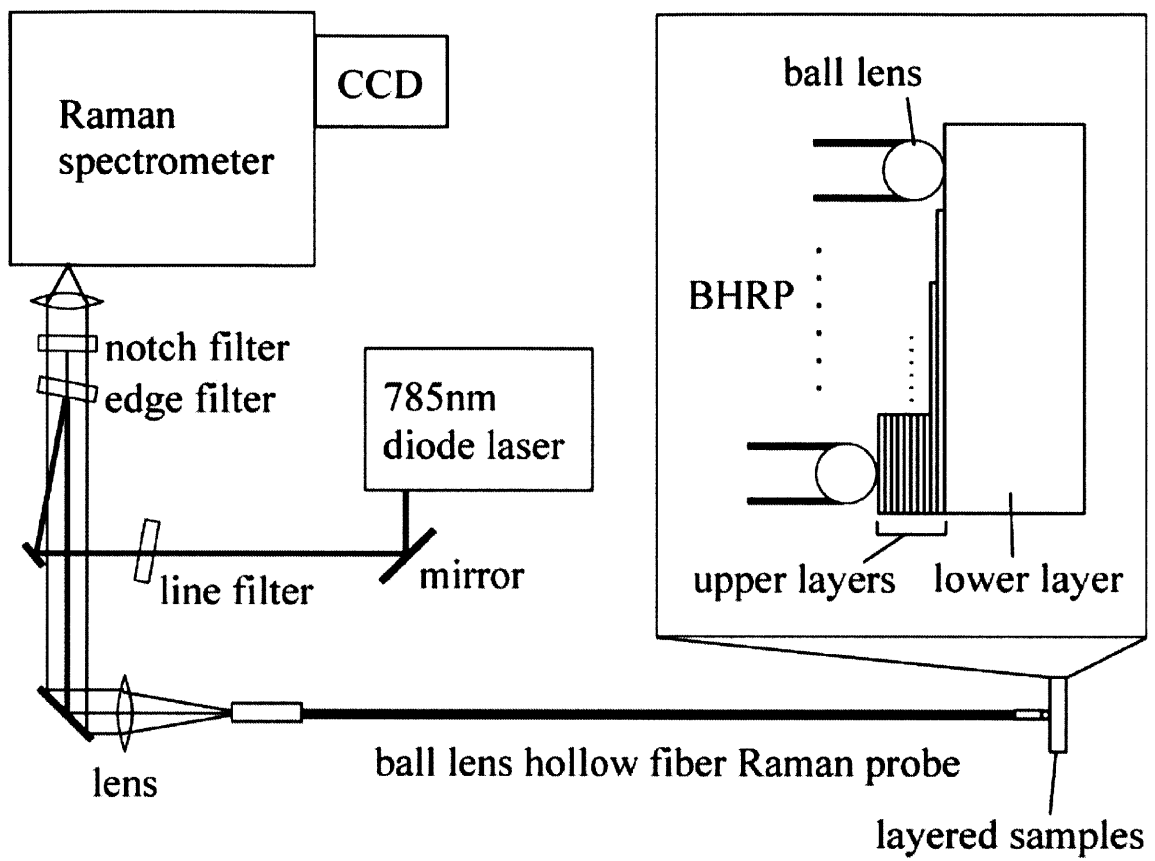
Figure 2.   Experimental setup of the BHRP Raman system and the model samples.
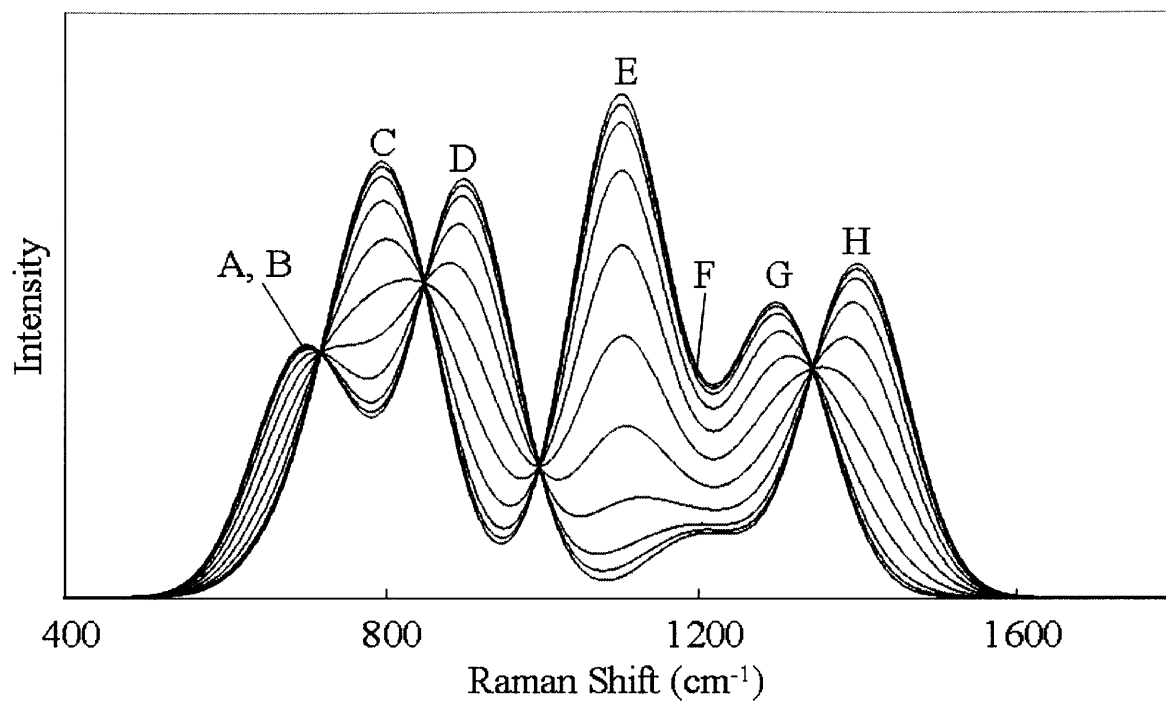
Figure 3.   Simulation spectra. Two different spectra are combined at different ratios. Bands A, C, E, and G belong to the first spectrum; bands B, D, F, and H belong to the second spectrum.
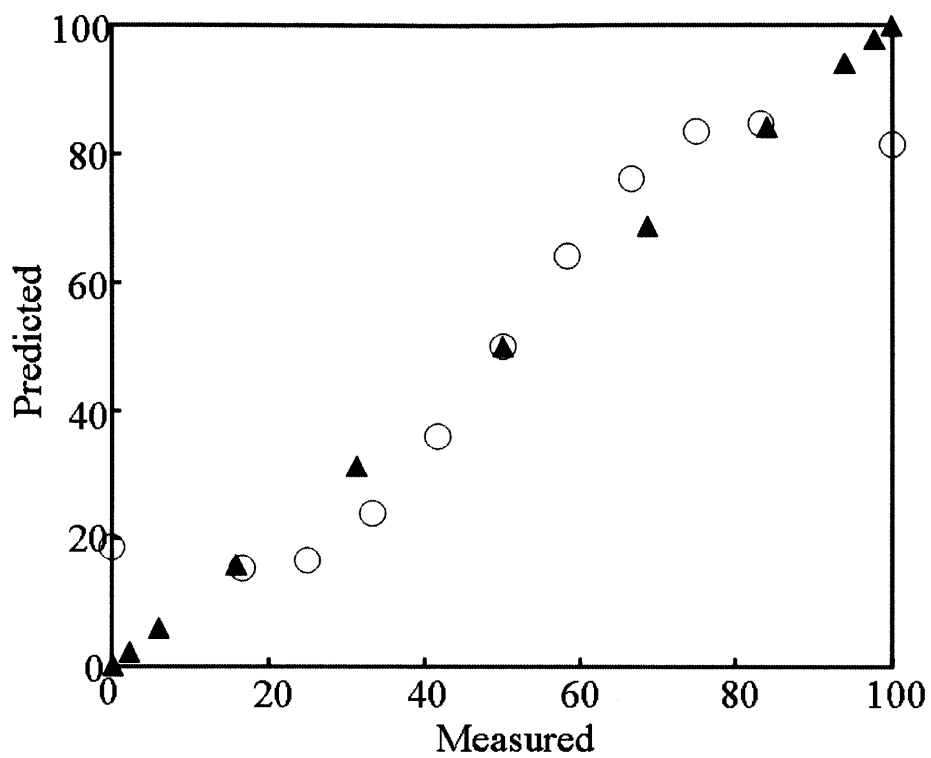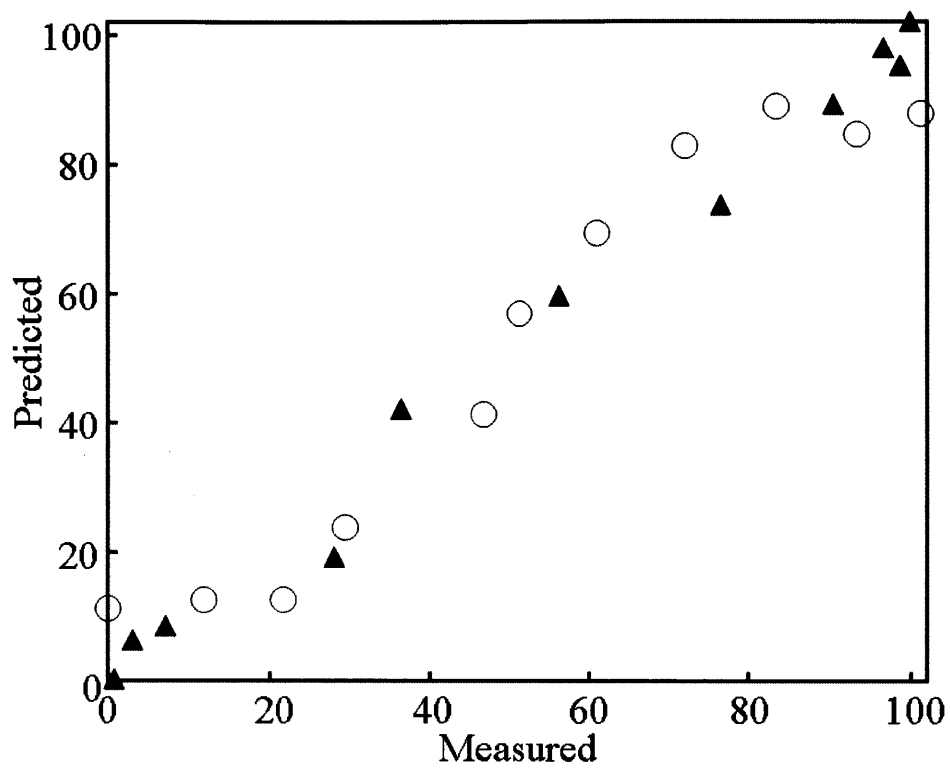
Figure 4. The PLSR prediction curves calculated (i) based on the simulation spectra and raw z-value (-○-) and (ii) based on the spectra and the linearized z (-▲-) with the integrated Gaussian curve.
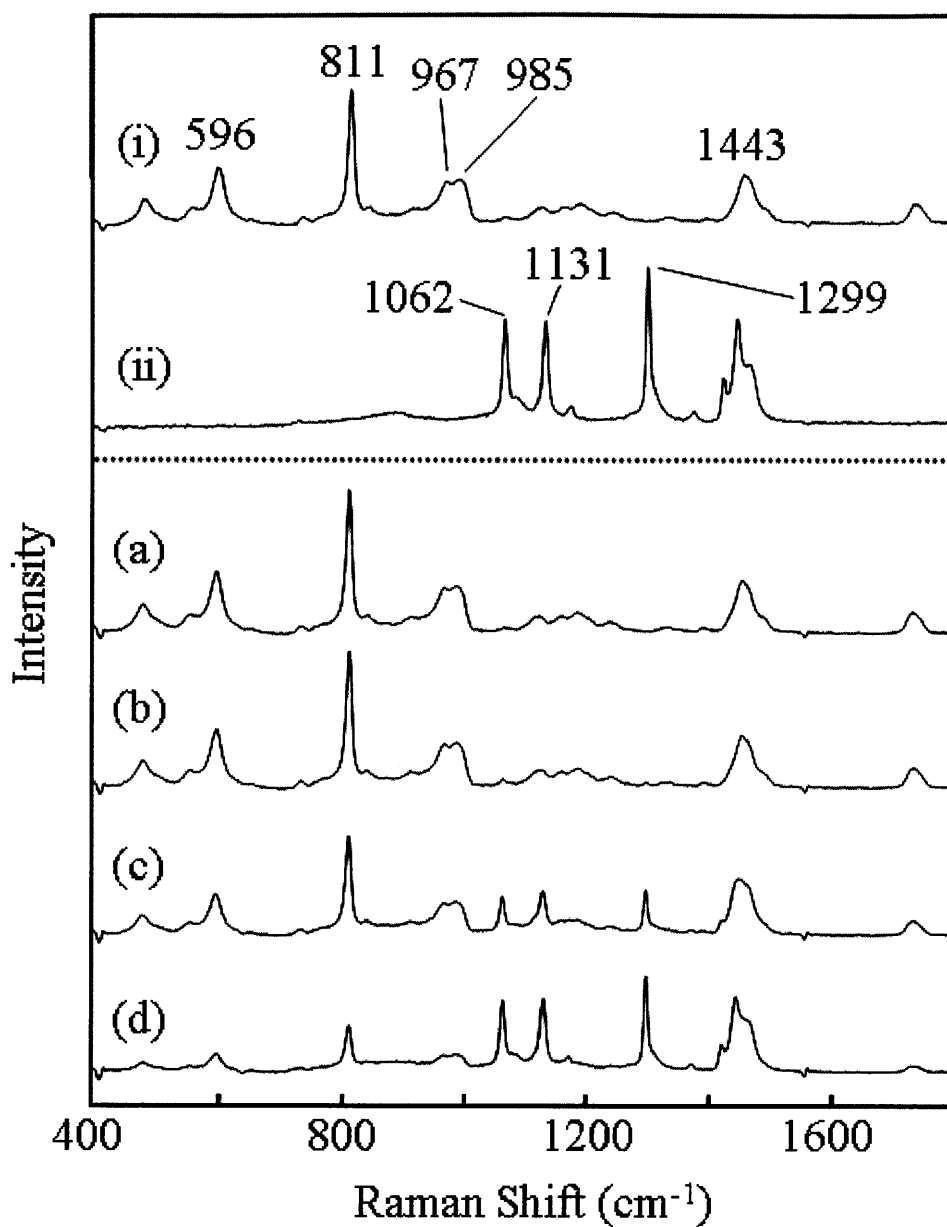
Figure 5. Raman spectra of (i) pure PMMA and(ii) pure PE, and their layered model samples. Thicknesses of PE are (a) 0.0μm, (b)11.9μm, (c) 46.7μm, and (d) 72.1μm.

Figure 6. The PLSR prediction curves calculated (i) based on the measured spectra and raw z-value (-○-) and (ii) based on the spectra and linearized z (-▲-) with the integrated Gaussian curve.
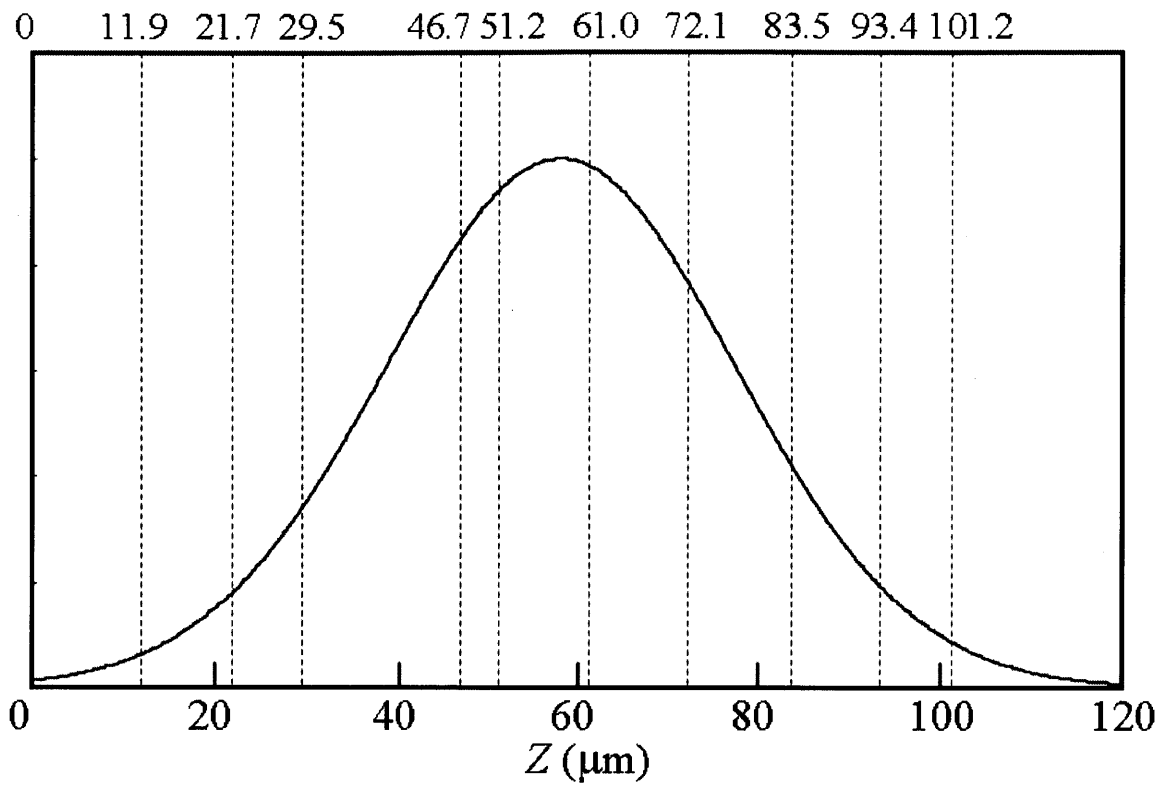
Figure 7. The Gaussian curve with the center, 58μm, and FWHM, 46μm, plotted for the z-values and thicknesses of the real samples indicated by dotted lines.

Chapter 4

Noninvasive Subsurface Analysis Using Multiple Miniaturized Raman Probes: Basic Study of Thin-Layered Transparent Models of Biomedical Tissues

Abstract

This study describes a basic theory for reconstructing pure Raman signalsof materials composing a multilayer sample from Raman spectra obtainedusing two types of miniaturized Raman probes. An illustrative example isdemonstrated using a multilayer system of samples composed of thetransparent plastics polymethylmethacrylate (PMMA) and polyethylene(PE) as a model of thin-layered biomedical tissues. When the same regionof an object is measured using Raman probes with different focalproperties, the Raman spectra provide different depth profile informationdepending on the level of light penetration. Thus, a detailed comparison ofthe spectra can provide an interesting opportunity to probe the differencesbetween the layers. A simple analytic form is presented for reconstructingthe pure Raman spectra of the embedded layer. The method applies anunderstanding of the Raman sampling volume in layered transparentmaterials to the interpretation of Raman spectra experimentallymeasured by multiple probes. The basic theory described here isnecessary for the expansion of the technique to turbid media, such asbiological samples, where light-scattering effects must be considered. Thepotential applications of the proposed method include material andcatalyst subsurface probing through different embedded materials, suchas assessment of silicon wafers, effective noninvasive screening for catalystsynthesis, and biomedical tissue research.

Introduction

Recent rapid progress in Raman spectroscopy has enabled the measurementof Raman spectra of biological materials under physiological conditions.[1-7]By using fiber-optic Raman probes together with an endoscope, we can directly observe diseased tissues inside bodies in a noninvasive or minimally invasive manner.[4-7] One of the major goals of diagnosis using Raman probes is to develop a noninvasive method ofdetermining the chemical composition of subsurface tissues. To detect embedded dysplasia, e.g., early gastric cancer and precancer in a submucosal layer,[8] by using Raman probes, it is critical to develop a methodology for obtaining a pure Raman spectrum of the embedded layer. Matousek and co-workers have succeeded in detecting depth-resolved Raman signals from a human bone *in vivo* with fiber optics by spatially offset Raman spectroscopy (SORS).[9] In combination with multivariate data analysis, the technique can extract almost pure Raman spectra of the underlying layers. Shim et al.[10] demonstrated depth-resolved Raman spectroscopy in an intralipid suspension phantom using a bundled fiber-optic probe with interchangeable beveled tips. As tips with increasing bevel angle were used, the collection region moved closer to the surface. The effective depths of tissue sampling are within a few millimeters of each other, and the probes must be applicable to tissue analysis. In summary, nondestructive analysis of embedded biological tissues by fiber-optic Raman probes has seldom been performed despite its importance.Komachi et al. installed a micro lens in the head of a miniaturized Raman probe to control the collection region and efficiency of the Raman scattered light.[11]

In the present study, we deal with another type of fiber-optic Raman probe, balllens hollow optical-fiber Raman probes (BHRPs),[12] as our first example to demonstrate the

possibility of obtaining a pure Raman spectrum of an embedded layer. We have already developed a miniaturized endoscope system for diagnosing diseases of the esophagus, stomach, colon, and rectum of mouse and rat,[5,6] and the BHRPs are able to be used together with this system. The BHRPs enable us to control the working distance (WD) and Raman collection area of the probes by selecting only the material and diameter of the ball lens attached to the distal end of the probe.[11]Particularly striking in this study is that we could reconstruct pure Raman spectra from embedded layers by knowing the Raman spectra measured by two types of multiple miniaturized Raman probe and the different optical properties at different depths and thicknesses of the layers. The formulas discussed here represent the basic theory for explainingthe relationship between the surface layer thickness of the layered sample and the spectra from the embedded layer.

This is a preliminary study, wherein transparent samples instead of diffusely scattering media are used to construct and evaluate the basic theory. With our previous study about subsurface sensing method by using a single BHRP,[12] we plan to expand it to biomedical samplesand consider light-scattering effects in our next study. The present technique provides basic knowledge of the sampling volumes of the Raman probes and the data processing methods, and is expected to facilitate future development of in situ measurements of diseased tissues.

Model description

General formulas for Raman spectra measured by multiple Raman probes

Here we derive the formulaeforreconstructingthe Raman spectrum of anembedded layer. Let us consider a semi-infinite, one-dimensional two-layered slab measured by two

different types of multiple fiber-optic Raman probe in contact mode, as shown in Fig. 1. A previous study showed that the sensitivity curve is represented approximately by a Gaussian curve.[13]The WD of the probe can be controlled by selecting an material and diameter for the ball lens.[12]Since the Raman spectra measured by the probes contain contributions from both the first and embedded layers at different rates, they are given by simple linear combinations of pure Raman spectra S and sampling volume A. For example, when the light penetrates deeper than the first layer, the Raman spectrum essentially includes contributions from both the first and second layers. We consider that the total sensitivity of the probe, in other words, the entire size of the Raman sampling volumes, is represented by the area under the Gaussian curve in Fig. 1. When we assume that the sampling volumes of these two probes (probes I and II) are the same, the two Raman spectra X^I and X^{II} measured by these probes become

$$X^I = A_1^I S_1 + A_2^I S_2 \qquad (1)$$

$$X^{II} = A_1^{II} S_1 + A_2^{II} S_2 \qquad (2)$$

whereX^I is the Raman spectrum measured by probe I, A is a function that describes the Raman sampling volume of the probe in a layer, and S is the pure Raman spectrum of the layer. A tunable parameter k is introduced here. The intensity contribution of the first layer from X^{II}can be removed by subtracting$X^I$and using a parameter k, as described below.

$$X^{II} - kX^I = S_1 \cdot \left(A_1^{II} - kA_1^I\right) + S_2 \cdot \left(A_2^{II} - kA_2^I\right) \qquad (3)$$

In Eq. (3), the term $A_1^{II} - kA_1^I$ on the right-hand side becomes zero when the entire contribution of the first layer (S_1) is removed. Thus, we find that

$$k = A_1^{II} / A_1^I \qquad (4)$$

and

$$S_2 \cdot \left(A_2^{II} - kA_2^I\right) = X^{II} - kX^I$$

$$(5)$$

and thus,

$$S_2 = \frac{X^{II} - kX^{I}}{A_2^{II} - kA_2^{I}} \qquad (6)$$

It is particularly striking that this formula, together with Eq. (4), indicates that the pure spectra S can be derived using only X^{I}, X^{II}, and k. In other words, the spectra of a layered samplemeasured by two types of Raman probe with different WD can be decomposed into the pure spectrum of each layer.

Total Raman sampling volumes

In an empirical study, the size of the Raman sampling volumes for each probe may diffeent. When the entire sizes of the Raman sampling volumes of probes I and II different, it will be convenient to standardize the measured spectra X^{raw} by the entire sizes of the Raman sampling volumes (A_{total}). The standard spectra for probes I and II, $X^{st,I}$, $X^{st,II}$, are as follows.

$$X^{st,I} = X^{raw,I} \times \frac{1}{A_{total}^{I}} \qquad (7)$$

$$X^{st,II} = X^{raw,II} \times \frac{1}{A_{total}^{II}} \qquad (8)$$

The total Raman sampling volumes can be obtained experimentally by simply measuring the Raman signals from a pure bulk material. According to the conditions, we can introduce the following relation.

$$X = X^{st}$$

$$(9)$$

Substituting these relations into Eqs. (4) and (6), we finally obtain the required expression for the pure spectrum from the embedded layer,

$$S_2 = \frac{\dfrac{1}{A_{total}^{II}} X^{raw,II} - \dfrac{k}{A_{total}^{I}} X^{raw,I}}{A_2^{II} - kA_2^{I}} \qquad (10)$$

$$c \cdot S_2 = \frac{1}{A_{total}^{II}} X^{raw,II} - \frac{k}{A_{total}^{I}} X^{raw,I} \qquad (11)$$

$$\left(c = A_2^{II} - kA_2^{I} \right)$$

Here, c is a scalar. It is possible to obtain A_{total}^{I}, A_{total}^{II}, $X^{raw,I}$, and $X^{raw,II}$ experimentally. The value of k is a function of the thickness of the first layer. The thickness of the first layer x can be measured experimentally by ultrasound[14] or optical coherence tomography (OCT).[15] The axial resolution of ultrasound is several tens of micrometers, and that of OCT is a few micrometers.

Functions describing Raman sampling volumes and k

For BHRPs, the functions representing the Raman collection efficiency along the z-axis (the depth direction) in transparent materials are Gaussian curves.[13] The Raman sampling volumes can be calculated as the integral of the Gaussian curves, with the interval $[-\infty, t]$ of the probability density function.

$$A = \int_{-\infty}^{t} \frac{1}{\sqrt{2\pi\sigma^2}} \exp\left(-\frac{(x-\mu)^2}{2\sigma^2} \right) dx = \frac{1}{2}\left(1 + erf\left(\frac{t-\mu}{\sigma\sqrt{2}} \right) \right) \qquad (12)$$

Here, *erf* is the error function encountered in integrating the normal distribution, which is a normalized form of the Gaussian function. This formula can be calculated for any numbers *t*,and the total integral must be 1. The value of *k* is expressed by the following equation.

$$k = \frac{A_1^{II}}{A_1^{I}} = \frac{1 + erf\left(\frac{x - \mu_{II}}{\sigma_{II}\sqrt{2}}\right)}{1 + erf\left(\frac{x - \mu_{I}}{\sigma_{I}\sqrt{2}}\right)} \qquad (13)$$

It is convenient to represent the values in Eq. (13)as empirical values that can be measured.The thickness of the first layer is represented by x;μ describes the WD of the probe, and $\sigma$is the distribution of the Raman sampling volume. The value of σcanbe transformed into the FWHM value of the Gaussian curve, as follows.

$$\sigma \cong \frac{FWHM}{2.35} \qquad (14)$$

Therefore,

$$k = \frac{1 + erf\frac{2.35 \times (x - \mu_{II})}{FWHM_{II}\sqrt{2}}}{1 + erf\frac{2.35 \times (x - \mu_{I})}{FWHM_{I}\sqrt{2}}} \qquad (15)$$

The WD and FWHM are characteristicsof the probe;we reported how to obtain these values in a previous paper.[13] Hence, all of the parameters used to calculate the pure spectrum of the embedded layer are experimentally obtained.

Experimental

Raman measurements

94

The experimental setup for the Raman measurements was described elsewhere.[12]Thehomemade BHRP was connected to a single polychromator via a specially developed coupling stage in which two long-pass filters were installed for reflecting the excitation light and blocking Rayleigh scattered light, respectively.[12]The 785-nm line of a diode laser (XTRA, Toptica, Germany) was employed as a light source.Thelaser power wastypically 10 mW at the sample. The measurements were made with the probes held perpendicular to the sample in contact mode with the surface of the polyethylene (PE) layer. The exposure time was typically 20 s.

The BHRPs consist of a hollow optical fiber and a ball lens at the distal end, as mentioned previously.[11]Here, we used three kinds of ball lenses: two made of sapphire glass (diameters, 0.50 and 0.79 mm, respectively; Edmund Optics, USA) and one made of fused silica (diameter, 0.50 mm; Swiss Jewel Co., USA). The total diameters of the probe heads were 0.64, 0.90, and 0.64 mm, respectively. The optical properties of the BHRPs are presented in Table 1. The total Raman sampling volumes were estimated from the spectral intensitiesofa thick pure PE substrate measured in contact mode.

The layered model samples consist of PE films and polymethylmethacrylate (PMMA) substrates. The PE films are attached to a flat PMMA substrate one by one in order to vary the thickness of the PE layer, as illustrated in Fig. 1. After the measurements, the model samples were cut vertically with a sharp cutter, and the thickness of the PE layer was measured with a laser microscope (VK-8500, Keyence, Japan).

Data processing and simulation study

The optical property WD and FWHM, was obtained empirically according to the method described in a previous report.[13] A background spectrum originating from the optical components in the Raman system was subtracted from the raw Raman spectra obtained from the layered model samples to eliminate noise. The Unscrambler software package (Ver. 7.8, CAMO Software Inc., USA) was employed for PLS regression analyses of the empirical and simulated spectra. PLS regression of the dependent variables wasconducted for the spectral region ranging from 400 to 1800 cm^{-1}. The prediction models were validated by the leave-one-out cross-validation method.

Results and Discussion

Relationship between k and the layer thickness

The parameters μ and σ, which represent the Raman sampling volumes of the BHRPs, are shown in Table 1.The total Raman sampling volumes are also shown in Table 1. The value of the sampling volume is standardized so that the value of probe I is 1. In summary, by calculating k from the dispersion of the Raman sampling volumes of multiple probes by using Eq. (13) or (15), we can estimate the quality of the pure spectrum of the embedded layer calculated from the empirical spectra by Eq. (11). Moreover, these results also illustrate the significance of selecting the Raman collection area of the probes depending on the thickness or depth of the target sample.

To clarify the properties of k, we plot the values of k calculated by Eq. (13) versus x,the thickness of the first layer. The theoretical and empirical results are compared in Fig. 2. The empirical k values were estimated from the Raman spectra of two-layered transparent materials measured by BHRPs. Figure 3 shows Raman spectra of a two-layered transparent

sample measured by two types of Raman probe in contact mode. Since PE and PMMA show independent sharp Raman bands, precise k valuescan be obtained experimentally directly from the spectra in the present model for the good comparison with the theoretical results.As shown in Fig. 2, k passes through a minimum value and goes to 1 with increasing x. The empirically obtained k values agree well with the theoretical result, validating the adequacy of the present theory. From Eq. (4), k is the ratio of the Raman sampling volumes in the first layer of probes I and II. When $k = 1$, the total Raman sampling volumes for the two probesarethe same, and neither spectrum measured by the probes has a detectable contribution from the second layer.Therefore, the accuracy of the estimated thickness and/or pure spectrum of the first and second layers becomes low when k is close to one. According to Fig.2a, $k$reaches approximately oneat an$x$value of 300 μm, which is slightly larger than the estimated detectable area of probe II, 200 μm (80 μm[WD] + 240 μm[FWHM]/2). The contribution from the embedded second layer becomes much smaller than that of the first layer when x is smaller than 300 μm. When probes I and III are used, as shown in Fig. 2b, k is less than one even at an$x$ value of 600 μm. This suggests that this pair of BHRPs has a wider applicable range. On the other hand, the $k$value for x from 30 to 100 μm does not change much. In fact, the empirically obtained$k$values are almost the same in this range of x. As the WDs of these probes are 48 and 400μm, respectively, the overlap in the total excitation volumes for these two probes is estimated to be relatively small. This suggests that the axial resolution decreases when the WDs of the two probes are too different.

It is possible to estimate the thickness of the first layer when the pure spectra of the materials composing the sample are available, according to the present theory.Note that there may be two x values for one$k$ value; k is 0.8 for $x = 50$ and 190 μm in the graph in Fig.

97

2a. These results indicate that it is important to designate a pair of probes suitable for the sample to be measured. Crude information on the thickness of the first layer must be available in advance when selecting the probes. This is generally a reasonable condition for biological samples because the thickness of tissues in the human body has been studied very well.

Pure spectrum reconstruction of the embedded layer

Figure 3 shows Raman spectra of a two-layered transparent sample measured by probes I and II in contact mode. The sample consists of 80 μm thick PE films covering a flat PMMA substrate. The value of k is estimated to be 0.5, according to Eq. (15). The spectrum of the embedded layer reconstructed according to Eq.(11) is very similar to the pure spectrum of PMMA.The signal-to-noise ratio in the reconstructed spectra is rather lower than that in the spectrum of pure PMMA. In Eq.(11), S_2 is a function of parameters $X^{raw,I}$ and $X^{raw,II}$, and the noise level in S_2 is described by basic error propagation as

$$\delta S_2 = \sqrt{\frac{k^2}{(A_2^{II} - kA_2^{I})^2 A_{total}^{I}{}^2}\left(\left|\frac{\partial S_2}{\partial X^{raw,I}}\right|\delta X^{raw,I}\right)^2 + \frac{1}{(A_2^{II} - kA_2^{I})^2 A_{total}^{II}{}^2}\left(\left|\frac{\partial S_2}{\partial X^{raw,II}}\right|\delta X^{raw,II}\right)^2} \quad (16)$$

Since k is less than one, the noise level of the spectra of probe II, which has a longer WD, contributes more than that of the spectra of probe I. Therefore, in practice, using multiple Raman probes, we simply measure the Raman spectra with lower noise levels to obtain the Raman spectra of an embedded layer with better quality.

Conclusion

In this paper, we presented a theoretical approach to reconstructingthe pure Raman spectrum of the embedded layer in a two-layered sample using two BHRPs.The method,which is based on an understanding of the Raman sampling volume,is very simple. Its viability is evaluated using a transparent model sample consisting of PE and PMMA layers.The reconstructed pure spectrum of the embedded layer is almost identical to the spectrum of the pure bulk material. The results strongly suggest that the theory is essentially correct. Since the present method depends only on the sampling volume of the Raman probe, this approach can be extended to light-scattering samples, e.g., biomedical tissue, if the scattering properties of the sample are known. We employa Monte Carlo simulation to depict the shapes of the Raman sampling volumes in light-scattering samples. The result will be described in a later paper.

References

[1] E. B. Hanlon, R. Manoharan, T. W. Koo, K. E. Shafer, J. T. Motz, M. Fitzmaurice, J. R. Kramer, I. Itzkan, R. R. Dasari, and M. S. Feld, *Phys. Med. Biol.* **45**, R1 (2000).

[2] T. C. B. Schut, M. J. H. Witjes, H. J. C. M. Sterenborg, O. C. Speelman, J. L. N. Roodenburg, E. T. Marple, H. A. Bruining, and G. J. Puppels, *Anal. Chem.* **72**, 6010 (2000).

[3] N. Stone, C. Kendall, J. Smith, P. Crow, and H. Barr, *Faraday Discuss.* **126**, 141 (2004).

[4] J. C. C. Day, R. Bennett, B. Smith, C. Kendall, J. Hutchings, G. M. Meaden, C. Born, S. Yu, and N. Stone, *Phys. Med. Biol.* **54**, 7077 (2009).

[5] Y. Hattori, Y. Komachi, T. Asakura, T. Shimosegawa, G. Kanai, H. Tashiro, and H. Sato, *Appl. Spectrosc.* **61**, 579 (2007).

[6] H. Sato, Y. S. Yamamoto, A. Maruyama, T. Katagiri, Y. Matsuura, and Y. Ozaki, *Vib. Spectrosc.* **50**, 125 (2009).

[7] Y. Matsuura, S. Kino, E. Yokoyama, T. Katagiri, H. Sato, and H. Tashiro, *IEEE J. Sel. Top. Quant.* **13**, 1704 (2007).

[8] T. L. Ang, C. J. L. Khor, and T. Gotoda, *Singap. Med. J.* **51**, 93 (2010).

[9] P. Matousek, I. P. Clark, E. R. C. Draper, M. D. Morris, A. E. Goodship, N. Everall, M. Towrie, W. F. Finney, and A. W. Parker, *Appl. Spectrosc.* **59**, 393 (2005).

[10] M. G. Shim, L. M. W. M. Song, N. E. Marcon, and B. C. Wilson, *Photochem. Photobiol.* **72**, 146 (2000).

[11] Y. Komachi, T. Katagiri, H. Sato, and H. Tashiro, *Appl. Opt.*, **48**, 1683 (2009).

[12] T. Katagiri, Y. S. Yamamoto, Y. Ozaki, Y. Matsuura, and H. Sato, *Appl. Spectrosc.* **63**, 103 (2009).

[13] Y. S. Yamamoto, Y. Oshima, H. Shinzawa, T. Katagiri, Y. Matsuura, Y. Ozaki, and H. Sato, *Anal. Chim. Acta* **619**, 8 (2008).

[14] T. J. Romer, J. F. Brennan, G. J. Puppels, A. H. Zwinderman, S. G. van Duinen, A. van der Laarse, A. F. W. van der Steen, N. A. Bom, and A. V. G. Bruschke, *Arterioscler., Thromb., Vasc. Biol.* **20**, 478 (2000).

[15] G. J. Tearney, M. E. Brezinski, B. E. Bouma, S. A. Boppart, C. Pitris, J. F. Southern, and J. G. Fujimoto, *Science* **276**, 2037 (1997).

Table 1.   Parameters representing the Raman sampling volumes of the BHRPs. *Working

distance for paraxial light calculated from the original formula of Katagiri et al.[12]

Name	Lens material	Lens Diameter (mm)	Working distance				Raman sampling volume
			Calculated		Measured		
			u	FWHM	Transparent plastics		
					u	FWHM	
Probe I	Sapphire	0.50	39	–	48	66	1.00
Probe II	Sapphire	0.79	62	–	80	240	1.00
Probe III	Fused silica	0.50	153	–	400	410	0.93
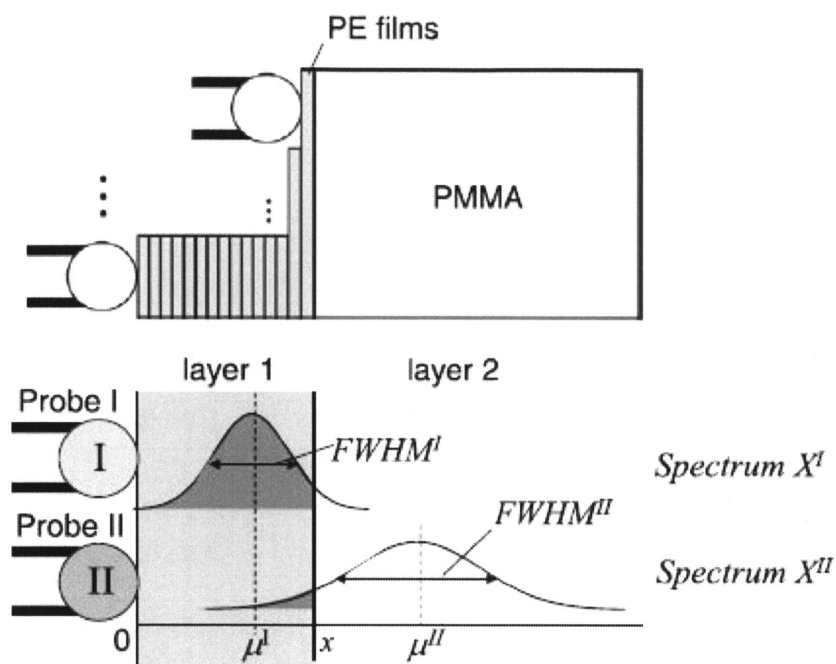
Figure 1. Schematic representations of the experimental setup of the sample arrangement and the Raman sampling volumes of the BHRP in two-layered transparent materials.
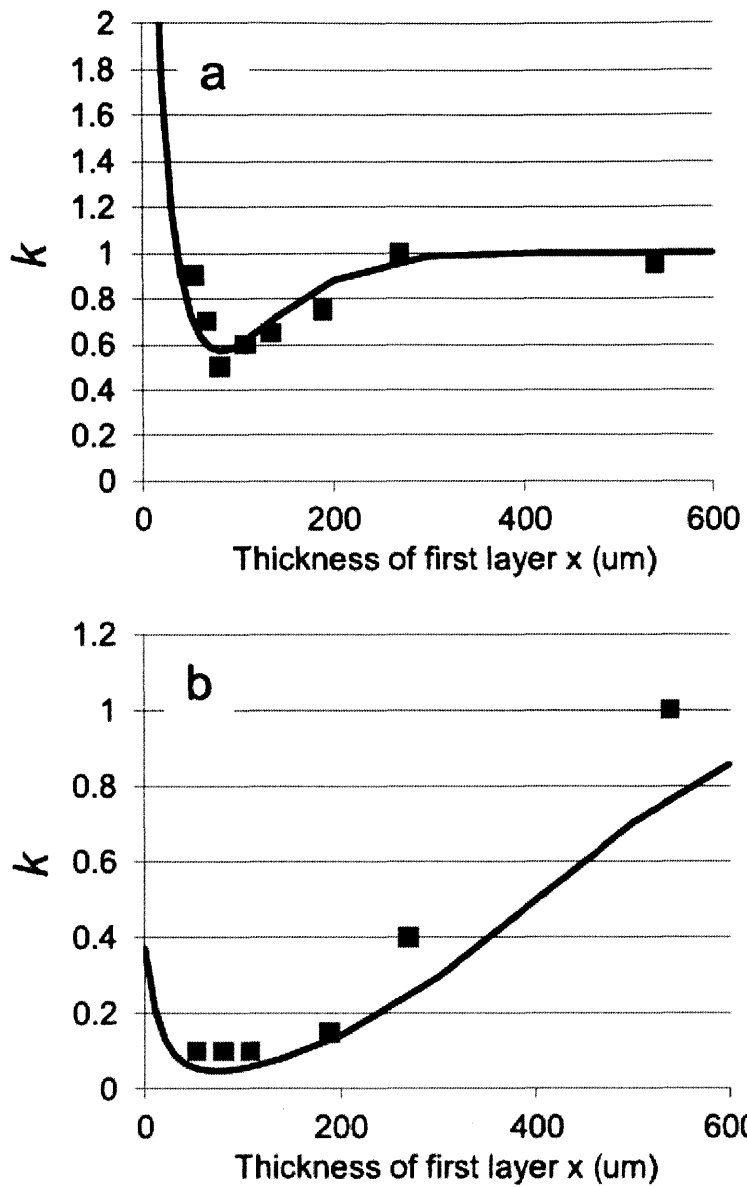
Figure 2. Intensity plots of k as a function of x, the thickness of the first layer, in two-layered transparent materials: (a) probe I and probe II, (b) probe I and probe III. Solid line indicates value of k calculated by Eq. (15).
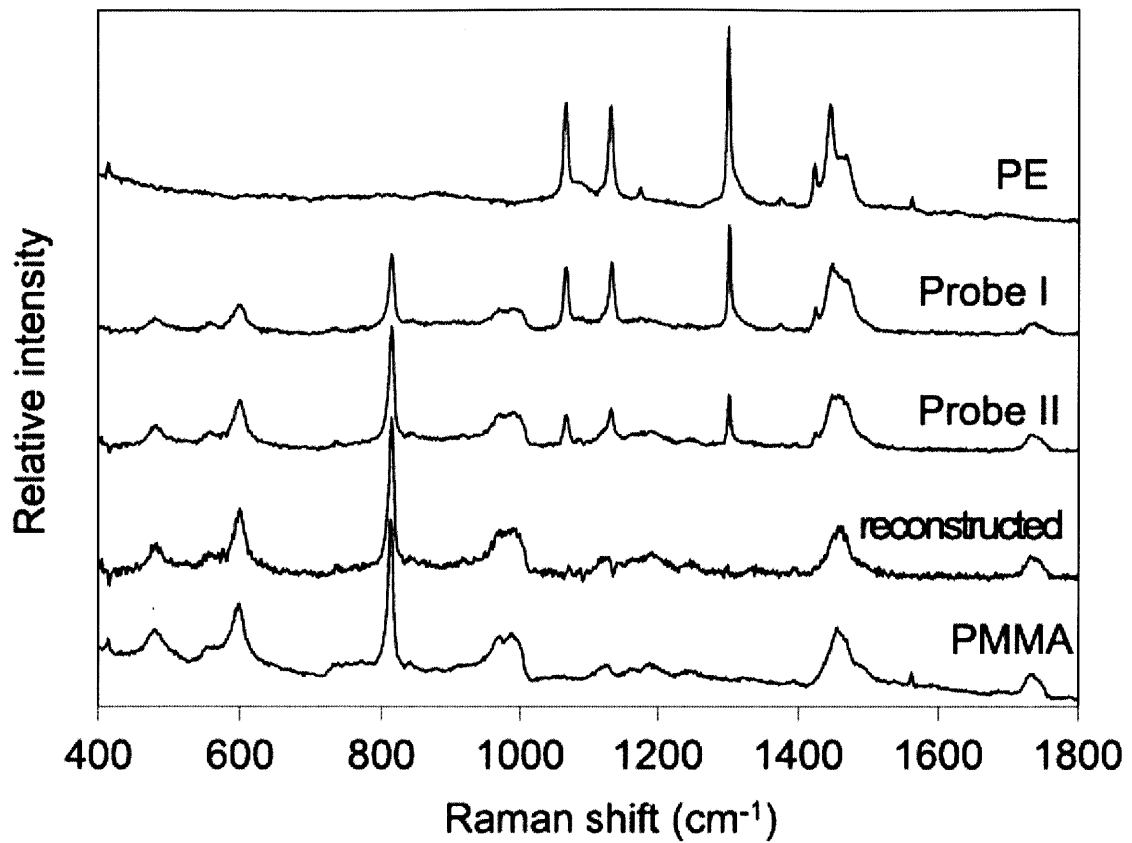
Figure 3. Raman spectra of a two-layer transparent sample in which an 80 μm thick PE film covers a flat PMMA substrate, measured with probes I and II in contact mode. Top and bottom spectra are those of pure PE and pure PMMA. Spectra are offset for clarity.

Chapter 5

Raman Study of Brain Functions in Live Mice and Rats: a Pilot Study

Abstract

Raman spectra of brain tissues of live mice and rats weresuccessfully obtained using a miniaturized Raman probe. The use of a ball lens hollow fiber Raman probe and a background-free electronically tuned Ti:sapphire laser enabledthe measurement of high-quality Raman spectra in the fingerprint region and high-wavenumber region at exactly the same measurement point at the same time. The measurements were performed on the animal under anesthesiabysodium pentobarbital, afterinhalation of diethyl ether (DE) vapor, and aftereuthanasia. The obtained spectra in the high-wavenumber region suggest that water concentration and water cluster conformation changewith changes in the condition of the animal, and the change shows site dependency in the brain. In the frontal cortex, a minor increase in the water cluster of a specific conformation was observed by theinhalation of DE vapor. On the other hand, water concentration decreased after the animal was euthanized. In the olfactory lobes, the water concentration increased both afterDE vapor inhalation and after euthanasia. No major spectral change was observed in the fingerprint region, suggesting that the functions of the water molecule are independent of other molecules. The study results demonstrate the high viability of Raman spectroscopy forstudying brain function in live experimental animals.

Introduction

Raman spectroscopy is a powerful tool for studying the molecular composition, molecular structure, and molecular interaction in a tissue in a completely nondestructive manner [1-6]. It is a vibrational spectroscopic technique with a high molecular specificity. No staining process is required to obtain information onthe sample, and a real-time *in vivo* noninvasive analysis can be carried out using a very small amount of the sample. Many researchers havemadeconsiderable efforts to develop clinically available tools and techniques for diagnosing brain tumor and diseases on the basis of Raman spectroscopy. For example, Mizuno et al. analyzed normal and tumor tissues in rat and human brains by near-infrared Raman spectroscopy in the 1990s[1,2]. Their study pioneered the use of Raman spectroscopy for analyzing brain tissues. A number of Raman studies provide evidence for the possibility of characterizing and identifying a large variety of normal and malignant brain tissues. Wolthuis et al. determined the water concentration in brain tissue by Raman spectroscopy[3]. They observed Raman bands in the high-wavenumber region (2600–3800 cm^{-1}) in which water has a strong band of the OH stretching mode and analyzed the water concentration by a multivariate statistical method. Koljenović et al. also observed the high-wavenumber region of Raman spectra to analyze brain tumor and bladder tissues[4]. They employed an unfiltered fiber optic Raman probe. Since anintense Raman signal of the core material of optical fibers hinders themeasurement of sample spectra, it is necessary to attach bandpass (BP) and long-pass (LP) filters to the distal end of the fiber probe to block unwanted light for the Raman measurement in the fingerprint region. However, the silica band is rather weak in the high-wavenumber region;therefore, it is possible to obtain sample spectra using the unfiltered probe. Koljenović et al. suggested that essentially, the same

diagnostic information is obtained in the fingerprint and high-wavenumber regions[4] Amharref et al. employed Raman spectral imaging to discriminate normal tissues from tumor and necrosis tissues[5]. They suggested that structural changes of tissue materials were related to qualitative and quantitative changes in lipid content, which were useful for a pathological analysis. Krafft et al. introduced a fiber optic Raman probe to obtain a Raman map for detecting metastases in mouse brains and compared the obtained results with thoseof FTIR imaging[6]. The Raman maps successfully detected tumor cells in the brain metastases of malignant melanomas but the FTIR imaging did not. Many studieshave revealed that Raman spectroscopy is one of the most effective techniques for analyzing brain tissues in terms of molecular theory and suggested that it has high viability in nondestructive *in vivo* analysis.

A molecular theoretical approach based on Raman spectroscopy may provide new insight into the understanding of mechanisms of brain function. Malonek and Grinvaldcharacterized activity-dependent changes in hemoglobin oxygenation and light scattering by imaging spectroscopy[7]. They reported that a localized increase in neuronal activity was accompanied by a metabolic process of the initial localized tissue hypoxia and vascular responses occurring within the first 3 seconds and the spreading of these responses over surrounding tissues. The brain function related to substantial actions and stimulations can be effectively observed by imaging spectroscopy;however,this technique does not appear to be sufficiently sensitive for detecting moderate brain functions such as consciousness. Therefore, it is necessary to develop a new techniquethat is sufficientlysensitive for observing weak and/or different types of physiological events.

We assume that water molecules play an important role in brain function because small molecules such as ethanol, diethyl ether (DE), and chloroform, which havea considerable effect on consciousness, alter the structure of water clusters. Therefore, it is important to observe the water band in the high-wavenumber region and Raman spectra in the fingerprint region at the same point and same time;moreover, this measurement must be carried out in a living animal. Hence, the objective of the present study is to demonstrate the viability of Raman spectroscopy for detecting molecular changes occurringdueto physiological changes in living brain tissues in situ. We employ a near-infrared Raman system equipped with a ball lens hollowfiber Raman probe (BHRP) and a background-free electronically tuned Ti:sapphire laser (BF-ETL)[8-14]. The BHRP consists of a single hollow optical fiber and a ball lens attached toits distal end and does not include any filter[8-10]. The BF-ETL provides high-purity laser light with high pointing stability[11,12]. Its wavelength and power can be controlled accurately usinga personal computer (PC). Detailed optical properties of the BHRP and BF-ETL are described elsewhere[8-12]. In this study, it is shown that the present Raman system is feasible for obtainingadequately reliable, stable, and high-quality Raman spectra of the brain tissue in live animals for analyzing minute spectral changesoccurring in the Raman bands of water clusters.

Experimental

1. Raman measurement

Figure 1 shows the experimental setup of the present Raman system. The BHRP is used to measure Raman spectra. As mentioned previously,the probe comprisesa single hollow fiber and a ball lens attached to its distal end. The BHRP is connected to a specially

developed coupling stage in which two LP filters (Semrock, Inc., USA) are installed for reflecting the excitation light and blocking Rayleigh scattered light. The length of the BHRP is 1.5 m,andits maximum diameter is 640 μm. The outer and inner diameters of the hollow fiber are 435 and 320 μm, respectively. The diameter of the sapphire ball lens attached to the probe head is 500 μm [10]. The collected Raman light is focused into a slit (100 μm) of a single polychromator(F/4.9, 320 mm, Photon Design Co., Ltd., Japan) with gratings (600 lines/mm, 850 nm brazed angle) and detected using a CCD detector (CCD; DU401-BR-DD, Andor Technology Co., Ltd., Northern Ireland). The spectral resolution of the Raman system is typically less than 10 cm^{-1}. A continuous wave (cw)-BF-ETL (TS-32, Megaopto Co., Ltd., Japan)is employed as a light source. Measurements of brain tissues of live mice and ratsare carried out using the probein the contact mode. Two excitation wavelengths—785 and 720 nm—are used to measure Raman spectra in the fingerprint region (600–1800 cm–1) and high-wavenumber region (2600–3800 cm–1), respectively, in order to avoid the low-sensitivity range (1000 nm<) of the CCD detector. The laser powers at the sample point are approximately 40 and 15 mWatwavelengths of 785 and 720 nm, respectively. The values of the laser power havea considerable degree of error because the transmission efficiency of the hollow optical fiber isdependent on its bending state. The exposure time is 300 s. Abackground spectrum originating from the optical elements in the Raman system is subtracted from the raw Raman spectra. The spectrum of a halogen lamp is used to correct the wavelength-dependent signal detection efficiency of the Raman system. No further treatment is carried out.

2. Sample preparation

The procedure of the present experiment was verified and permitted by the ethical committee of RIKEN. Mice (C57BL/6, male, 12–16 weeks) and rats (Wister, male, 8 weeks) were purchased from Japan SLC, Inc. The mice and rats were deeply anesthetized by anintraperitoneal administration of 50 mg/kg sodium pentobarbital (SP) and placed on a stereotaxic instrument. The body temperature of the animals was maintained by placing a hotwater bag in their bed. The skull was exposed and a small hole was drilled at the sites shown in Fig. 2 in order to insert the BHRP. The locations of drilling were selected such that theywere away from major blood vessels. The diameter of the hole was less than 1 mm in order for the probe to access the brain surface directly. The arachnoid membrane was carefully removed as much as possible by a needle. The Raman probe was set carefully by avoiding blood vessels in contact with the exposed brain surface. Raman spectra of the olfactory lobe of theratsand the frontal cortex of the mice were measured. In the experiment on rats, holes were madeon both sides of the olfactory lobes, and the surface cortex tissue (~100 μm) of only the right side was removed to expose the subsurface tissue layer. In the experiment on mice, a hole was madeon the right side of the frontal cortex.

After performing Raman measurements of the animals under anesthesia, a petri dish containing DE was placed under their mouthsfor them to inhale its vapor, and then, Raman spectra were measured again. Next,the mice and rats were euthanized by an intraperitoneal injection of an excess amount (×5~10) of SP. The death of the animal was confirmed by the termination of its respiration. The measurement was begun several minutes after the termination of respiration, and spectra were measuredtwo times. No change was observed in these two spectra, and the second spectrum was used for further analysis. The Raman measurement of the dead tissue was performed within 30 min after the

termination of respiration.Data on the frontal cortices of two mice and data on the right and left olfactory lobes of one rat were obtained.

Results and discussion

Figure 3 showsthe Raman spectra of the frontal cortex of a live mouse brain in the fingerprint (A) and high-wavenumber (B) regions. The spectra in the fingerprint region from 600 to 1800 cm^{-1} were measured with a 785 nm excitation wavelength and those inthe high-wavenumber region from 2600 to 3800 cm^{-1} were measured with a 720 nm excitation wavelength. The spectra of the high-wavenumber Raman shift region (2600–3800 cm^{-1})with the excitation wavelength of 720 nm lie in a wavelength range (886–991 nm) in which the CCD detector has high sensitivity. The present system equipped with the BHRP is suitable for using multiple excitation wavelengths because no filter is attached to its distal end. Since a typical miniaturized Raman probe made of glass fibers contains BP and LP filters at the end of the optical fibers to block strong Raman scattered light generated by the core material of the fibers, it must be used with a fixed excitation wavelength restricted by the transmissible wavelength of the filters[13,14] Although the LP filters are included in the coupling stage of the present Raman system, they do not interfere with the measurement inthe high-wavenumber region using the excitation wavelengthof720 nm. Since the cutoff wavelength of the LP filters is 793 nm, i.e., in the wavelength range of 886–991 nm, they are transparent with respect to light in the high-wavenumber region. The cw-BF-ETL does not generate background noise because of the fluorescence of the laser medium and high pointing stability during the changing wavelength and power. The laser wavelength and power are completely regulated by the PC[11]. Hence, in the present study,measurements in

both the fingerprint region and the high-wavenumber region can be carried out without making any changes in the optical setup, resulting in high stability of both the spectral intensity and spectral quality.

Spectra (a), (b), and (c) in Fig. 3A and 3B are those measured in the frontal cortex of a mouse under anesthesia by SP only, after inhaling DE vapor, and after euthanasia, respectively. The band indicated by the asterisk mark is attributed to the oxygen in the air in the hollow fiber. According to our previous work, the working distance of the BHRP is 58 μm and the focal depth, which is defined by FWHM, in a polyethylene film is 46 μm,and the correspondingvalues in water are 30 and 24 μm, respectively[10]. These values suggest that the Raman spectra of the brain areobtained from the brain tissue locatedapproximately 20 to 40 μm beneath the brain surface. The features of the spectrashown in Fig. 3A are rather similar. Bands at 1664, 1446, and 1003 cm^{-1} are assigned to the amide I mode, CH bending mode, and a breathing mode of phenylalanine of the protein species, respectively. A broad band with small peaks at 1344, 1301, and 1268 cm^{-1} is due to the amide III mode of the protein species. Although the Raman signals of the lipid species are generally much stronger than those of the protein species, the lack of a band at 718 cm^{-1} assignable to phospholipids indicates that the measured tissue in the frontal cortex is rich in protein and its lipid content is very low. No band due to hemoglobin is observed, indicating that the measurement point was successfullypositioned away from blood vessels[15]. The spectra shown in Fig. 3B arein good agreement in the high-wavenumber region as well. Bands at 2846, 2881, and 2928 cm^{-1} are assigned to the CH stretching modes of the protein and lipid species. Raman spectra in the high-wavenumber region of white matter, mesencephalon, and gray matter of the brain are presented in ref. 6. On the basis of the relative intensities of the

three CH stretching bands, it is concluded that the spectra shown in Fig. 3 are due to gray

matter. Gray matter is distributed at the surface of the cerebral cortex and consists mainly of

nerve cell bodies [6]. In the cortex tissues, the most drastic change directly related to the

brain function may be expected to occur in the gray matter. Broad bands at 3297 and 3397

cm^{-1} are assigned to the OH stretching modes of water molecules. A band due to the NH

stretching mode of the amide group at 3293 cm^{-1}appears to overlap with the band due to

water [6]. Spectrum (a) in Fig. 4 is the Raman spectrum of normal saline solution (NSS) in

the high-wavenumber region, measured at 37°C. The intensity of the 3297 cm^{-1} shoulder in

the brain tissue decreases in the spectrum of NSS because of the lack of the NH band.

To analyze minor spectral changes, subtracted spectra are calculated and shown in

Fig. 5A and 5B. The spectra denoted by (d) and (e) are subtraction results of spectra (b)–(a)

and (c)–(a) shown in Fig. 3A and 3B. Spectrum (f) is the subtraction result of two spectra

measured within several minutes of each otherwhen the animal is under anesthesia by SP.

No bands are observed in spectrum (f),implying that the Raman system is adequately stable

for analyzingminute spectral changes. Spectra (d) and (e) in the fingerprint region (Fig. 5A)

have no bands, suggesting that the basic molecular structure and composition of tissue

materials, including the conformation of protein species in the brain tissue,do not change,

even by the death of the animal. The reason why the baseline is not flat in the subtracted

spectra is unknown. Spectra (d) and (e)in the high-wavenumber region (Fig. 5B) show weak

bands due to the OH group of water. The coefficient of subtraction is adjusted to minimize

the contribution of the CH stretching bands. This is because the spectra in the fingerprint

region, except for the spectrum due to water molecules, which does not have a strong band

in the fingerprint region, reveal that no change occurs in the conformation and composition

of tissue materials. The coefficients for obtaining spectra (d) and (e) shown in Fig. 5B are 0.99 and 1.05, respectively. The reason for the presence of the trace band due to the CH stretching mode in the subtracted spectrum (d)is unknown. We have succeeded in obtaining data from two mice. The CH stretching band disappears in the subtracted spectrum of the other mouse. Spectrum (d) shown in Fig. 5B reflects the effect of inhalation of DE vapor, suggesting that DE affects the conformation of water clusters in the brain tissue. The ratio of the intensity of the band in spectrum (d) to the intensity of the original band due to water in the tissue is 2.8%. A similar spectral change is observed in the spectrum of NSSto which DE is added.Spectrum (b) in Fig. 4 is the difference spectrum betweenthe spectrum ofonly NSS and the spectrum of DE-added NSS;spectrum (b') is the enlarged version of spectrum (b). Bands at 2880, 2939, and 2986 cm^{-1} are assigned to the CH stretching modes of DE. The band at 3453 cm^{-1}due to water cluster species indicates that the conformational change of the water clustersoccurs due to theaddition of DE. It is supposed that DE, which can pass through the blood-brain barrier,enters the brain tissue and affects the structure of water clusters, although the concentration of DE in the tissue is considerably lower than that in the normal saline-DE solution. The fact that no bands due to DE appear in the spectrum of the brain tissue reveals that the concentration of DE in the tissue is considerably low. Spectrum (e) reflects the effect of death of the animal. The broad band at 3380 cm^{-1} is assigned to the OH stretching modes of the water cluster species. The negative band indicates a reduction in the water density in the tissue. The intensity of the band due to water decreases by approximately 7.7%. The spectral feature of the water band in spectrum (e) shows good agreementwiththe features of the spectrum of the NSS. The result suggests that the temporal reduction of water concentration in the frontal cortex tissue is an indication of the

termination of brain function. Similar spectral changes are observed in subsequent experiments, suggesting thatthey are independent of individual characteristics of the animals. There still remains one possibility that the reduction in the water concentration is the result of the termination of blood flow. If this possibility is true, the reduction in the water concentration must be observed in other brain tissues as well.

Spectrum (a) in Fig. 6 is the Raman spectrum of the subsurface layer of the olfactory lobe of a rat. Approximately several hundreds of micrometers of the surface layer were surgically removed, and the subsurface layer was exposed to measure Raman spectra. The spectrum of the surface layer onthe other side of the olfactory lobe (not shown) has similar featuresto that of the frontal cortex of mice. The comparison of spectra of the surface tissue and subsurface tissue reveals that the relative intensity of the water band to the CH stretching bands is larger in the subsurface tissue, suggesting that water concentration in the subsurface tissue is higher than that in the surface tissue. Spectra (b) and (c) in Fig. 6areobtained by the subtractionof the spectrum of the olfactory lobe of the rat under anesthesiaby SP from that of the rat that inhaled DE vapor andthe subtraction of the spectrum of the olfactory lobe of the rat under anesthesia by SP fromthat after euthanasia, respectively. The CH stretching bands could not be removed completely in the subtracted spectra. The reason for this may be the dislocation of the measurement point because the right and left lobes were measured alternately using one BHRP in this experiment. No major difference was observed between the subtracted spectra of the surface (data not shown) and subsurface tissues. According to spectrum (b) in Fig. 6, the water density increased by the inhalationof DE vapor, similar to the behavior observed in thespectrum of the frontal cortex of the mouse. Spectrum (c) showsan increase in the water density by the death of the animal,

which is opposite tothe behaviorobserved from the spectrum of the frontal cortex. The results suggest that the state of alterations in the density and conformation of the water clusters depends on their location in the brain. It is confirmed that the reduction in the water concentration observed in the frontal cortex is not due to the termination of blood flow, suggesting that water plays an important role in brain function.

Conclusion

The present study successfully demonstrated that Raman spectroscopy using the BHRP is a powerful tool for investigating brain function on the basis of the molecular composition and structural changes of tissue materials. No alteration in the protein and lipid specieswas observed by theinhalation of DE vapor and theeuthanasia of the animal;however,changes in water concentration and its cluster conformation were observed. The inhalation of DE vapor causes an increase in certain water clusters in the brain tissues. The death of the animal causeda decrease in the water concentration in the frontal cortex and an increase in thewater concentration in the olfactory lobes. The results strongly suggest that water and its cluster system play an important role in brain function. In this study, as all the measurements were carried out on unconsciousanimals so that they would not suffer or undergo pain, the measurement resultsare not sufficientfor explaining the effect of anesthesia itself. To study brain function in greater detail, it is necessary to measure Raman spectrain conscious animals. It suggested that the present system is feasible for measuring spectra of the brain of live animals. The BHRP is sufficiently narrow and flexible; therefore,its tip can be easily attached to the brain. It would be interesting to study spectral changes occurring during activities of conscious mice. This wouldprovide new insight into the mechanisms of the effect of small molecules that causeunconsciousness in animals.

References

[1] A. Mizuno, T. Hayashi, K. Kawauchi, S. Muraishi and Y. Ozaki, *Neurosci. Lett,*.**141**, 47 (1992).

[2] A. Mizuno, H. Kitajima, K. Kawauchi, S. Muraishi and Y. Ozaki,*J. Raman Spectrosc.,* **25**, 25 (1994).

[3] R. Wolthuis, M. van Aken, K. Fountas, J.S. Robinson, Jr., H.A. Bruining and G.J. Puppels, *Anal. Chem.,***73**, 3915 (2001).

[4] S. Koljenović, T.C. Bakker Schut, R. Wolthuis, B. de Jong, L. Santos, P.J. Caspers, J.M. Kros and G.J. Puppels, *J. Biomed. Opt.,***10**, 03116-1 (2005).

[5] N. Amharref, A. Beljebbar, S. Dukic, L. Venteo, L. Schneider, M. Pluot and M. Manfait, *Biochim. Biophys. Acta,***1768**, 2605 (2007).

[6] C. Krafft, M. Kirsch, C. Beleits, G. Schackert and R. Salzer, *Anal. Bioanal. Chem.,***389**, 1133 (2007).

[7] D. Malonek and A. Grinvald, *Science,***272**, 551 (1996).

[8] Y.Komachi, H. Sato, Y. Matsuura, M. Miyagi and H.Tashiro, *Opt. Lett.,***30**, 2942 (2005).

[9] Y. Matsuura, S. Kino, E. Yokoyama, T. Katagiri, H. Sato and H. Tashiro, *IEEE J. Selected Topics in Quantum Electronics,***13**, 1704 (2007).

[10] Y.S. Yamamoto, Y.Oshima, H. Shinzawa, T.Katagiri, Y. Matsuura, Y. Ozakiand H. Sato, *Anal. Chim. Acta,***619**, 8 (2009).

[11] H. Sato, S. Wada, M. Ling and H. Tashiro, *Appl. Spectrosc.,***54**, 1163(2000).

[12] H. Sato, S. Wada and H. Tashiro, *Appl. Spectrosc.,***56**, 1303(2002).

[13] Y. Komachi, H.Sato, K.Aizawa andH.Tashiro, *Appl. Opt,*.**44**, 4722 (2005).

[14] Y. Hattori, Y. Komachi, T. Asakura, T. Shimosegawa, G. Kanai, H. Tashiro and H. Sato, *Appl. Spectrosc.*,**61**, 579 (2007).

[15] H. Sato, S. Wada, Y. Ozaki and H. Tashiro, *Vibrational Spectros*c.,**34**, 149 (2004).
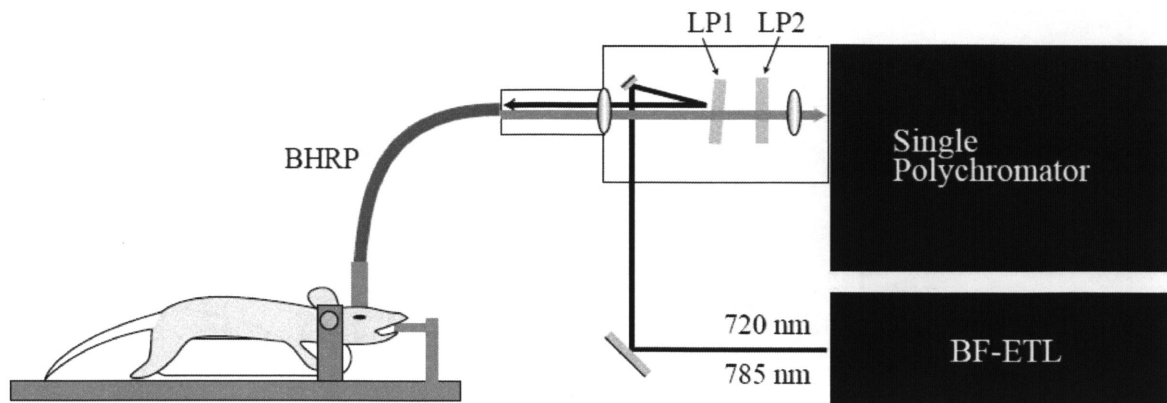
Figure 1.   Schematic representation of experimental setup.
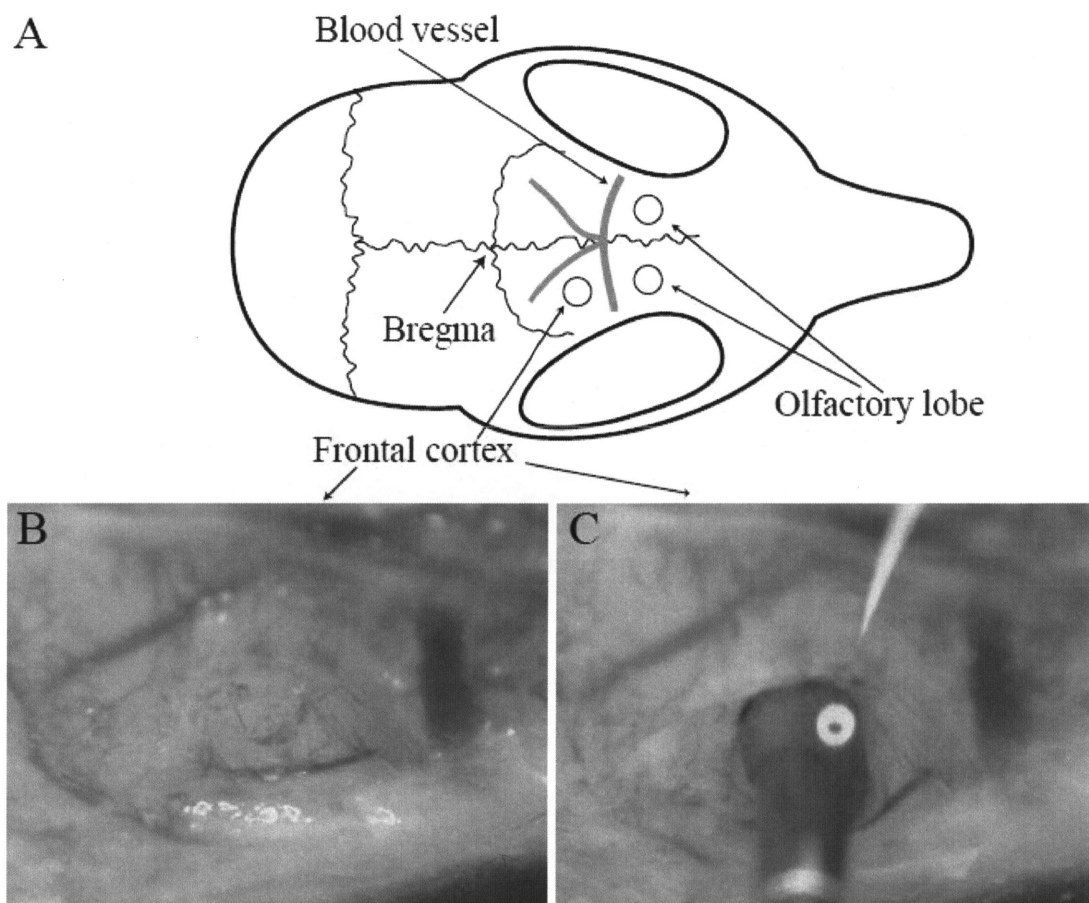
Figure 2. Raman measurement site (A) on the skull of mouse and rat. Holes were made on the skull such that blood vessels were avoided (B). The tip of the BHRP gently touched the surface of the brain (C) to measure the spectrum.
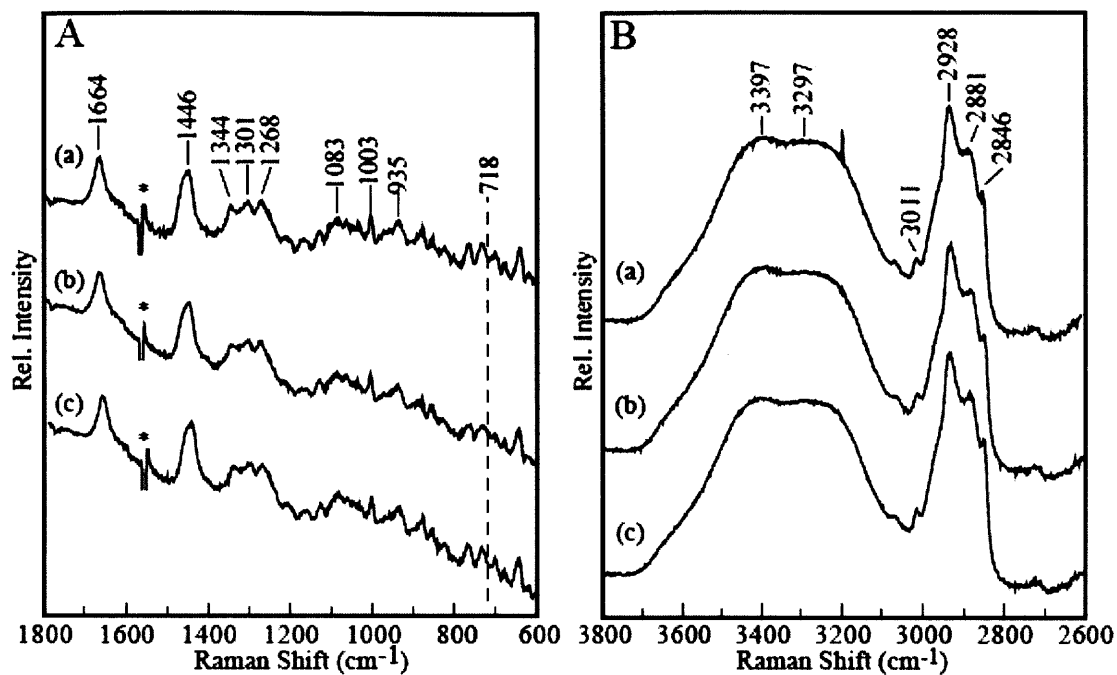
Figure 3. Raman spectra of frontal cortex of a mouse brain in the fingerprint region (A) and high-wavenumber region (B). The spectra were measured when the animal was under anesthesia by SP (a), when the animalinhaled DE vapor (b), and after the animal was euthanized (c).

125
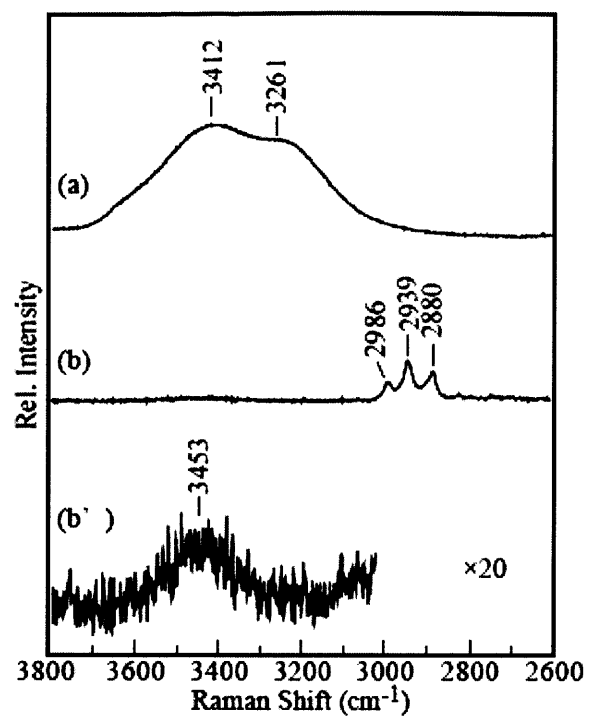
Figure 4.   Raman spectrum of NSS (a). Resultantsubtractedspectrumof NSS spectrum from

spectrum of NSS + DE (b) and partly enlarged version of spectrum (b) (×20; b′).
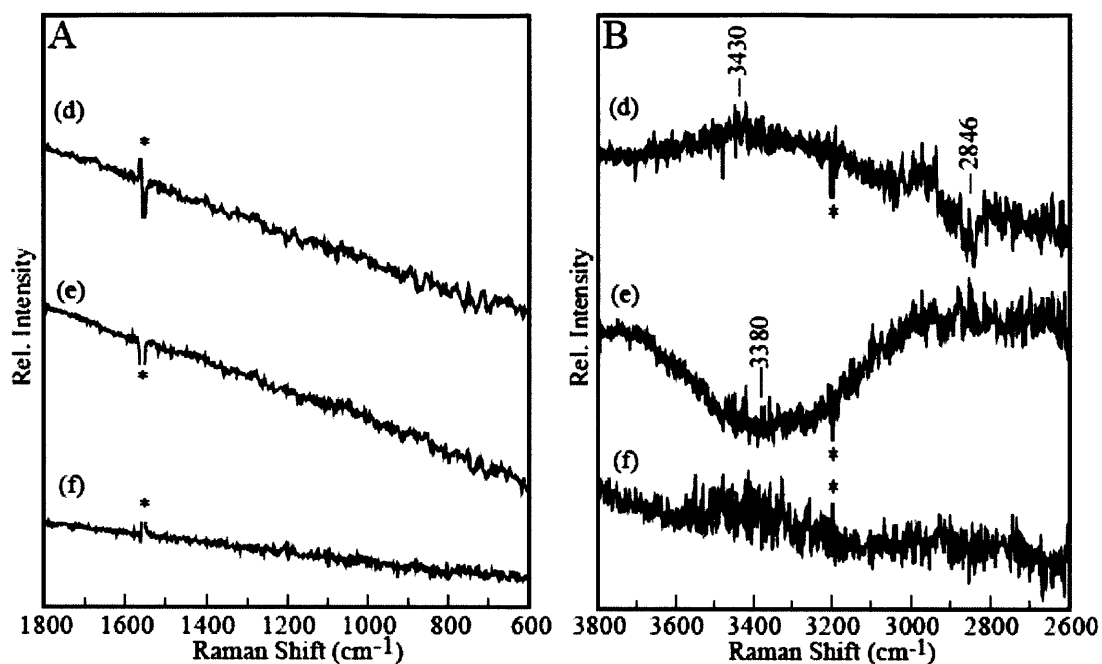
Figure 5. Subtracted Raman spectra of frontal cortex of a mouse brain in the fingerprint

region (A) and high-wavenumber region (B). Resultantsubtracted spectra of the spectrum

measured under anesthesia from that measured under the inhalation of DE (d) and from that

measured after euthanasia (e). Spectrum (f) is the subtraction result of spectra measured

twice after anesthesia.
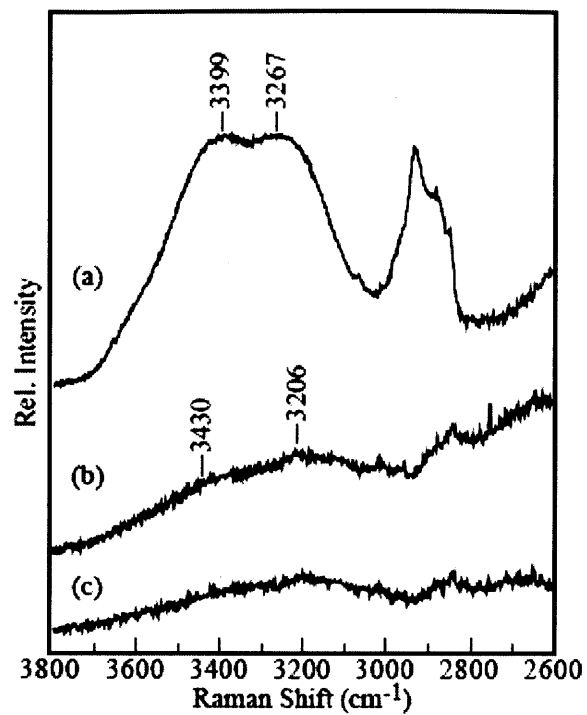
Figure 6. Raman spectra of exposed subsurface tissue of olfactory lobe of rat brain in the high-wavenumber region (a). Subtracted spectra of spectrum measured under anesthesia from that measured under the inhalation of DE vapor (b) and from that measured after euthanasia (c).

grateful to all members in Ozaki laboratory and Sato laboratory in KwanseiGakuin University, especially to Mr. Ken Nakamura and Mr. Yuhei Tanaka, for their emotional assistance.

Moreover, I give special thanks to my family for their financial supports and fancy encouragements.

List of Publications

Papers

Original Papers:

(1) <u>Yuko S. Yamamoto</u>, Yusuke Oshima, Hideyuki Shinzawa, Takashi Katagiri, Yuji

Matsuura, Yukihiro Ozaki, and Hidetoshi Sato,"Subsurface Sensing of Biomedical

Tissues Using a Miniaturized Raman Probe: Study of Thin-layered Model Samples"

AnalyticaChimicaActa, Elsevier, **619**, 8 (2008)

(2) TakashiKatagiri, <u>Yuko S. Yamamoto</u>, Yukihiro Ozaki, Yuji Matsuuraand Hidetoshi

Sato"High axial resolution Raman probe made of single hollow optical fiber"

Appl.Spectrosc.,**63**, 103(2009)

(3) Hidetoshi Sato, <u>Yuko S. Yamamoto</u>,Atsushi Maruyama, TakashiKatagiri, Yuji Matsuura,

and Yukihiro Ozaki,"Raman study of brain functions in live mice and rats: A pilot

study"

Vib. Spectrosc.,**50**, 125 (2009)

(4) <u>Yuko S. Yamamoto</u>, Hideyuki Shinzawa, Yuji Matsuura, Yukihiro Ozaki, and Hidetoshi

Sato, "Noninvasive Subsurface Analysis Using Multiple Miniaturized Raman Probes,

Part I: Basic Study of Thin-Layered Transparent Models of Biomedical Tissues"

Appl.Spectrosc,**65**, 34 (2011).

(5) <u>Yuko S. Yamamoto</u>, Hidetoshi Sato, and Yukihiro Ozaki, "Basic Study of Subsurface

Probing through Diffusely Scattering Media Using Raman Microscope"

To be submitted.

131

Proceedings:

(1) <u>Yuko S. Yamamoto</u>, Yuichi Komachi, Hideyuki Shinzawa, Atsushi Maruyama, Bibin B.
Andriana, Yuji Matsuura, Yukihiro Ozaki, and Hidetoshi Sato, "Noninvasive subsurface
analyzing technique using multiple miniaturized Raman probes"
Proceedings of SPIE, 7173-27(2009)

総説:

(1) 佐藤英俊、<u>山本裕子</u>、大嶋佑介、鈴木利明、「ラマン分光法を用いた生体分析技
術-光バイオプシー技術の展望-」
ぶんせき 5 巻、229(2010)

(2) 佐藤英俊、小杉浩司、RetnoHariyani、<u>山本裕子</u>、Bibin. B. Andriana、小町裕一、
金井源一、「ラマン分光分析によるバイオプシー技術の展望」
日本レーザー医学会誌 31 巻 4 号、420 (2011)

Presentations

Oral Presentations:

(1) <u>山本裕子</u>、大嶋佑介、新澤英之、盛田伸一、尾崎幸洋、佐藤英俊
「生体組織診断用極細径ラマンプローブの高度化：ラマンデプスプロファイル解
析技術の研究」
(社)レーザー学会学術講演会第 28 回年次大会、I1-31aV、2008 年 1 月(名古屋)

(2) <u>Yuko S. Yamamoto</u>, Yuichi Komachi, Hideyuki Shinzawa, Atsushi Maruyama,
Bibin B. Andriana, Yuji Matsuura, Yukihiro Ozaki, and Hidetoshi Sato

"Noninvasive subsurface analyzing technique using multiple miniaturized Raman probes",

BiOS, a part of SPIE 2009, 7173-27, Jan 2009, San jose, US(2009)

(3) 山本裕子

「細径ラマンプローブを用いたデプスプロファイル計測技術」

バイオメディカルオプティクスと光バイオプシー技術に関する産学連携会議、 no.15、2009 年 12 月(和光)

(4) 山本裕子、ビビン・B・アンドリアーナ、松浦祐司、佐藤英俊、尾崎幸洋

「極細径ラマンプローブを用いた層状生体組織の定量的計測:複数プローブの併用」

(社)レーザー学会学術講演会第 30 回年次大会、I-30108、2010 年 2 月(千里)

(5) 山本裕子、佐藤英俊、尾崎幸洋

「極細径ラマンプローブを用いたデプスプロファイル分析手法の開発」

第 57 回応用物理学関係連合講演会、20a-K-9、2010 年 3 月(平塚)

(6) 山本裕子、ビビン・B・アンドリアーナ、松浦祐司、佐藤英俊、尾崎幸洋

「極細径ラマンプローブを用いたデプスプロファイル分析手法の開発：生体組織計測への応用」

第 71 回応用物理学会学術講演会、16p-C-3、2010 年 9 月(長崎)

(7) Yuko S. Yamamoto, Yuji Matsuura, Yukihiro Ozaki, and Hidetoshi Sato,

「Depth Profiling Analysis of Layered Tissues by Miniaturized Raman Probes」

Pacifichem2010,no.120, Dec 2010, Hawaii

(8) 山本裕子、尾崎幸洋、佐藤英俊

「光ファイバラマンプローブを用いた非破壊的サブサーフェス計測手法の基礎検討」

第 58 回応用物理学関係連合講演会、26p-BH-14、2011 年 3 月(神奈川)、 (但し大会自体は東日本大震災に伴い中止)

Poster Presentations:

(1) 山本裕子、大嶋佑介、佐藤英俊、尾崎幸洋

「経血管癌診断用細径ラマンプローブの高度化：層状構造体のラマンデプスプロファイル」分析化学会近畿支部第 1 回平成夏期セミナー、2007 年 8 月(神戸)

(2) Yuko S. Yamamoto, Yusuke Oshima, Shin-ichi Morita, Yukihiro Ozaki, Hidetoshi Sato

"Subsurface Sensing of Biomedical Tissues Using a Miniaturized Raman Probe: Study of Thin-Layered Model Samples"

The 9th Asian Conference on Analytical Sciences (Asianalysis 2007), P-AT-TUE-04, Jeju island, Jeju city, Korea, Nov 2007.

(3) 山本裕子、小町祐一、片桐崇史、丸山篤史、鈴木利明、松浦祐司、尾崎幸洋、佐藤英俊

「極細径ラマンプローブによる層状生体組織計測技術の開発およびその応用研究:光散乱モデルの解析」

日本分析化学会第 57 年会、Y1006、2008 年 9 月 （福岡）

(4) Yuko S. Yamamoto, Yuji Matsuura, Yukihiro Ozaki, and Hidetoshi Sato

"Subsurface Sensing of Biomedical Tissues Using a Miniaturized Raman Probe: Study

of Thin-Layered Model Samples"

TOIN International Symposium on Biomedical Engineering 2008, BE24, 2008 年 10 月

（横浜）

(5) Yuko S. Yamamoto

"Noninvasive subsurface sensing using multiple miniaturized Raman probes: evaluation

using model samples"

HOPE ミーティング 2009、09024、2009 年 9 月 （箱根）

(6) 山本裕子、新澤英之、松浦祐司、尾崎幸洋、佐藤英俊

「極細径ラマンプローブによる層状生体組織計測技術の開発：複数プローブを用

いた定量計測」

日本分析化学会第 58 年会、Y1001、2009 年 9 月 （札幌）

Awards:

(1) Best Poster Award

Yuko S. Yamamoto, Yusuke Oshima, Shin-ichi Morita, Yukihiro Ozaki, Hidetoshi Sato

"Subsurface Sensing of Biomedical Tissues Using a Miniaturized Raman Probe: Study

of Thin-Layered Model Samples"

The 9th Asian Conference on Analytical Sciences (Asianalysis XI), Jeju island, Jeju city,

Korea, Nov 2007

(2) 優秀論文発表賞

山本裕子、大嶋佑介、新澤英之、盛田伸一、尾崎幸洋、佐藤英俊

「生体組織診断用極細径ラマンプローブの高度化：ラマンデプスプロファイル解

析技術の研究」

(社)レーザー学会学術講演会第 28 回年次大会、2008 年 1 月 （名古屋）

(3) Award of Excellence

Yuko S. Yamamoto, Yuji Matsuura, Yukihiro Ozaki, and Hidetoshi Sato

"Subsurface Sensing of Biomedical Tissues Using a Miniaturized Raman Probe: Study

of Thin-Layered Model Samples"

TOIN International Symposium on Biomedical Engineering 2008、2008 年 10 月（横浜）